AD-A055 854 AIR FORCE FLIGHT DYNAMICS LAB WRIGHT-PATTERSON AFB OHIO F/G 17/2
THE SMALL SIGNAL RESPONSE OF FLUID TRANSMISSION LINES, INCLUDIN--ETC(U)
MAR 78 E F MOORE

UNCLASSIFIED AFFDL-TR-78-12 NL

1 OF 2
AD
A055 854

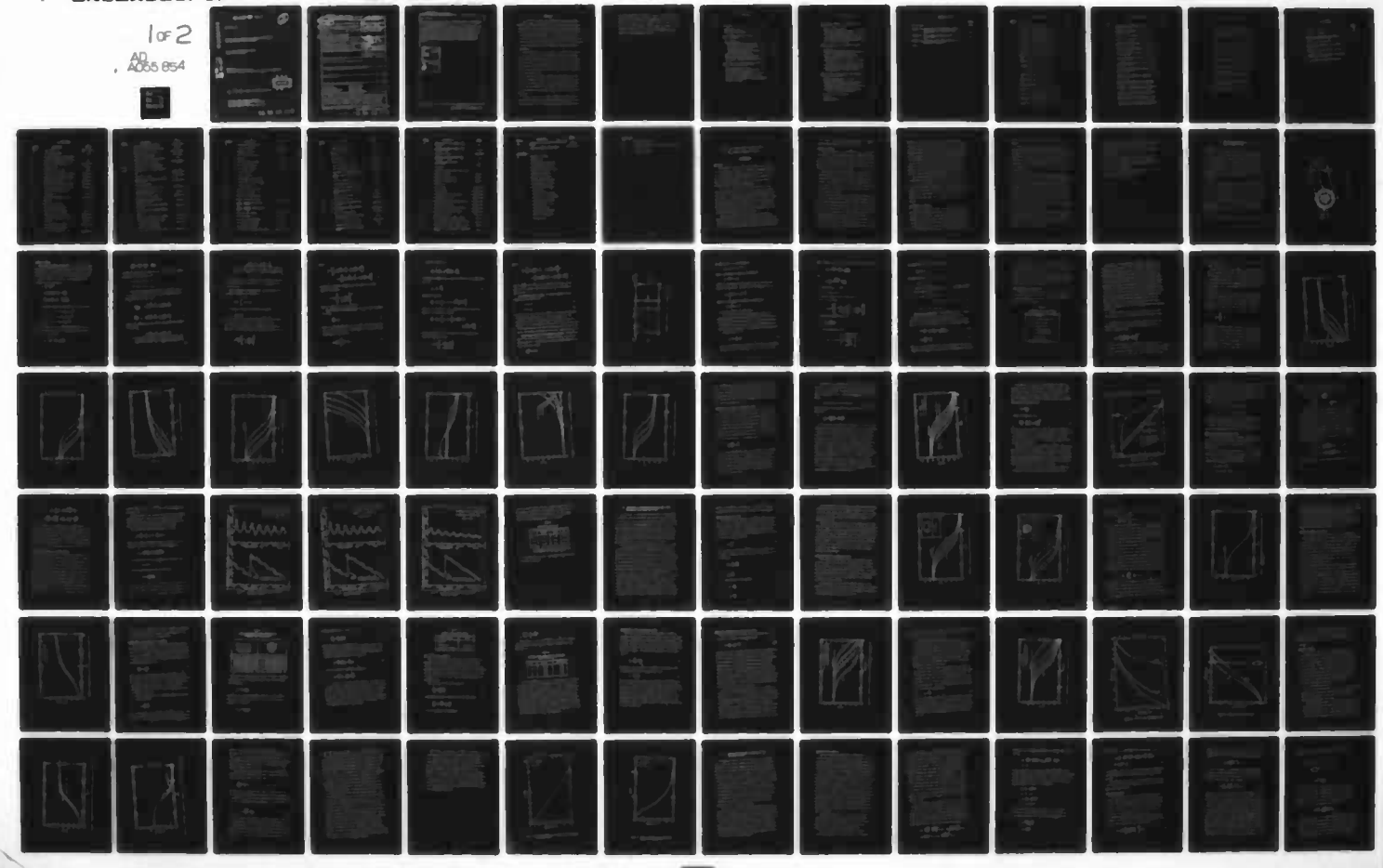

1 OF 2

AD
A055 854

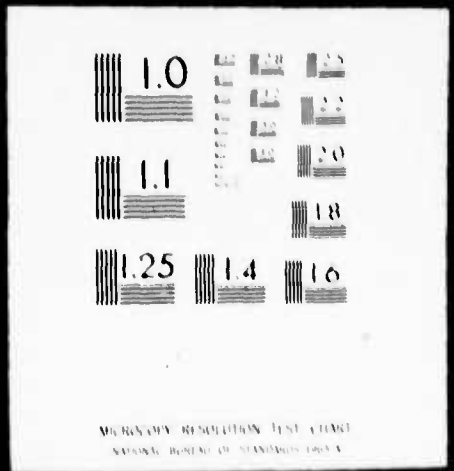

AFFDL-TR-78-12

THE SMALL-SIGNAL RESPONSE OF FLUID TRANSMISSION LINES, INCLUDING DEVELOPED MEAN FLOW EFFECTS

Control Systems Development Branch
Flight Control Division

March 1978
TECHNICAL REPORT AFFDL-TR-78-12
Final Report for Period 3 January 1973 through 16 December 1977

AIR FORCE FLIGHT DYNAMICS LABORATORY
AIR FORCE WRIGHT AERONAUTICAL LABORATORIES
AIR FORCE SYSTEMS COMMAND
WRIGHT-PATTERSON AIR FORCE BASE, OHIO 45433

UNCLASSIFIED

SECURITY CLASSIFICATION OF THIS PAGE (When Date Entered)

REPORT DOCUMENTATION PAGE

READ INSTRUCTIONS BEFORE COMPLETING FORM

1. REPORT NUMBER: AFFDL-TR-78-12	2. GOVT ACCESSION NO.
3. RECIPIENT'S CATALOG NUMBER	
4. TITLE (and Subtitle): THE SMALL SIGNAL RESPONSE OF FLUID TRANSMISSION LINES, INCLUDING DEVELOPED MEAN FLOW EFFECTS.	5. TYPE OF REPORT & PERIOD COVERED: Final Technical Report. 3 Jan 1973 - 16 Dec 1977.
	6. PERFORMING ORG. REPORT NUMBER
7. AUTHOR(s): Ernest F. Moore, Lt Colonel, USAF	8. CONTRACT OR GRANT NUMBER(s)
9. PERFORMING ORGANIZATION NAME AND ADDRESS: Air Force Institute of Technology, Wright-Patterson Air Force Base, Ohio 45433	10. PROGRAM ELEMENT, PROJECT, TASK AREA & WORK UNIT NUMBERS: Program Element 62201F, Project 2403, Task 240302, Work Unit 24030201
11. CONTROLLING OFFICE NAME AND ADDRESS: Air Force Flight Dynamics Laboratory (FGL), AF Wright Aeronautical Laboratories, AFSC, Wright-Patterson Air Force Base, Ohio 45433	12. REPORT DATE: March 1978
	13. NUMBER OF PAGES: 188
14. MONITORING AGENCY NAME & ADDRESS (if different from Controlling Office)	15. SECURITY CLASS (of this report): Unclassified
	15a. DECLASSIFICATION/DOWNGRADING SCHEDULE

16. DISTRIBUTION STATEMENT (of this Report)

Approved for public release; distribution unlimited.

17. DISTRIBUTION STATEMENT (of the abstract entered in Block 20, if different from Report)

18. SUPPLEMENTARY NOTES

19. KEY WORDS (Continue on reverse side if necessary and identify by block number)

Small Signal	Transient Response
Frequency Response	Hydraulic Lines
Fluid Transmission Lines	Pneumatic Lines
Through Flow Effects	Hydraulic Transients

20. ABSTRACT (Continue on reverse side if necessary and identify by block number)

Mathematical models of fluid transmission lines of arbitrary cross section were developed to describe the propagation of small signals through developed mean flow. The mean flow may be either laminar or turbulent and the fluid, either compressible or incompressible. Expressions for both the frequency and time domain dynamic responses are derived. A characteristic radius is defined for any line of arbitrary cross section, which essentially defines

(over)

DD FORM 1 JAN 73 1473 EDITION OF 1 NOV 65 IS OBSOLETE

UNCLASSIFIED

SECURITY CLASSIFICATION OF THIS PAGE (When Date Entered)

Item 20 (cont'd):

an equivalent circular line having the same dynamic response. The characteristic radius used in dynamic analysis is roughly analogous to the hydraulic radius used in steady flow analysis.

In developing the models, the frequency response of annular transmission lines was solved and compared to existing solutions for circular and rectangular lines. Next, the frequency and time domain solutions applicable to arbitrary lines carrying laminar mean flow were obtained in terms of equivalent circular lines. Finally, the concept of a characteristic radius was extended to arbitrary fluid lines carrying turbulent mean flow. The results are shown to be relatively very easy to apply, yet comparable in accuracy to existing, very complex models. The new models should be of significant value to the practicing engineer in fluid systems design and analysis.

FOREWORD

This technical report is being issued under the Control Systems Development Branch, Flight Control Division, Air Force Flight Dynamics Laboratory, Air Force Wright Aeronautical Laboratories, Wright-Patterson Air Force Base, Ohio, under Project 2403, "Flight Control," Task 240302, "Flight Control Systems Development." This report was a dissertation prepared by Ernest F. Moore, M. S., Lt Colonel, USAF, and presented to the Faculty of the School of Engineering of the Air Force Institute of Technology in partial fulfillment of the requirements for the degree of Doctor of Philosophy.

This dissertation is part of a sequence of studies being conducted at the Air Force Institute of Technology to build a sound technology base concerning the propagation of signals in fluid transmission lines. The central objective of this dissertation was to develop the frequency and transient response of transmission lines of arbitrary cross section carrying fully developed laminar or turbulent mean flow of a compressible or incompressible fluid.

A legacy of many computer programs and large quantities of data, much too voluminous for inclusion in this work, has been organized and bound for the convenience and use of the next AFIT student who desires to continue this endeavor. It is safe to say that the solution of one problem surfaces at least two more, so that the quest is not ended with this work.

There are many people to thank. Captains G. R. Farney and J. D. Vining, who provided much of the additional experimental data needed to verify the models, and who worked closely with me in developing some of

the computer programs, deserve special thanks. I wish to thank the members of the AFIT Research Advisory Committee, composed of Dr. M. E. Franke, Dr. A. J. Shine, Dr. C. H. Houpis, Major J. T. Karam, Jr., and 1Lt. R. Merz for their guidance. Special thanks are extended to the chairman, Dr. Franke, for his patience and encouragement, and for the sound advice given throughout this work.

TABLE OF CONTENTS

SECTION		PAGE
I.	Introduction	1
	Background	1
	Problem Description	2
	Organization and Contents	3
II.	The Small-Signal Response of Annular Fluid Transmission Lines	6
	Introduction	6
	Frequency Response	8
	Small-Signal Equations and Solution	8
	Series Impedance of the Annular Line	10
	Shunt Admittance of the Annular Line	11
	Equivalent Electric Circuit	13
	Characteristic Impedance and Propagation Operator	13
	Characteristic Frequencies	17
	Numerical Results and Discussion	18
	Comparison with Circular and Rectangular Lines	29
	High and Low Frequency Approximations	34
	Experimental Confirmation of Annular Theory	36
III.	Correlation of the Linear Response of Circular and Noncircular Fluid Transmission Lines	42
	Frequency Response Solutions	43
	Generalized Response of Noncircular Lines	44
	Numerical Results and Discussion	49
	Determination of the Characteristic Frequency	51
	Use of the Hydraulic Diameter	54
	Determination of the Characteristic Radius	56
	Comparison of Characteristic and Hydraulic Radii	57
	Impedance Matching	63

Contents (cont'd)

		Page
IV.	The Transient Response of Noncircular Fluid Transmission Lines	71
	Frequency Domain Equations	72
	Pressure (Flow) Response of Noncircular Lines to a Step Input of Pressure (Flow)	79
	Pressure (Flow) Response of Noncircular Lines to a Step Input of Flow (Pressure)	83
	Physical Implications of the Fluid Line Step Responses and Dimensionless Parameters	92
	Summary of Transient Responses	93
V.	Laminar Oscillatory Flow Combined with Steady Developed Mean Flow	94
	Background	94
	Physical Considerations of Combined Oscillatory and Steady Developed Mean Flow	96
	Steady and Oscillatory Boundary Layers	97
	A Mean Flow Characteristic Frequency for Circular Lines	99
	Characteristic Frequency and Radius - Turbulent Mean Flow	103
	Low Frequency Domain - Turbulent Mean Flow	105
	Mid-Frequency Domain - Turbulent Mean Flow	111
	High Frequency Domain - Turbulent Mean Flow	115
	Comparison of High Frequency Results with Previous Work	121
VI.	The Transient Response of Fluid Lines Carrying Developed Turbulent Mean Flow	128
	Frequency and Time Domain Equations	128
	Line Attenuation Factor	129
	Pressure (Flow) Response to a Step Input of Pressure (Flow), Turbulent Mean Flow	130
	Pressure (Flow) Response to a Step Input of Flow (Pressure), Turbulent Mean Flow	134
	Physical Implications of the Fluid Line Step Response with Turbulent Mean Flow	136
VII.	Conclusions and Recommendations	140
	Conclusions	140
	Recommendations	142

Contents (cont'd)

		Page
Bibliography		144
Appendix A:	DC Resistance and DC Inductance of Fluid Transmission Lines Carrying Developed Laminar Flow	147
Appendix B:	High Frequency Approximations for Annular Lines	153
Appendix C:	Derivation of Small Signal Equations in Cylindrical Coordinates	157
Vita		169

LIST OF ILLUSTRATIONS

Figure		Page
1	Annular Transmission Line	7
2	Equivalent Circuit of Transmission Line	14
3	Magnitude of Characteristic Admittance Ratio	21
4	Phase Angle of Characteristic Admittance	22
5	Phase Velocity and Wavelength Ratios	23
6	Attenuation Per Line Wavelength for Annular Lines	24
7	Ratio of Frequency Dependent to Viscous (DC) Resistance	25
8	Ratio of Frequency Dependent to Adiabatic Inductance	26
9	Ratio of Frequency Dependent Conductance to Adiabatic Capacitance	27
10	Ratio of Frequency Dependent to Adiabatic Capacitance	28
11	Comparison of Attenuation of Annular and Rectangular Lines	31
12	Ratios of Viscous (DC) Resistances	33
13	Correlation of Experimental Results with Annular Line Theory	38
14	Correlation of Experimental Results with Annular Line Theory	39
15	Correlation of Experimental Results with Annular Line Theory	40
16	Attenuation Per Line Wavelength for Rectangular Lines	45
17	Attenuation Per Line Wavelength for Annular Lines	46
18	Attenuation Per Line Wavelength for Circular, Rectangular, and Annular Lines	48
19	Wavelength Ratio for Circular, Rectangular, and Annular Lines	50

LIST OF ILLUSTRATIONS (cont'd)

Figure		Page
20	Comparison of Attenuation Per Line Wavelength of Rectangular Lines	58
21	Comparison of Attenuation Per Line Wavelength of Annular Lines	60
22	Radius Ratios of Rectangular Lines	61
23	Radius Ratios of Annular Lines	62
24	Characteristic Admittance Ratio for Circular, Rectangular and Annular Lines	64
25	Phase Angle of Characteristic Admittance for Circular, Rectangular and Annular Lines	65
26	Ratio of Characteristic Frequencies of Rectangular to Circular Lines	69
27	Ratio of Characteristic Frequencies of Annular to Circular Lines	70
28	Logarithmic Approximation of Attenuation Ratio for Circular Lines	78
29	Comparison of Pressure (Flow) Response to a Unit Step Input of Pressure (Flow) for Liquid-Filled Circular Lines	80
30	Pressure (Flow) Response to a Step Input of Pressure (Flow) for Air-Filled Lines of Arbitrary Cross Section	82
31	Normalized Approximations of the Integrals of Characteristic Impedance and Admittance	87
32	Comparison of Pressure Response to a Step Input of Flow for Liquid-Filled Circular Lines	88
33	Comparison of Flow Response to a Step Input of Pressure for Liquid-Filled Circular Lines	89
34	Pressure Response to a Step Input of Flow for Air-Filled Lines of Arbitrary Cross Section	90
35	Flow Response to a Step Input of Pressure for Air-Filled Lines of Arbitrary Cross Section	91

LIST OF ILLUSTRATIONS (cont'd)

Figure		Page
36	Variation of Low Frequency Attenuation with Reynolds Number in Circular Lines	108
37	Attenuation and Phase Velocity in Circular or Noncircular Lines, Laminar or Turbulent Mean Flow, Constant LRC Model	112
38	Normalized Attenuation Data in Water Medium	114
39	Phase Velocity Ratio Data in Water Medium	114
40	Variation of Unadjusted Frequency Dependent Attenuation with Reynolds Number in Circular and Noncircular Lines	117
41	Frequency Dependent Attenuation in Circular and Noncircular Lines, Laminar or Turbulent Mean Flow . .	120
42	Attenuation in Circular and Noncircular Lines, Laminar or Turbulent Mean Flow, High Frequency Model	124
43	Comparison of Experimental and Predicted Results for Attenuation Factor in Circular Lines, Turbulent Mean Flow	127
44	Pressure (Flow) Response to a Step Input of Pressure (Flow) for Air-Filled Lines of Arbitrary Cross Section, Carrying Turbulent Mean Flow	133
45	Pressure Response to a Step Input of Flow for Air-Filled Lines of Arbitrary Cross Section, Carrying Turbulent Mean Flow	137
46	Flow Response to a Step Input of Pressure for Air-Filled Lines of Arbitrary Cross Section, Carrying Turbulent Mean Flow	138

List of Tables

Table		Page
I	Properties of Air at 80°F	18
II	Ambient Test Conditions	41
III	Fully Developed Laminar Flow Parameters for Rectangular and Annular Lines	52
IV	Geometric Cross Section Factor	54
V	Frequency Ratio Parameters for Rectangular Lines for $D_{hr} = D_c$	55
VI	Turbulent Steady Flow Inertance Factor (K_{L_t}) for Circular Lines	103
VII	Equivalent Circular Line Steady Flow Parameters for Figures 44, 45, and 46	132
B-I	First Order High Argument Approximations of J_0, J_1, K_0, K_1	155

List of Symbols

Symbol	Description	Units
a,AR	aspect ratio, b/h	dimensionless
A	cross-sectional area	in^2
AC	frequency dependent flow condition	--
b	width of rectangular cross section	in
B	arbitrary coefficient, Eq. (13)	dimensionless
c	phase velocity	in/sec
c_a	adiabatic speed of sound	in/sec
c_p	specific heat at constant pressure	Btu/lbm-°R
c_v	specific heat at constant volume	Btu/lbm-°R
C	capacitance/unit length	cis-sec/psi-in
C_a	adiabatic capacitance/unit length	cis-sec/psi-in
C_i	isothermal capacitance/unit length	cis-sec/psi-in
C_1,C_2	arbitrary constants, Eq. (31)	psi
db	line gain	decibels
D	arbitrary coefficient, Eq. (14)	dimensionless
D	diameter	in
DC	steady flow condition	--
D_h	hydraulic diameter, $4A/P_W$	in
e	base of natural logarithms	2.718 •••
erfc	complementary error function	dimensionless
E	arbitrary coefficient, Eq. (12)	dimensionless
f	frequency	Hertz
f	friction factor, Eq. (129)	dimensionless
f( )	general function notation	--
F	arbitrary coefficient, Eq. (12)	dimensionless

Symbol	Description	Units
g	transfer pressure gain modulus	dimensionless
gc	gravitational acceleration, 386.088	in/sec^2
$g(\phi)$	complex function, Eq. (167)	dimensionless
G	conductance/unit length	cis/psi-in
h	height of rectangular cross section	in
$h(\phi)$	complex function, Eq. (170)	dimensionless
Imag	imaginary part of complex number	--
J_0, J_1	Bessel functions, standard notation	--
j	$\sqrt{-1}$	dimensionless
k	constant, Eq. (195)	dimensionless
K	proportionality constant, Eqs. (103), (109), (195)	dimensionless
K_B	fluid bulk modulus	psi
K_C	geometric shape factor, Eq. (79)	dimensionless
K_H	high frequency proportionality constant, Eq. (194)	neper/in
K_L	inertance constant, L_V/L_a	dimensionless
K_L	low frequency proportionality constant, Eq. (194)	neper/in
K_R	resistance proportionality constant, Eq. (73)	dimensionless
K_0, K_1	Bessel functions, standard notation	--
ℓ	length	in
L	inductance or inertance/unit length	psi-sec/cis-in
L_a	adiabatic inductance/unit length	psi-sec/cis-in
L_V	DC inductance/unit length	psi-sec/cis-in
L^{-1}	inverse Laplace transform	--
m	exponent, Eqs. (103), (109), (195)	dimensionless

Symbol	Description	Units
M	impedance parameter, Eq. (18)	in
n	polytropic exponent	dimensionless
n	exponent, Eq. (135)	dimensionless
N	admittance parameter, Eq. (27)	in
P	pressure	psi
P_r	received dynamic pressure	psi-rms
P_s	sent dynamic pressure	psi-rms
P_w	line wetted perimeter	in
Q	volume flow rate	cis
r	radial dimension	in
r_A	area equivalent radius, $\sqrt{A/\pi}$	in
r_c	characteristic radius, $\sqrt{6\nu/\omega_{cx}}$	in
r_h	hydraulic radius, $D_h/2$	in
r_i	annular line, inside radius	in
r_o,R	circular line radius	in
r_o	annular line, outside radius	in
r^*	annular radius ratio, r_i/r_o	dimensionless
r_{ν_ℓ}	viscous laminar characteristic radius, $\sqrt{8\nu/\omega_{\nu_\ell}}$	in
r_{ν_t}	viscous turbulent characteristic radius, $\sqrt{8\nu/\omega_{\nu_t}}$	in
R	resistance/unit length	psi/cis-in
Re	Reynolds number	dimensionless
Real	real part of complex number	--
R_v	DC resistance/unit length	psi/cis-in
s	Laplace domain variable	1/sec
SN	characteristic frequency ratio, $4\omega R^2/\nu$	dimensionless

Symbol	Description	Units
t	time	sec
t_c	characteristic time	sec
T	adiabatic delay time, ℓ/c_a	sec
T	temperature	°F or °R
u	line axial velocity	in/sec
$u(t)$	unit step input	dimensionless
$U(t)$	step input including magnitude	variable
Y	shunt admittance/unit length	cis/psi-in
Y_0	characteristic admittance, $\sqrt{Y/Z}$	cis/psi
Y_{so}	lossless characteristic admittance, $\sqrt{C_a/L_a}$	cis/psi
z	line axial coordinate	in
Z	series impedance/unit length	psi/cis-in
Z_o	characteristic impedance, $\sqrt{Z/Y}$	psi/cis
Z_{so}	lossless characteristic impedance, $\sqrt{L_a/C_a}$	psi/cis
α	attenuation/unit length	neper/in
α_{Br}	attenuation factor, Eq. (153)	dimensionless
$\bar{\alpha}_{Ht}$	high frequency attenuation factor, Eq. (178)	dimensionless
$\bar{\alpha}_{Lt}$	low frequency attenuation factor, Eq. (166)	dimensionless
β	phase shift/unit length	radian/in
β_p	coefficient of thermal expension, $-1/\rho\ (\partial\rho/\partial T)_p$	1/°R
γ	ratio of specific heats, c_p/c_v	dimensionless
Γ	propagation operator, $\alpha + j\beta$	1/in
δ_T	thermal nonadiabatic skin depth, $\sqrt{2\nu_T/\omega}$	in

Symbol	Description	Units
δ_v	steady flow viscous boundary layer thickness	in
δ_ω	frequency dependent boundary layer thickness, $\sqrt{2\nu/\omega}$	in
Δ	incremental change	variable
Δ	fictitious laminar boundary layer thickness, Eq. (179)	in
ε	isothermal compressibility, $1/\rho\ (\partial\rho/\partial p)_T$	1/psi
λ	wavelength	in
λ	integration variable, Eqs. (113), (114)	--
μ	dynamic viscosity	psi-sec
ν	kinematic viscosity, μ/ρ	in^2/sec
ν_T	thermal diffusivity, ν/σ^2	in^2/sec
π	3.14159···	--
ρ	fluid density	$psi\text{-}sec^2/in^2$
σ^2	Prandtl number	dimensionless
τ	normalized time, $\omega_c t$, $\omega_\nu t$, etc.	dimensionless
τ'	normalized time, $t\nu/R^2$	dimensionless
τ_0	normalized delay time, $\omega_c T$, $\omega_\nu T$, etc.	dimensionless
τ_0'	normalized time, $T\nu/R^2$	dimensionless
ϕ	Bessel function argument, Eq. (169)	dimensionless
Φ	dissipation function, Eq. (180)	dimensionless
ω	angular frequency	rad/sec
ω_c	DC characteristic frequency, R_v/L_v	rad/sec
ω_ν	viscous characteristic frequency, R_v/L_a	rad/sec
ω_T	thermal characteristic frequency, ω_ν/σ^2	rad/sec
$\omega_{\nu\ell}$	laminar viscous characteristic frequency, R_{v_ℓ}/L_a	rad/sec

Symbol	Description	Units
ω_{ν_t}	turbulent viscous characteristic frequency, R_{ν_t}/L_a	rad/sec
Ω	normalized frequency ratio, $\omega R^2/\nu$	dimensionless

Subscripts

a	adiabatic condition
c	circular line
H	high frequency or short time
H_B	high break frequency ratio
i	inside radius of annular line
i	isothermal condition
ℓ	laminar flow condition
L	low frequency or long time
L_B	low break frequency ratio
M	middle frequency or time
n	annular line
o	circular or outside radius
o,c	characteristic line parameter
r	receiving station in line
s	sending station in line
s	lossless condition
t	turbulent flow condition
T	thermal or temperature
x	arbitrary line

Superscripts

$(\bar{})$	average or normalized
$(\,)'$	instantaneous deviation from average or alternate form
$(\,)^*$	reference conditions
$(\,)^\circ$	degrees temperature

THE SMALL-SIGNAL RESPONSE OF FLUID TRANSMISSION LINES INCLUDING DEVELOPED MEAN FLOW EFFECTS

I. Introduction

Background

The propagation of small signals through ducts or lines filled with a fluid has been of interest to scientists and engineers for some time. With the advent of fluidics and fluerics in the late 1950's and up to the present time, many investigations have been completed, both analytically and experimentally, in order to predict and measure the parameters governing small signal propagation.

The modeling of fluid-filled transmission lines has progressed from the basic lossless line model, to the line whose losses might be called linear with mean velocity, to the present frequency-dependent friction models. Solutions have been obtained in the frequency domain for lines of circular and rectangular cross section, as these cross sections are commonly found in fluid systems. For the fluid-filled circular line, the transient response to small amplitude impulse and step inputs has been obtained in various forms.

Recently, investigations have been carried out and models developed to determine and to describe the response of liquid-filled circular lines to oscillatory inputs, where the inputs are superimposed on a steady developed flow, and where the steady developed flow may be

either laminar or fully turbulent. A limited amount of experimental data has provided some degree of credence to these models.

Problem Description

During the literature search preceding this work, it appeared that a majority of the investigations were very specialized and that an effort to synthesize the results obtained by others was in order. Much of the previous work relating to transient response in the time domain, and to combined oscillatory and steady developed flow, was restricted to liquid-filled circular lines.

A solution for the small-signal response of fluid lines of concentric annular cross section appeared to be a useful first step in synthesizing and expanding the applicability of transmission line modeling. Since the annular line includes the circular line as a special case (when the inside radius is equal to zero) and approaches the parallel plate configuration in its other extreme, a solution was first obtained for this line.

In studying the solutions available for circular and rectangular lines as well as the solution for annular lines given herein, it appeared that a method of expressing the frequency dependent response of lines of arbitrary cross section in terms of only the circular line might be developed. Through the use of the various analogies between electrical transmission line theory and fluid dynamics, and in particular by constructing and analyzing the equivalent electrical circuit of a generalized fluid transmission line, such a method was found.

It followed that if the frequency dependence of a line of arbitrary cross section could be expressed in terms of an equivalent

circular line, then: (1) The small signal transient (time domain) response of lines of arbitrary noncircular cross section might be found, since this response is known for circular lines; (2) The characteristic impedance of lines of noncircular cross section may be expressed in terms of equivalent circular lines; consequently, impedance matching of lines of different cross section may be possible; (3) The computer modeling of all lines of any cross section in a fluid system might be reduced to modeling the equivalent circular lines; (4) A method of determining the small signal response of fluid lines of arbitrary cross section, carrying fully developed mean flow might be found.

All of these possibilities were investigated and the associated problems were solved, subject to the restrictions specified herein. It is noted that where possible the simplest model achievable is used, in accord with Oldenberger's observation that only those models which are reasonably uncomplicated find wide use. This observation is particularly appropriate to fluid systems, which generally contain a myriad of components and lines, some of which are usually noncircular in cross section.

Organization and Contents

Since this work covers a rather broad range of transmission line problems, specific background information and references will be introduced as appropriate. Further, where specific examples are deemed necessary, these will be given in terms of the more common rectangular and annular cross sections for which a relatively larger body of technical reference material exists. Lengthy mathematical details which are of minor import in understanding the various developments, as well

as certain examples and error analyses, have been relegated to the appendices.

In Section II, the exact theory describing the small-signal response of fluid transmission lines of annular cross section is presented. The results are compared with those obtained by others for circular and rectangular lines. Thus, Section II serves also as an introduction to the synthesis of results applicable to circular and noncircular lines. High and low frequency approximations are developed for the annular line, and experimental results are presented which confirm the theory.

In Section III, a characteristic frequency and corresponding characteristic radius are determined, which allow the frequency response of noncircular lines to be presented in terms of equivalent circular lines. The results are compared with those previously obtained for rectangular and annular lines by using the classical hydraulic radius together with circular line theory. The results predicted using the characteristic radius and circular line theory are shown to be clearly superior to the results predicted using the classical hydraulic radius and circular line theory. However, the hydraulic radius may be adjusted to allow its use in the circular line theory. A concept of impedance matching is also developed in Section III.

Many practical problems are more concerned with the time domain response of transmission lines. In Section IV, the results of others, which describe the impulse and unit step response of circular lines only, are adapted to lines of noncircular cross section and also compared with existing experimental data.

Section V is devoted to the simplification and synthesis of results describing the combination of steady developed turbulent mean flow, and laminar oscillatory flow produced by a small sinusoidal pressure input signal. The solutions are extended to include lines of noncircular cross section.

In Section VI, the frequency domain results of Section V are transposed into the time domain, and the various combinations of downstream pressure and flow response to upstream step inputs of pressure or flow are presented.

In Section VII, the last section of this work, a summary of the conclusions and recommendations is presented.

II. The Small-Signal Response of Annular Fluid Transmission Lines

Introduction

The small-signal frequency response of fluid transmission line of circular cross section has been obtained in various forms [1-3][1]. Nichols [3] expressed the results in a manner similar to that used for electrical transmission lines. Schaedel [4] followed closely the approach used by Nichols and obtained the response for lines of rectangular cross section. In both of these studies, a distributed parameter line model was developed and results were obtained for the impedance, admittance, propagation operator and characteristic impedance of the line.

There are a number of applications, such as aircraft pitot-static systems, hydraulic mining, and instrumentation, where annular lines are used and the small signal frequency response characteristics are of interest. The purpose of this section is to present the small-signal response of rigid pneumatic transmission lines of annular cross section, Figure 1. The analytical approach taken is similar to that used by Nichols [3] and Schaedel [4]. The detailed analytical development is presented in Appendix C. Finally, the annular line results will be compared with those obtained for circular and rectangular lines.

---

[1]Numbers in brackets designate Bibliography at end of dissertation.

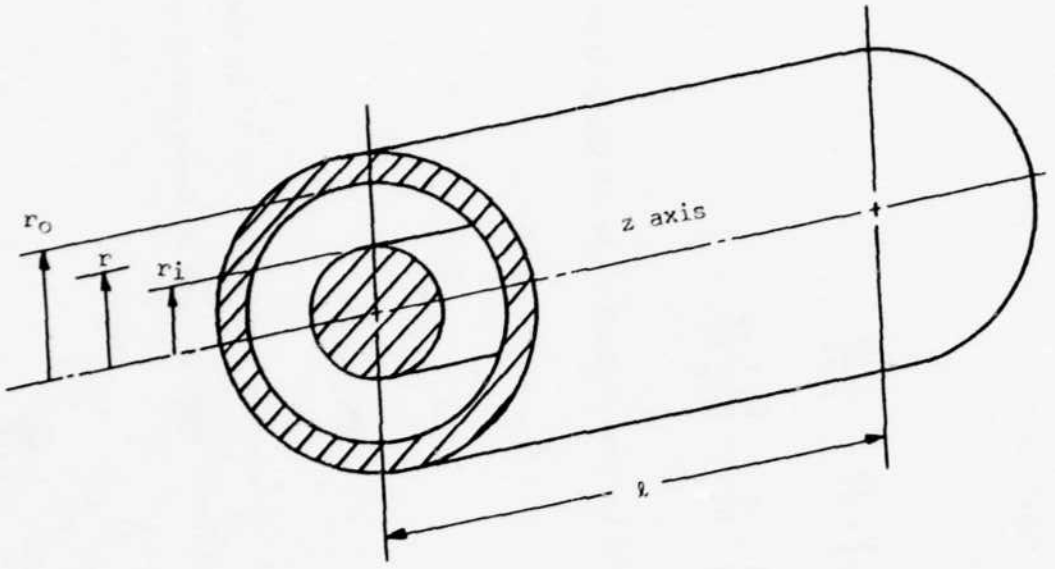

Figure 1. Annular Transmission Line

Frequency Response

Small Signal Equations and Solution. The equations expressing conservation of mass, momentum, and energy for laminar small signal oscillatory flow in a pneumatic line of annular cross section are those used by Nichols [3] to obtain a frequency response solution for lines of circular cross section: The development of these equations is given in Appendix C.

$$-\frac{\partial \rho}{\partial t} = \frac{\partial (\rho u)}{\partial z} \tag{1}$$

$$-\frac{\nu}{r}\frac{\partial}{\partial r}\left[r\frac{\partial u}{\partial r}\right] + \frac{\partial u}{\partial t} = -\frac{1}{\rho}\frac{\partial P}{\partial z} \tag{2}$$

$$\frac{\nu_T}{r}\frac{\partial}{\partial r}\left[r\frac{\partial T}{\partial r}\right] - \frac{\partial T}{\partial t} = -\frac{\beta_p\, T}{\rho\, c_p}\frac{\partial P}{\partial t} \tag{3}$$

The dependent variables are assumed to be of the following form

$$T(r,z,t) = \overline{T} + T' = \overline{T} + \Delta T(r,z)\, e^{j\omega t} \tag{4}$$

$$u(r,z,t) = \bar{u} + u' = \bar{u} + u(r,z)\, e^{j\omega t} \tag{5}$$

$$P(z,t) = \overline{P} + P' = \overline{P} + \Delta P(z)\, e^{j\omega t} \tag{6}$$

where, for example, $\overline{T}$ is the average temperature and T' is the instantaneous temperature fluctuation. Substitution of these variables into equations (2) and (3) gives

$$\frac{\partial^2 u}{\partial r^2} + \frac{1}{r}\frac{\partial u}{\partial r} - \frac{j\omega u}{\nu} = \frac{1}{\nu\rho}\frac{\partial \Delta P}{\partial z} \tag{7}$$

$$\frac{\partial^2 \Delta T}{\partial r^2} + \frac{1}{r}\frac{\partial \Delta T}{\partial r} - \frac{j\omega \Delta T}{\nu_T} = -\frac{j\omega \Delta P}{\rho c_p \nu_T} \tag{8}$$

Assuming isothermal walls and zero velocity at the walls, the boundary conditions for the annular line are

$$\Delta T = 0,\ u = 0 \quad \text{at} \quad r = r_i \tag{9}$$

$$\Delta T = 0,\ u = 0 \quad \text{at} \quad r = r_o \tag{10}$$

The momentum and energy equations are thus identical in form, and the solutions for the dimensionless velocity and temperature profiles are Bessel functions of zero order.

$$\frac{j\omega u}{-\frac{1}{\rho}\frac{\partial \Delta p}{\partial z}} = 1 + BJ_0\left(\sqrt{\frac{\omega}{\nu}}\, r j^{\frac{3}{2}}\right) + DK_0\left(\sqrt{\frac{\omega}{\nu}}\, r j^{\frac{1}{2}}\right) \tag{11}$$

$$\frac{\rho c_p \Delta T}{\Delta P} = 1 + EJ_0\left(\sqrt{\frac{\omega}{\nu_T}}\, r j^{\frac{3}{2}}\right) + FK_0\left(\sqrt{\frac{\omega}{\nu_T}}\, r j^{\frac{1}{2}}\right) \tag{12}$$

The arbitrary coefficients (B,D,E, and F) obtained from the boundary conditions are

$$B = \frac{K_0\left(\sqrt{\frac{\omega}{\nu}}\, r_o j^{\frac{1}{2}}\right) - K_0\left(\sqrt{\frac{\omega}{\nu}}\, r_i j^{\frac{1}{2}}\right)}{J_0\left(\sqrt{\frac{\omega}{\nu}}\, r_o j^{\frac{3}{2}}\right) K_0\left(\sqrt{\frac{\omega}{\nu}}\, r_i j^{\frac{1}{2}}\right) - J_0\left(\sqrt{\frac{\omega}{\nu}}\, r_i j^{\frac{3}{2}}\right) K_0\left(\sqrt{\frac{\omega}{\nu}}\, r_o j^{\frac{1}{2}}\right)} \tag{13}$$

$$D = \frac{J_0\left(\sqrt{\frac{\omega}{\nu}}\, r_i j^{\frac{3}{2}}\right) - J_0\left(\sqrt{\frac{\omega}{\nu}}\, r_o j^{\frac{3}{2}}\right)}{J_0\left(\sqrt{\frac{\omega}{\nu}}\, r_o j^{\frac{3}{2}}\right) K_0\left(\sqrt{\frac{\omega}{\nu}}\, r_i j^{\frac{1}{2}}\right) - J_0\left(\sqrt{\frac{\omega}{\nu}}\, r_i j^{\frac{3}{2}}\right) K_0\left(\sqrt{\frac{\omega}{\nu}}\, r_o j^{\frac{1}{2}}\right)} \tag{14}$$

The coefficients E and F of equation (12) are identical to B and D, respectively, except ν is replaced by ν_T in the arguments of the Bessel functions.

Series Impedance of the Annular Line. The mass rate of flow at the reference pressure P* is given by

$$\rho^* Q^* = \int_{r_i}^{r_o} (\rho u)\, 2\pi r dr \tag{15}$$

and by analogy to electrical transmission line theory

$$-\frac{\partial \Delta P}{\partial z} = Z Q^* \tag{16}$$

where Z is the frequency dependent series impedance per unit length, ΔP is analogous to voltage and Q^* is analogous to current. Solving for (ρu) from equation (11), performing the integration of equation (15), and using equation (16), an expression for Z is obtained:

$$Z = \frac{j\omega\rho^*}{A_n}\left[1 + \frac{2\pi M}{A_n \sqrt{\frac{\omega}{\nu}}\, j^{\frac{3}{2}}}\right]^{-1} \tag{17}$$

where

$$M = B\left[r_o J_1\left(\sqrt{\frac{\omega}{\nu}}\, r_o j^{\frac{3}{2}}\right) - r_i J_1\left(\sqrt{\frac{\omega}{\nu}}\, r_i j^{\frac{3}{2}}\right)\right] +$$

$$- jD\left[r_o K_1\left(\sqrt{\frac{\omega}{\nu}}\, r_o j^{\frac{1}{2}}\right) - r_i K_1\left(\sqrt{\frac{\omega}{\nu}}\, r_i j^{\frac{1}{2}}\right)\right] \qquad (18)$$

Introducing the adiabatic inductance per unit length, $L_a = \rho^*/A_n$, equation (17) becomes,

$$Z = j\omega L_a\left[1 + \frac{2\pi M}{A_n\sqrt{\frac{\omega}{\nu}}\, j^{\frac{3}{2}}}\right]^{-1} \qquad (19)$$

where Z is shown to be frequency dependent.

Shunt Admittance of the Annular Line. From electrical transmission line theory,

$$-\frac{\partial Q^*}{\partial z} = Y\Delta P \qquad (20)$$

where Y is the shunt admittance per unit length. Upon differentiating equation (15) with respect to z, using equation (1), and substituting into equation (20), Y becomes

$$Y = \frac{2\pi}{\rho^*\Delta P}\int_{r_i}^{r_o}\frac{\partial \rho}{\partial t}\, r\, dr \qquad (21)$$

It is shown in Appendix C that

$$\frac{\partial \rho}{\partial t} = \frac{\rho \varepsilon}{\gamma} \frac{\partial P}{\partial t} + \beta_p \rho \left[\frac{\beta_p T}{\rho c_p} \frac{\partial P}{\partial t} - \frac{\partial T}{\partial t} \right] \tag{22}$$

Introducing the complex time notation for $\partial P/\partial t$ and $\partial T/\partial t$ and using the relation

$$c_p - c_v = \frac{\beta_p^2 T}{\rho \varepsilon} \tag{23}$$

equation (22) becomes

$$\frac{\partial \rho}{\partial t} = \frac{\rho \varepsilon}{\gamma} j\omega \Delta P \left[1 + (\gamma - 1) - \frac{(\gamma - 1)\, \rho\, c_p\, \Delta T}{\Delta P} \right] \tag{24}$$

where $\beta_p = 1/T$ for a perfect gas. Substituting for $\rho\, c_p\, \Delta T/\Delta P$ from equation (12), equation (24) becomes

$$\frac{\partial \rho}{\partial t} = \frac{\rho \varepsilon}{\gamma} j\omega \Delta P \left\{ 1 - (\gamma - 1) \left[E J_0\left(\sqrt{\frac{\omega}{\nu_T}}\, r j^{\frac{3}{2}} \right) + F K_0\left(\sqrt{\frac{\omega}{\nu_T}}\, r j^{\frac{1}{2}} \right) \right] \right\} \tag{25}$$

Substituting equation (25) into equation (21) and performing the indicated integration yields

$$Y = j\omega C_a \left[1 + \frac{2\pi(1-\gamma)\, N}{A_n \sqrt{\frac{\omega}{\nu_T}}\, j^{\frac{3}{2}}} \right] \tag{26}$$

where

$$N = E\left[r_o J_1\left(\sqrt{\frac{\omega}{\nu_T}} r_o j^{\frac{3}{2}}\right) - r_i J_1\left(\sqrt{\frac{\omega}{\nu_T}} r_i j^{\frac{3}{2}}\right)\right] +$$

$$- jF\left[r_o K_1\left(\sqrt{\frac{\omega}{\nu_T}} r_o j^{\frac{1}{2}}\right) - r_i K_1\left(\sqrt{\frac{\omega}{\nu_T}} r_i j^{\frac{1}{2}}\right)\right] \qquad (27)$$

and $C_a = \frac{\varepsilon\rho\ A_n}{\gamma P^*}$ = the adiabatic capacitance per unit length. For an ideal gas, $C_a = A_n/\gamma P^*$. Tabulated Bessel functions of interest are given in [5,6].

Equivalent Electrical Circuit. The series impedance and shunt admittance may be expressed as

$$Z = R + j\omega L \qquad (28)$$

$$Y = G + j\omega C \qquad (29)$$

where R,L,G, and C are the circuit parameters of resistance, inductance, conductance, and capacitance, per unit length, respectively. The equivalent circuit for a transmission line of dz length is shown in Figure 2. The circuit parameters are all real numbers and are dependent on the signal frequency, the cross-sectional area, and the radii of the annular line through the expressions for Z and Y, equations (19) and (26).

Characteristic Impedance and Propagation Operator. Equations (16) and (20) are used to obtain the governing differential equations for pressure and flow. Differentiating equation (16) with respect to z and using equation (20) gives

$$\frac{\partial^2(\Delta P)}{\partial z^2} = ZY(\Delta P) \qquad (30)$$

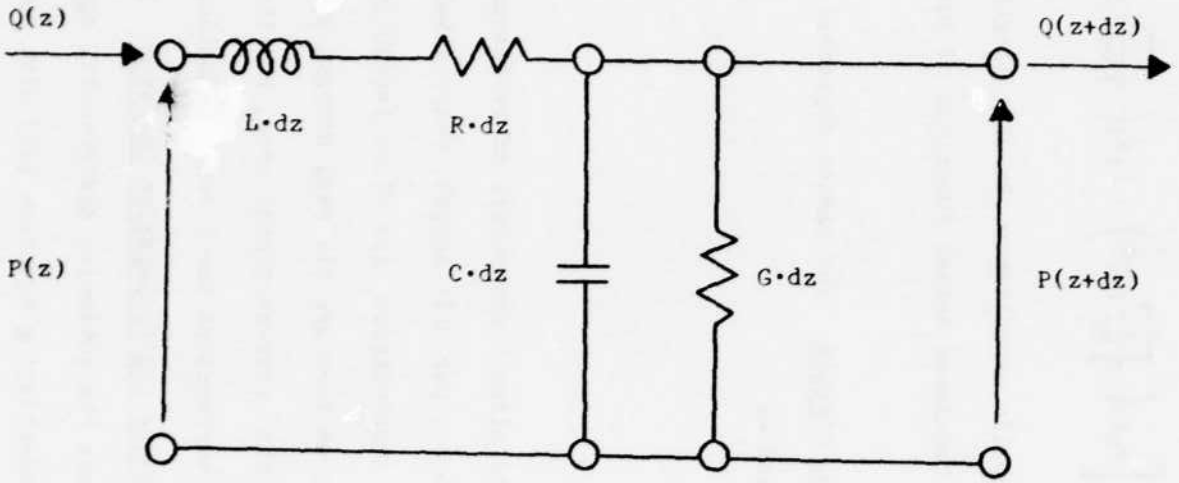

Figure 2. Equivalent Circuit of Transmission Line

The general solution for the pressure is

$$\Delta P = C_1 e^{-\Gamma z} + C_2 e^{+\Gamma z} \tag{31}$$

where Γ, the propagation operator, is defined as

$$\Gamma = \sqrt{ZY} = \alpha + j\beta \tag{32}$$

where α is the attenuation per unit length and β is the phase angle increase per unit length. The solution for the volumetric flow is

$$Q = \frac{1}{Z_0}\left(C_1 e^{-\Gamma z} - C_2 e^{+\Gamma z}\right) \tag{33}$$

where Z_0, the characteristic impedance, is defined as

$$Z_0 = \sqrt{Z/Y} = 1/Y_0 \tag{34}$$

and Y_0 is the characteristic admittance.

The characteristic impedance and propagation operator are generally complex quantities and are convenient for describing the pressure and flow in the transmission line. An excellent review of the significance and use of Z_0 and Γ in various representations of fluid lines for system analysis is given by Goodson and Leonard [7].

The phase velocity is

$$c = \lambda f = \frac{\lambda\omega}{2\pi} = \frac{\omega}{\beta} \tag{35}$$

where λ is the wavelength and β increases 2π radians per wavelength. The phase velocity c is in general not equal to c_a, the adiabatic

speed of sound. For a lossless line the characteristic admittance is

$$Y_{s0} = \sqrt{C_a/L_a} = \frac{A}{\rho^* c_a} = \frac{A}{\sqrt{\gamma \rho^* P^*}} \tag{36}$$

and

$$c_a = \frac{\omega}{\beta_a} = \sqrt{\frac{\gamma P^*}{\rho^*}} = \frac{1}{\sqrt{L_a C_a}} \tag{37}$$

For a lossless line $\alpha = 0$, thus

$$\Gamma_s = j\beta_a = j\omega/c_a \tag{38}$$

Y_0, defined in equation (34), is normalized with respect to the lossless line as follows:

$$Y_0/Y_{s0} = \left\{ \left[1 + \frac{2\pi(1-\gamma)\ N}{A_n \sqrt{\frac{\omega}{\nu_T}}\, j^{\frac{3}{2}}} \right] \left[1 + \frac{2\pi M}{A_n \sqrt{\frac{\omega}{\nu}}\, j^{\frac{3}{2}}} \right] \right\}^{1/2} \tag{39}$$

The normalized propagation operator is

$$\frac{j\Gamma}{\Gamma_s} = \frac{j(\alpha + j\beta)}{j\omega/c_a} \tag{40}$$

or upon rewriting equation (40),

$$\alpha\, c_a/\omega + j\beta\, c_a/\omega = \left[\frac{1 + \frac{2\pi(1-\gamma)\ N}{A_n \sqrt{\frac{\omega}{\nu_T}}\, j^{\frac{3}{2}}}}{1 + \frac{2\pi M}{A_n \sqrt{\frac{\omega}{\nu}}\, j^{\frac{3}{2}}}} \right]^{1/2} (j) \tag{41}$$

The propagation velocity ratio or wavelength ratio is

$$\frac{c}{c_a} = \frac{\lambda}{\lambda_a} = \frac{\beta_a}{\beta} \tag{42}$$

The neper attenuation in $\lambda_a/2\pi$ distance is

$$\alpha\, c_a/\omega = \alpha\, \lambda_a/2\pi \tag{43}$$

To convert the attenuation from nepers to the more common decibel, the following equations are used:

$$(\alpha\lambda_a)\ \text{db} = 40\pi\ (\log_{10}e)\ \alpha\ c_a/\omega$$

$$= 54.575\ \alpha\ c_a/\omega\ \text{db per}\ \lambda_a \tag{44}$$

$$(\alpha\lambda)\ \ \text{db} = 54.575\ \alpha/\beta\ \text{db per}\ \lambda \tag{45}$$

Characteristic Frequencies. Following Nichols [3] it is convenient to define two characteristic frequencies which will aid in the presentation of the results and facilitate comparison of the annular line results with those obtained for circular and rectangular lines:

$$\omega_\nu = \frac{8\pi\nu}{A_n} = \frac{8\nu}{r_o^2 - r_i^2} = \frac{8\nu}{r_o^2(1-r^{*2})} \tag{46}$$

$$\omega_T = \frac{8\pi\nu_T}{A_n} = \frac{\omega_\nu}{\sigma^2} \tag{47}$$

where $r^* = r_i/r_o$ is defined as the annular radius ratio. The viscous characteristic frequency ω_ν is used to form the dimensionless frequency

ratio ω/ω_ν which is used in presenting the numerical results. Because the characteristic frequency ω_ν is defined to be proportional to the ratio ν/A, the frequency dependence of all sizes of annular lines of the same radius ratio are represented by a single curve when the results are plotted against ω/ω_ν. This is analogous to the frequency dependence of all sizes of circular lines and of rectangular lines of the same aspect ratio when plotted against ω/ω_ν.

Numerical Results and Discussion

The numerical results were calculated on a CDC 6600 computer using the standard properties of air at 80°F given in Table I. Plots are given for frequency ratios ω/ω_ν from 0.1 to 1000 and annular radius ratios of 0, 0.1, 0.5, and 0.8.

TABLE I

Properties of Air at 80°F [3]

P^*	14.696 psia
ρ^*	1.1017×10^{-7} lb_f-$sec^2/in.^4$
ν^*	0.02432 $in.^2/sec$
ν_T^*	0.03435 $in.^2/sec$
σ^2	0.7080 dimensionless
γ	1.4017 dimensionless
c_a	13,674 in./sec
g_c	386.088 $in./sec^2$

The influence of the frequency and radius ratio on annular line performance is easily seen in Figures 3 through 6. The modulus of the admittance ratio given by equation (39) is plotted in Figure 3 and the phase angle of the characteristic admittance is plotted in Figure 4. It can be seen that at high frequencies the magnitude of the characteristic admittance approaches that of the lossless line, while the phase angle approaches zero. At low frequencies the phase angle approaches 45 degrees. The propagation velocity ratio c/c_a, or wavelength ratio, λ/λ_a, equation (42), is plotted in Figure 5. For a given flow area and frequency, the propagation velocity decreases with increasing radius ratio. The db attenuation per line wavelength, equation (45), is plotted in Figure 6. For given fluid properties, flow area, and frequency, the attenuation per line wavelength increases with increasing aspect ratio.

The circuit parameters R,G,L, and C are normalized with respect to suitable reference values and the results plotted in Figures 7 through 10.

The ratio R/R_{vn} is plotted in Figure 7, where R_{vn} is the viscous laminar steady flow (DC) resistance of the annular line, and is defined in terms of r^* [8].

$$R_{vn} = \frac{8\pi\mu}{A_n^2}\left[\frac{1+r^{*2}}{1-r^{*2}} + \frac{1}{\ln r^*}\right]^{-1} \tag{48}$$

Equations for determining the DC properties of circular, annular, and rectangular lines are derived in Appendix A. As the frequency ω approaches zero, R approaches R_{vn}; however, R_{vn} is a good approximation for R when $\omega/\omega_v \leq 1$ for all r^*. For the larger values of r^* shown in Figure 7,

the range of applicability of the constant resistance model is extended to higher values of ω/ω_ν.

Figure 8 shows the frequency dependence of L/L_a where L_a is the adiabatic inductance. The tendency of the frequency dependent inductance to approach its adiabatic value at high frequencies is clearly shown. For low frequency ratios, say $\omega/\omega_\nu \leq 1$, the inductance is primarily dependent on r^* and essentially independent of ω/ω_ν. The value of L/L_a at low frequency ratios varies between approximately 1.2 and 1.33, depending on r^*.

The ratios $G/\omega_T C_a$ and C/C_a are plotted in Figures 9 and 10. In Figure 9 the conductance is shown to be essentially zero when $\omega/\omega_\nu \leq 1$ for all r^*. For values of $\omega/\omega_\nu > 10$ the conductance increases significantly. This increase is more pronounced at large values of r^*. Figure 10 shows the general thermodynamic behavior of the model:

$$\frac{C}{C_a} = \frac{\frac{A_n}{nP}}{\frac{A_n}{\gamma P}} = \frac{\gamma}{n} \tag{49}$$

where γ is the adiabatic exponent (approximately 1.4 for air at standard conditions) and n is the polytropic exponent. At low frequencies $\gamma/n \approx 1.4$; thus, $n \approx 1$, which is the isothermal exponent. At high frequencies $\gamma/n \approx 1.0$, thus, $n \approx \gamma$, the adiabatic exponent. The process is therefore isothermal at low frequencies and adiabatic at high frequencies. As r^* increases, the transition from isothermal to adiabatic behavior occurs at higher values of ω/ω_ν.

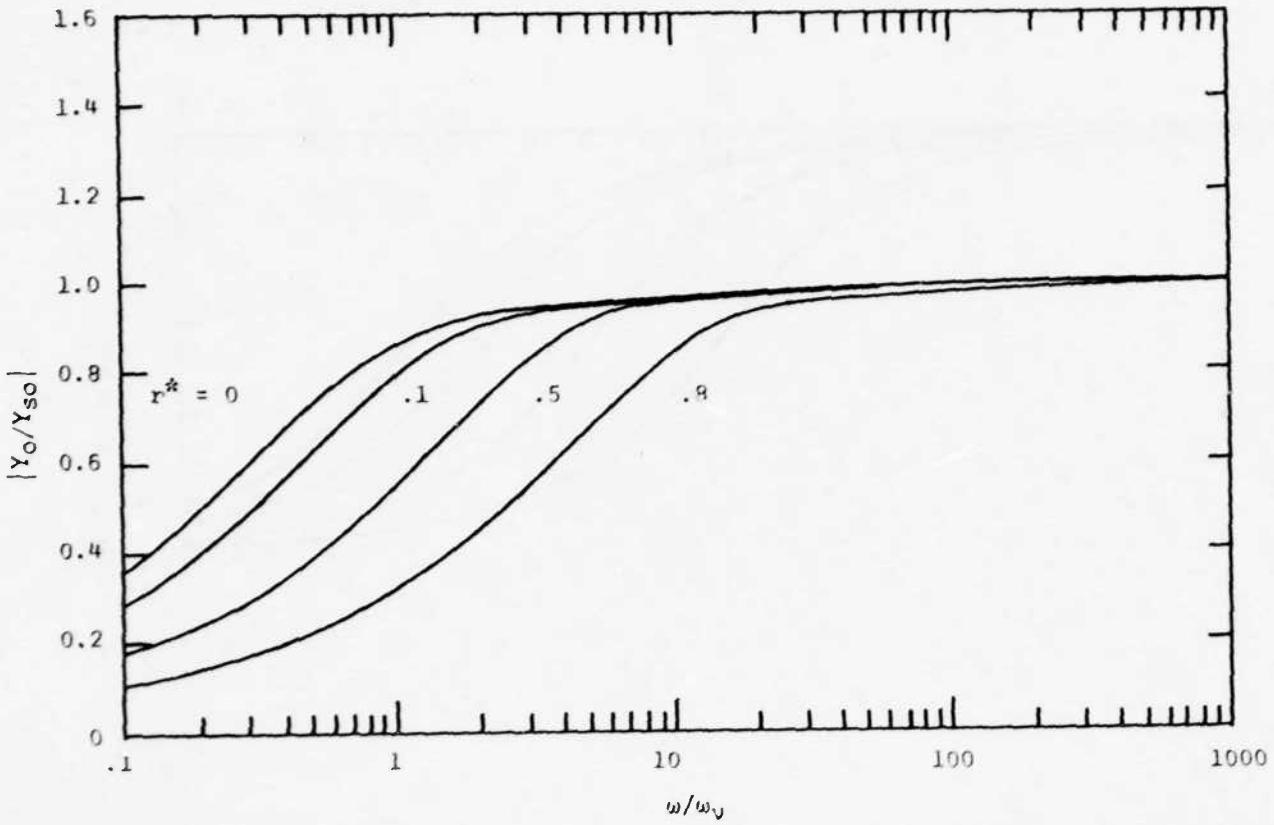

Figure 3. Magnitude of Characteristic Admittance Ratio

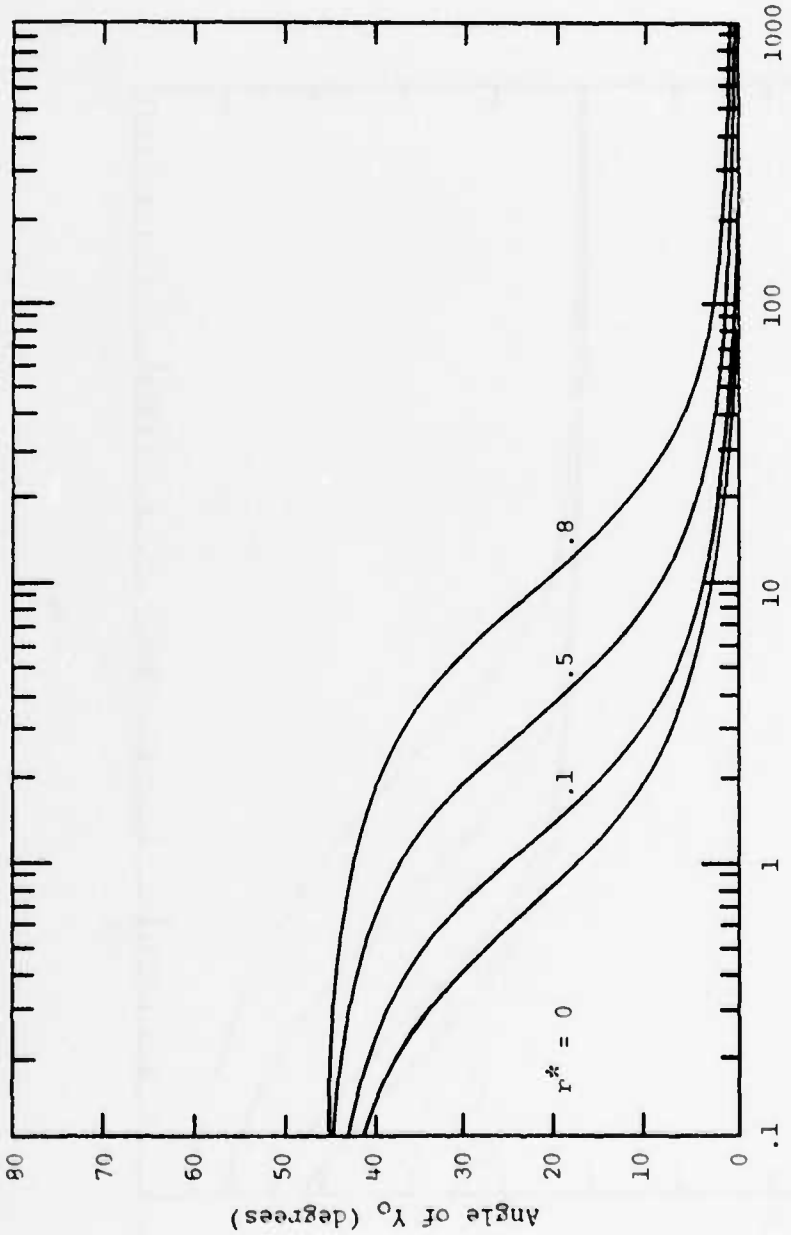

Figure 4. Phase Angle of Characteristic Admittance

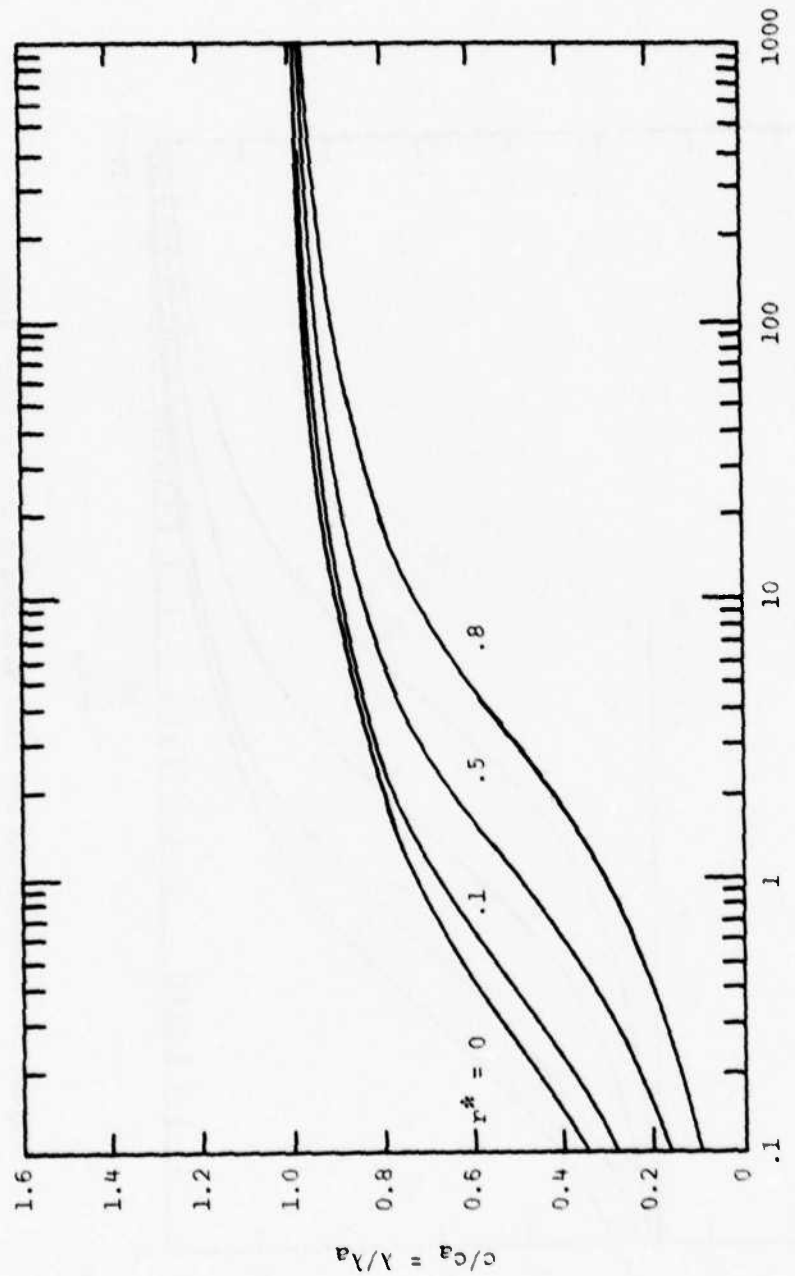

Figure 5. Phase Velocity and Wavelength Ratios

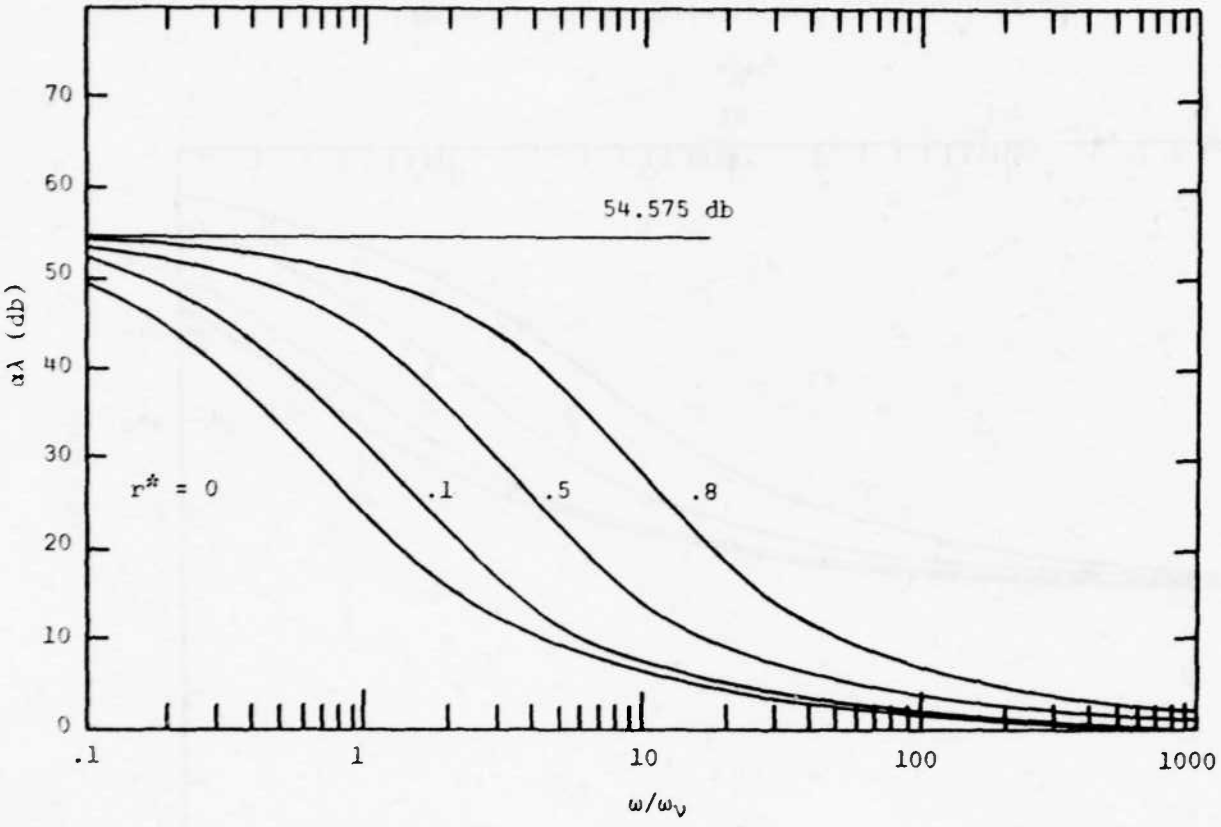

Figure 6. Attenuation Per Line Wavelength for Annular Lines

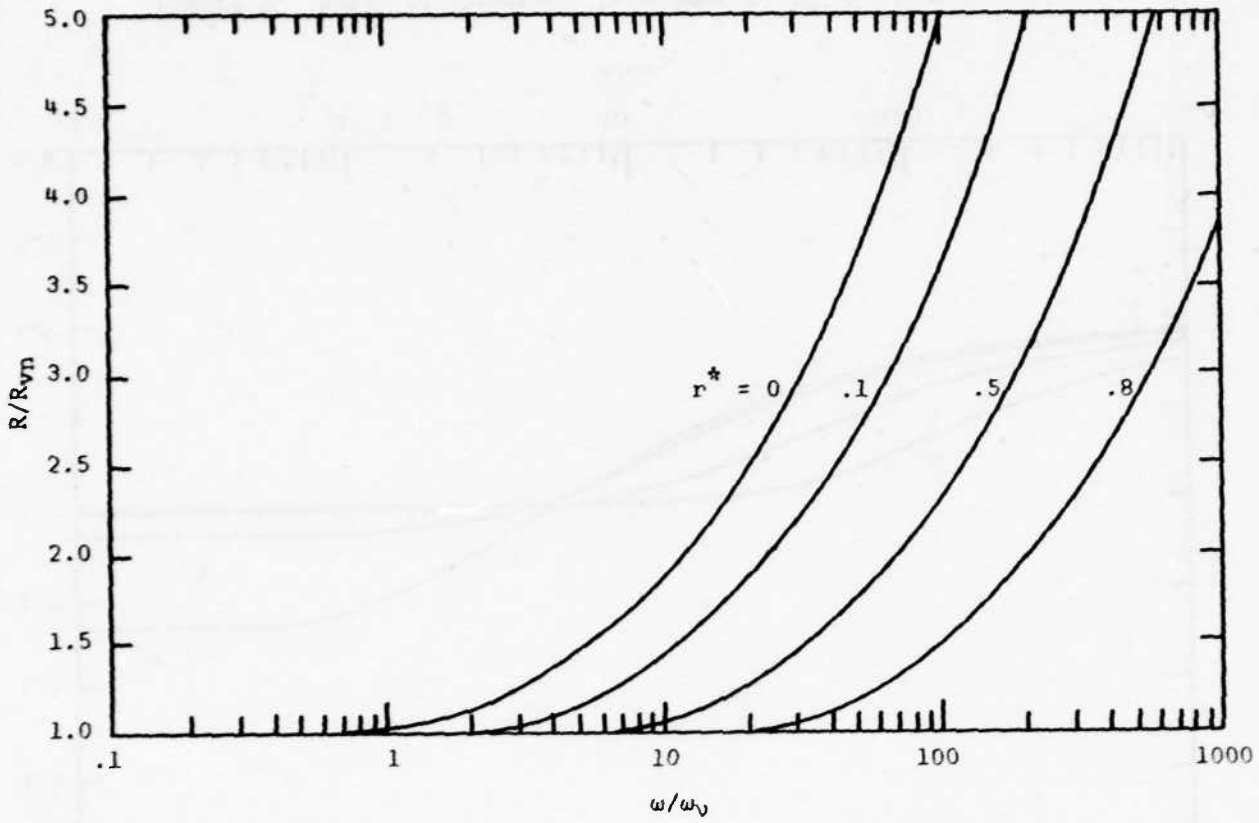

Figure 7. Ratio of Frequency Dependent to Viscous (DC) Resistance

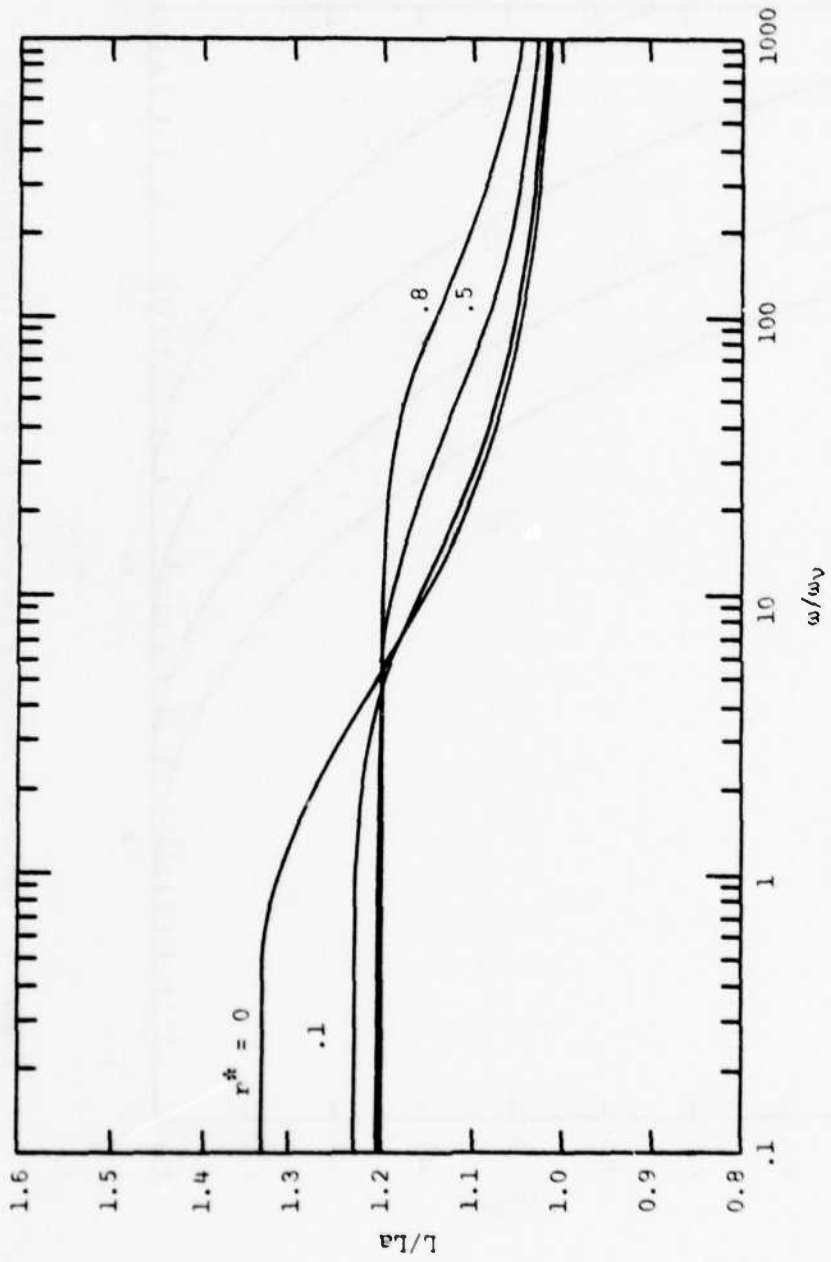

Figure 8. Ratio of Frequency Dependent to Adiabatic Inductance

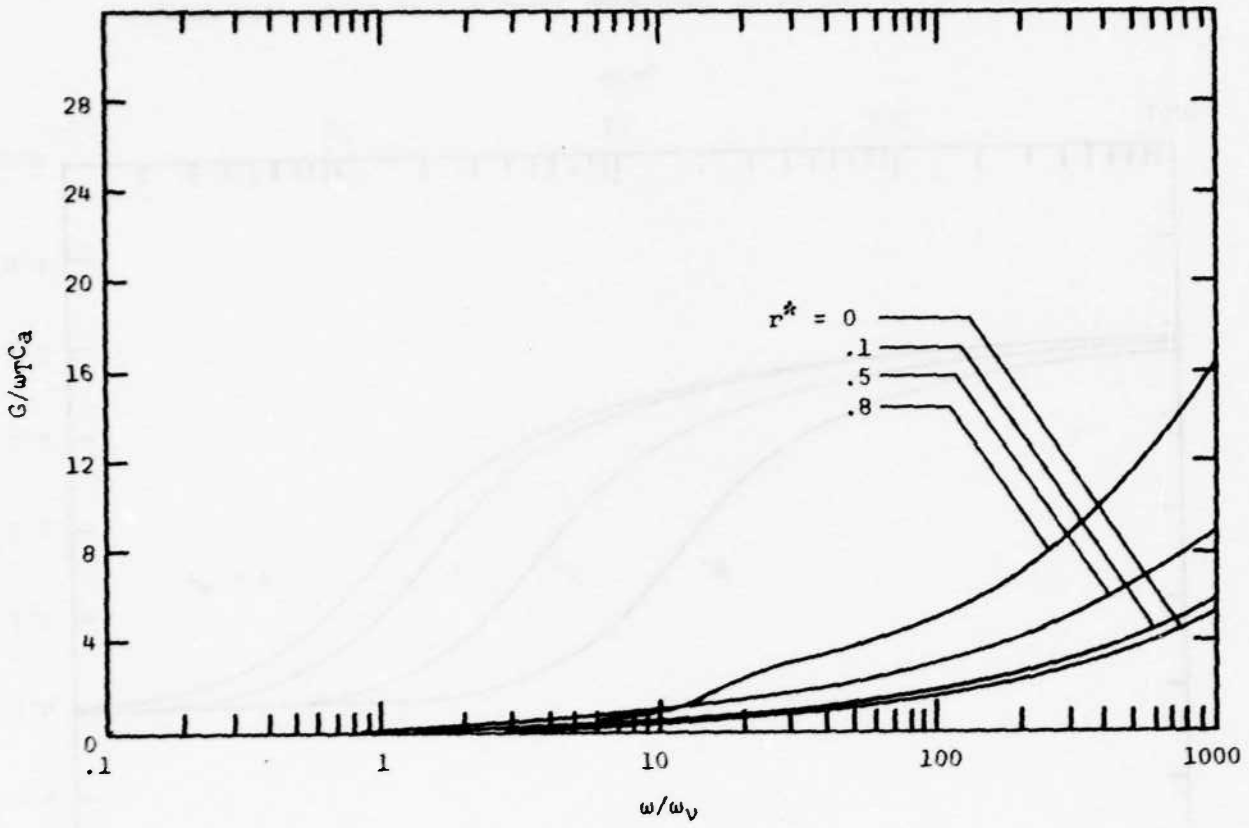

Figure 9. Ratio of Frequency Dependent Conductance to Adiabatic Capacitance

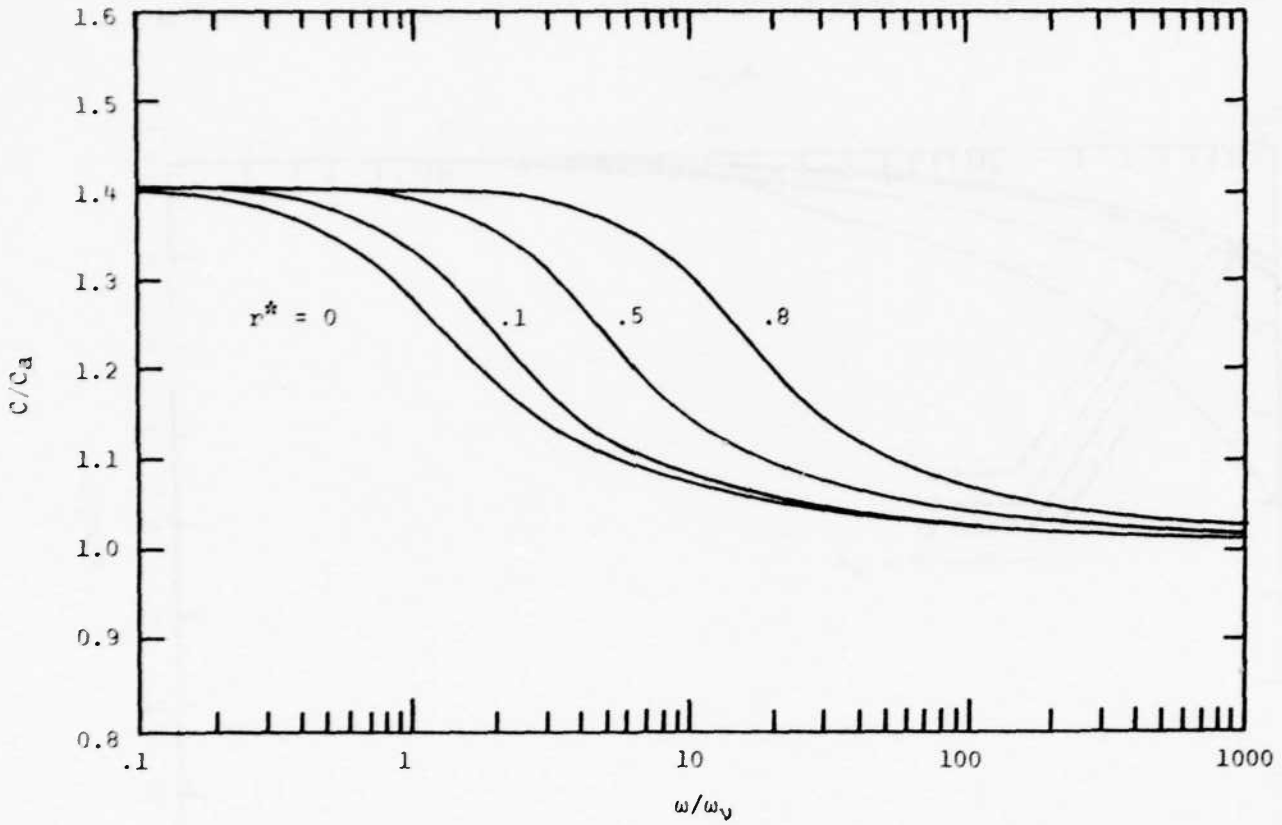

Figure 10. Ratio of Frequency Dependent to Adiabatic Capacitance

In summary, at low frequencies the equivalent circuit, see Figure 2, consists essentially of constant value elements of resistance, inductance, and capacitance and no conductance. At high frequencies, the inductance and capacitance approach their adiabatic values; however, the resistance and conductance are very large and are strongly dependent on frequency and radius ratio.

Comparison with Circular and Rectangular Lines

The results obtained for the annular line are now compared with those obtained for circular and rectangular lines. The comparison is made on the basis that the respective cross-sectional areas are equal.

Generally, the annular results approach those for circular lines as the inner radius of the annulus approaches zero and the losses attributable to the inner wall become small. It can be shown that the circular line velocity and temperature profiles of Nichols [3] may be obtained directly from equations (11) and (12) for the special case of the annular line with $r_i = 0$. The Bessel function

$$K_0\left(\sqrt{\frac{\omega}{\nu}}\, r_i j^{\frac{1}{2}}\right)$$

is infinite at the origin and ceases to be a solution in equations (11) and (12). Thus, when $r_i = 0$, the constants D and F are identically zero. Applying the boundary conditions of equation (10) at the outer wall $r = r_o$ and obtaining new relationships for B and E leads to Nichols' expressions for the velocity and temperature profiles. In all of the figures the curves for $r^* = 0$ are identical with those of Nichols for circular lines.

The annular results converge to those of Schaedel [4] for rectangular lines as $r^* \to 1$. The comparison is made by defining an equivalent aspect ratio for the annular line. The aspect ratio of the rectangular line is defined here as $AR_r = b/h \geq 1$. For equal rectangular and annular flow areas,

$$bh = \pi(r_o^2 - r_i^2) = \pi(r_o + r_i)(r_o - r_i) \tag{50}$$

where choosing $b = \pi(r_o + r_i)$ and $h = r_o - r_i$, the annular aspect ratio is defined as

$$AR_n = \frac{\pi(r_o + r_i)}{(r_o - r_i)} = \frac{\pi(1 + r^*)}{(1 - r^*)} \tag{51}$$

Since the annular line side walls of dimension h do not physically exist and are not considered in the theory, greater losses are expected in rectangular lines when compared to annular lines of the same area and aspect ratio. However, as aspect ratio becomes large, the losses attributable to the short walls of the rectangular line become small compared to the losses on the long walls. Consequently, the results for annular and rectangular lines converge with increasing aspect ratio. Figure 11 is a comparison of the attenuation per unit wavelength ($\alpha\lambda$) of annular and rectangular lines where here ω_ν is defined to correspond to that used by Schaedel [4]; i.e., $\omega_\nu = 4\nu/A$. Of interest is the rather close agreement at moderately low aspect ratios. Agreement within 10% is achieved for all frequency dependent properties when $AR \geq 7$ ($r^* \geq 0.38$). Thus, either model will give approximate predictions of the performance of the other model when $AR > 7$.

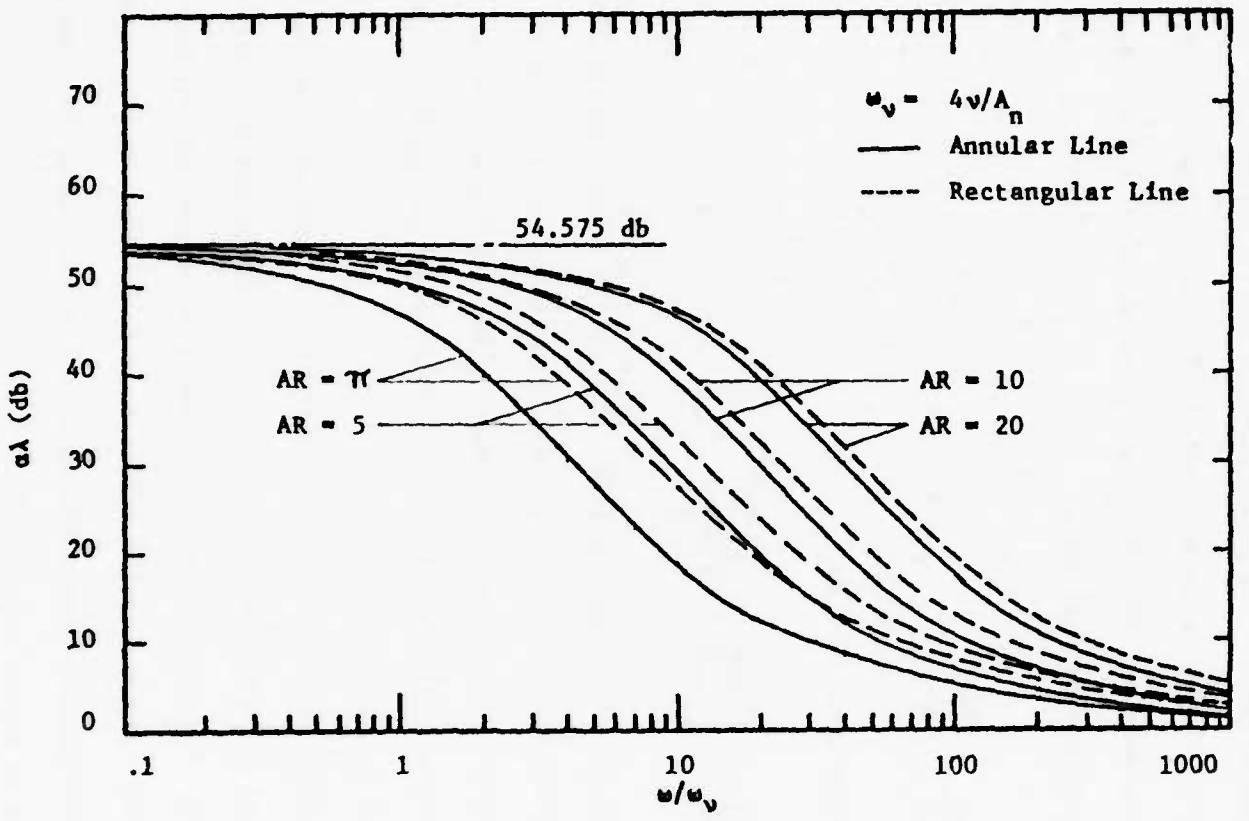

Figure 11. Comparison of Attenuation of Annular and Rectangular Lines

The differences in the circular, rectangular, and annular line results for equal areas are due mainly to differences in the steady-flow (DC) resistances. The differences in the DC resistances are illustrated by the DC resistance ratios plotted in Figure 12. The viscous resistance per unit length of circular lines is the classical Hagen-Poiseuille flow resistance

$$R_{vc} = \frac{8\pi\mu}{A_c^2} \tag{52}$$

For equal flow areas $A_n = A_c$,

$$\frac{R_{vn}}{R_{vc}} = \left[\frac{1+r^{*2}}{1-r^{*2}} + \frac{1}{\ln r^*}\right]^{-1} \tag{53}$$

where R_{vn} is given by equation (48). The ratios R_{vr}/R_{vc} and R_{vn}/R_{vr} are also given, where R_{vr} is the viscous resistance of rectangular lines given by Schaedel [4]. The ratios R_{vn}/R_{vc} and R_{vr}/R_{vc} are nearly linear functions of AR for AR >4. The convergence of R_{vn}/R_{vr} to unity for large AR is easily seen.

In summary, the small signal performance of annular lines has been presented and includes the performance of circular lines as a special case ($r^* = 0$). The small signal performance of annular and rectangular lines converge with increasing aspect or radius ratio. Useful approximations of rectangular line performance may be made using the annular line results at higher aspect ratios, or vice versa.

It is important to note that whereas the numerical results are presented for air at 80°F, any other fluid could have been used. If

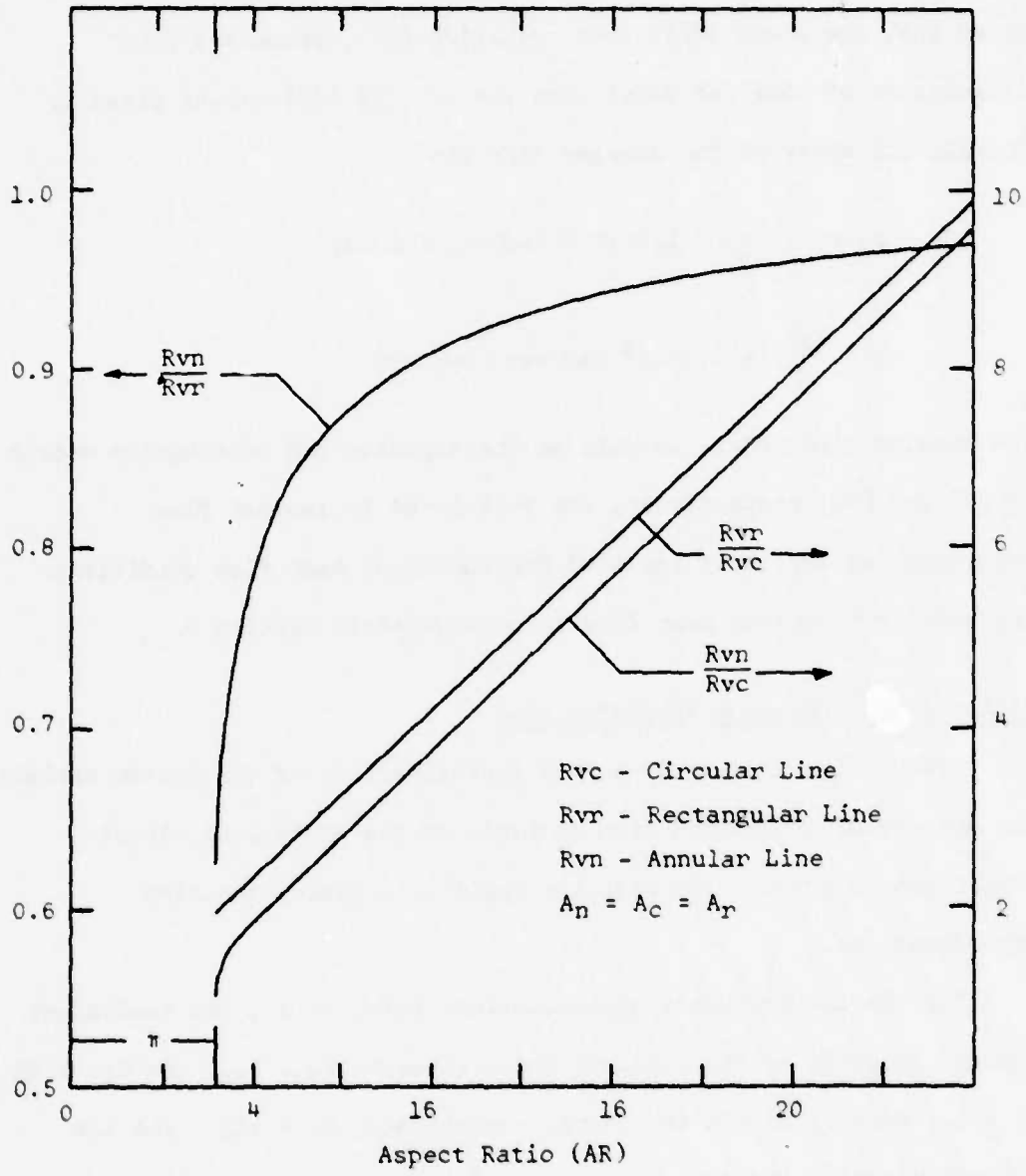

Figure 12. Ratios of Viscous (DC) Resistances

the fluid is considered incompressible, the results are easily adapted, and considerably simplified by assuming $\gamma = 1$, and by taking the speed of sound as $c = \sqrt{K_B/\rho}$ where K_B is the bulk modulus of the fluid. It is noted that the shunt admittance, equation (26), becomes a pure capacitance of constant value when $\gamma = 1$. The limitations given by Iberall [1] apply to the annular line also:

$$r_o - r_i > \frac{\nu}{c_a} \quad (\approx 1.8\times10^{-6} \text{ inches, for air})$$

$$\omega < \frac{c_a^2}{\nu} \quad (= 7.7\times10^{9} \text{ rad/sec, for air})$$

The annular line model, as well as the circular and rectangular models of [3] and [4], respectively, are restricted to laminar flow. Discrepancies are to be expected for turbulent mean flow conditions. The case of turbulent mean flow is considered in Section V.

High and Low Frequency Approximations

Useful high and low frequency approximations of the system variables are most readily obtained from analysis of the equivalent circuit components in conjunction with the applicable Bessel function approximations.

For the low frequency approximations ($\omega/\omega_\nu << 1$), the equivalent circuit consists of the constant value elements R_{v_n}, L_{v_n}, and C_i, with $G_i = 0$. Here C_i is the isothermal capacitance, $C_i = \gamma C_a$. The low frequency series impedance and shunt admittance are respectively,

$$Z_{L_n} = R_{v_n} + j\omega L_{v_n}$$

$$Y_{L_n} = G_i + j\omega C_i = j\omega\gamma C_a \qquad (54)$$

Using the inequality $\omega L_{v_n}/R_{v_n} << 1$ and equations (34) and (54), the low frequency characteristic admittance and propagation operator become

$$Y_{0_L} = \sqrt{Y_{L_n}/Z_{L_n}} = \sqrt{\frac{\gamma C_a \omega}{2R_{v_n}}}\,(1+j) \tag{55}$$

$$\Gamma_L = \sqrt{Z_{L_n}/Y_{L_n}} = \alpha + j\beta = \sqrt{\frac{\gamma}{2} R_{v_n} C_a \omega}\,(1+j) \tag{56}$$

It is seen that the phase lag β is approximately numerically equal to the attenuation α, and that the phase angle of the admittance is approximately $\pi/4$ radians. For $\omega/\omega_\nu \leq 0.1$, equations (55) and (56) give Γ and Y_0 within one percent of the exact value, for all r^*. Expressions for R_{v_n} and L_{v_n} are derived in Appendix A.

The high frequency approximations are derived in Appendix B using the standard asymptotic expansions of the Bessel functions [5,6], along with other approximations. For $\omega/\omega_\nu >> 1$, the inequalities, $R/\omega L << 1$ and $G/\omega C << 1$, apply. The high frequency series impedance and shunt admittance become

$$Z_{H_n} = j\omega L_{a_n} \left\{ 1 + \frac{\pi r_o}{A_n} \sqrt{\frac{2\nu}{\omega}} [(r^*-1) + j(r^*+1)] \right\}^{-1} \tag{57}$$

$$Y_{H_n} = j\omega C_{a_n} \left\{ 1 + \left(\frac{\gamma-1}{\sigma}\right) \frac{r_o}{A_n} \sqrt{\frac{2\nu}{\omega}} [(r^*-1) + j(r^*+1)] \right\} \tag{58}$$

The high frequency propagation operator and characteristic admittance become

$$\Gamma_H = \alpha_H + j\beta_H = \frac{1}{4c_a}\left(1 + \frac{\gamma-1}{\sigma}\right)\sqrt{\frac{1+r^*}{1-r^*}}\sqrt{\omega\omega_v} + j\frac{\omega}{c_a} \qquad (59)$$

$$Yo_H = \sqrt{\frac{Y_H}{Z_H}} \approx \sqrt{\frac{C_a}{L_a}}\left[1 + j\left(\frac{R}{\omega L} - \frac{G}{\omega C}\right)\right] \approx \sqrt{\frac{C_a}{L_a}} \qquad (60)$$

It is of interest that the expression for α_H in equation (59) for annular lines is identical to that obtained by Karam and Franke [9] for circular lines for the special case $r^* = 0$. The expression for β_H is identical to that given in [9]. It should therefore be possible to obtain a solution in the time domain for annular lines using Karam's approach [19,20]. The frequency to time domain transformations for circular, rectangular and annular lines are covered in Section III.

Experimental Confirmation of Annular Theory

The experimental verification of the annular line theory was the primary purpose of a M.S. thesis completed by Captain G. R. Farney at the Air Force Institute of Technology [10]. Farney measured the small signal amplitude and phase shift frequency response of a blocked annular pneumatic transmission line at five different radius ratios. The outer line was approximately three feet long and had an internal diameter of 0.187 inches. The five radius ratios were achieved by inserting and centering five different sized rods within the basic line. Farney observed that the experimental gains were within ± 1 db and the phase shift angles within ±15 degrees of those predicted by the annular line theory. Further, the predicted analytical results fell within the measurement capability of the experimental instrumentation used.

A description of the experimental apparatus and test procedures used is given in [10].

Additional equations are required to account for the sending and receiving conditions. These are standard equations of electrical transmission line theory, available in many references such as [11] and are repeated herein for the convenience of the reader.

For a given line, the transfer pressure gain is [12]:

$$g = \left|\frac{P_r}{P_s}\right| = \frac{Z_r}{Z_s} \cosh \Gamma\ell - \frac{Z_r}{Z_0} \sinh \Gamma\ell \tag{61}$$

where r and s denote sending and receiving locations and ℓ is the distance between these locations. The sending impedance is

$$Z_s = Z_0 \frac{Z_r \cosh \Gamma\ell + Z_0 \sinh \Gamma\ell}{Z_0 \cosh \Gamma\ell + Z_r \sinh \Gamma\ell} \tag{62}$$

For a blocked line, the receiving impedance Z_r is infinite, thus

$$Z_s = Z_0 \coth \Gamma\ell \tag{63}$$

The phase lag angle between sender and receiver is

$$\beta\ell = \arctan \frac{\text{Imag } (g)}{\text{Real } (g)} \tag{64}$$

The pressure gain, equation (61) converted to decibels, and the phase lag angle, equation (64) in degrees, are plotted as functions of excitation frequency in Figures 13, 14, and 15, for annular radius ratios of 0.07, 0.23, and 0.67, respectively. The experimental data

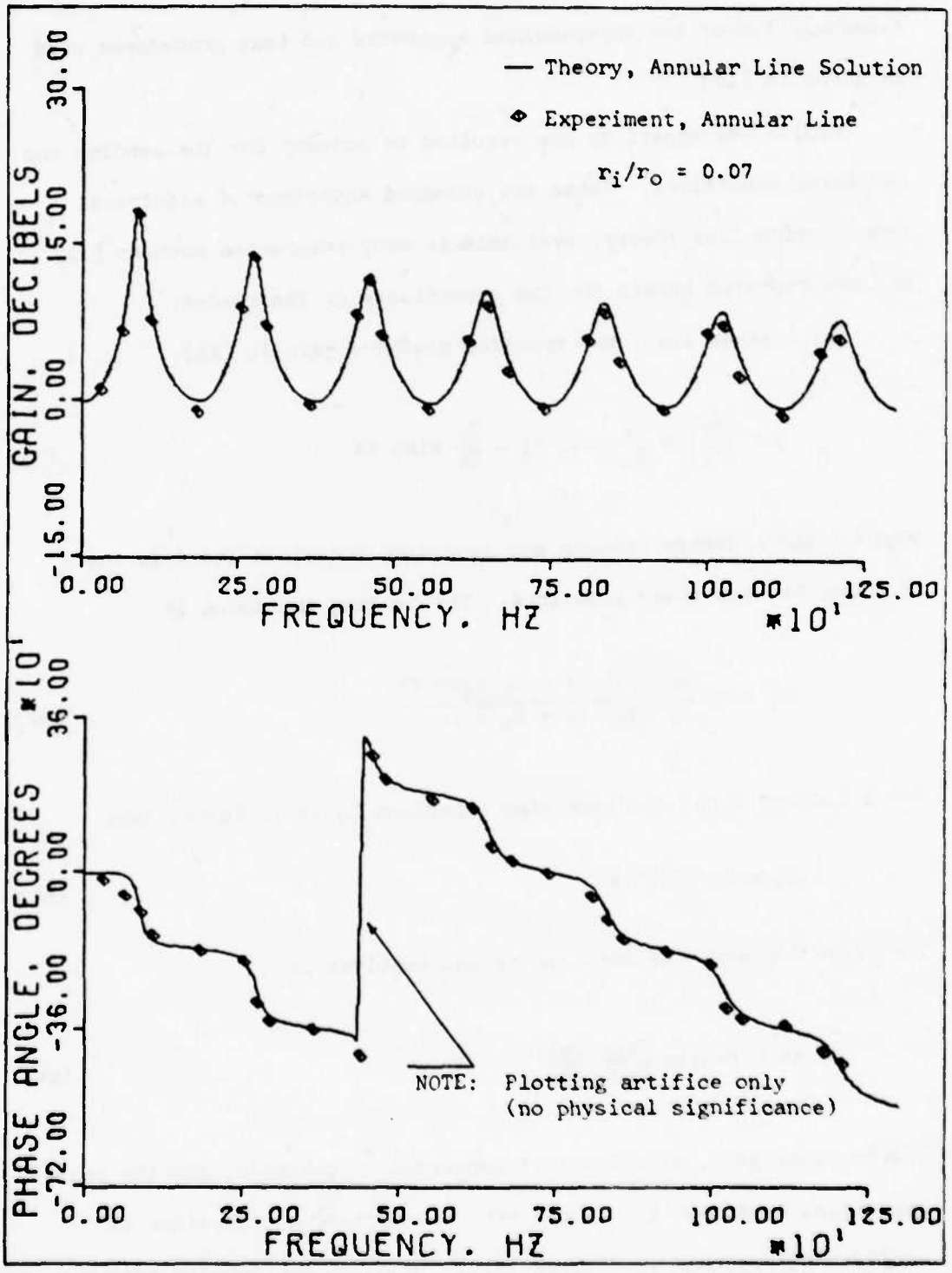

Figure 13. Correlation of Experimental Results with Annular Line Theory

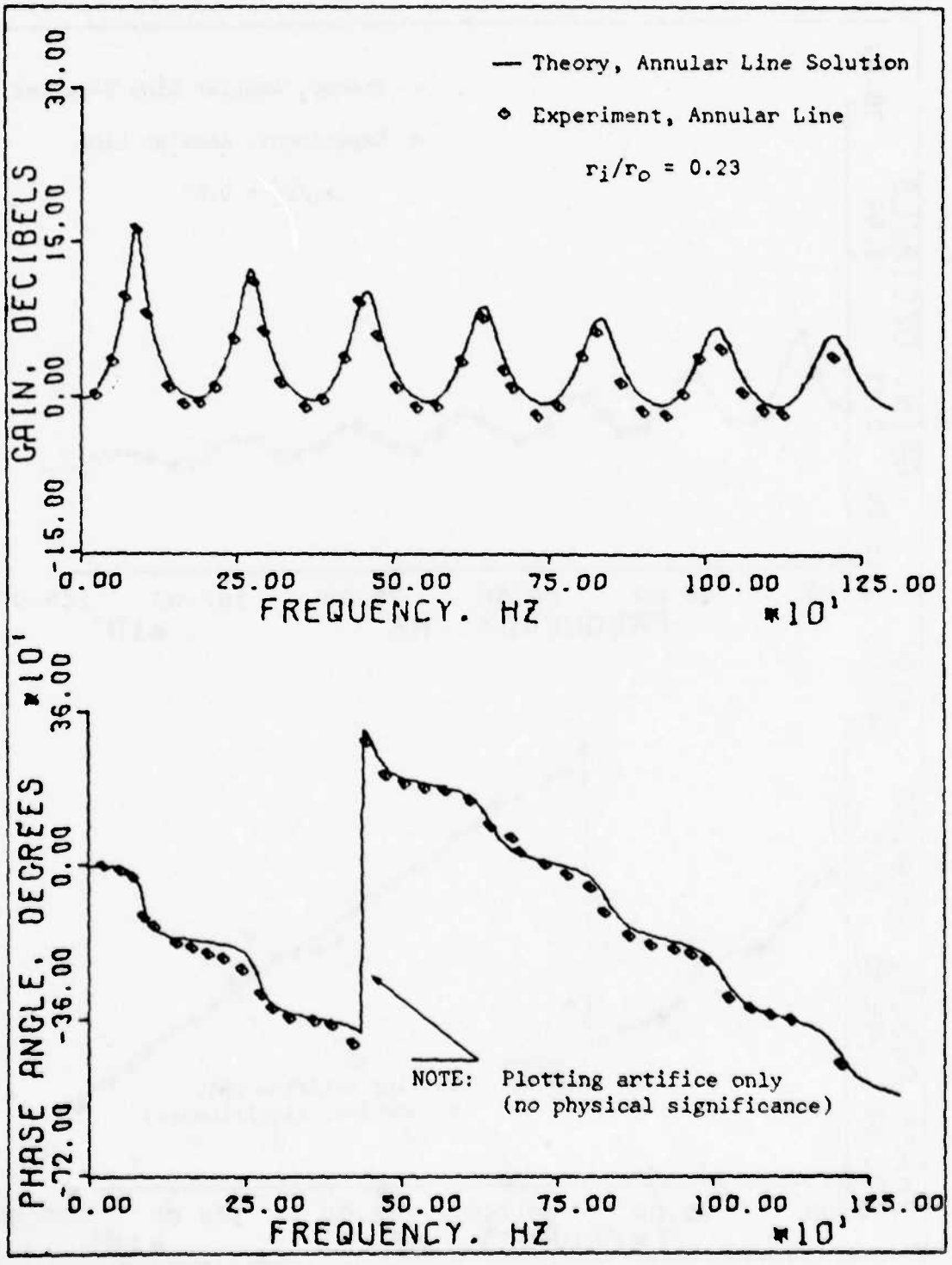

Figure 14. Correlation of Experimental Results with Annular Line Theory

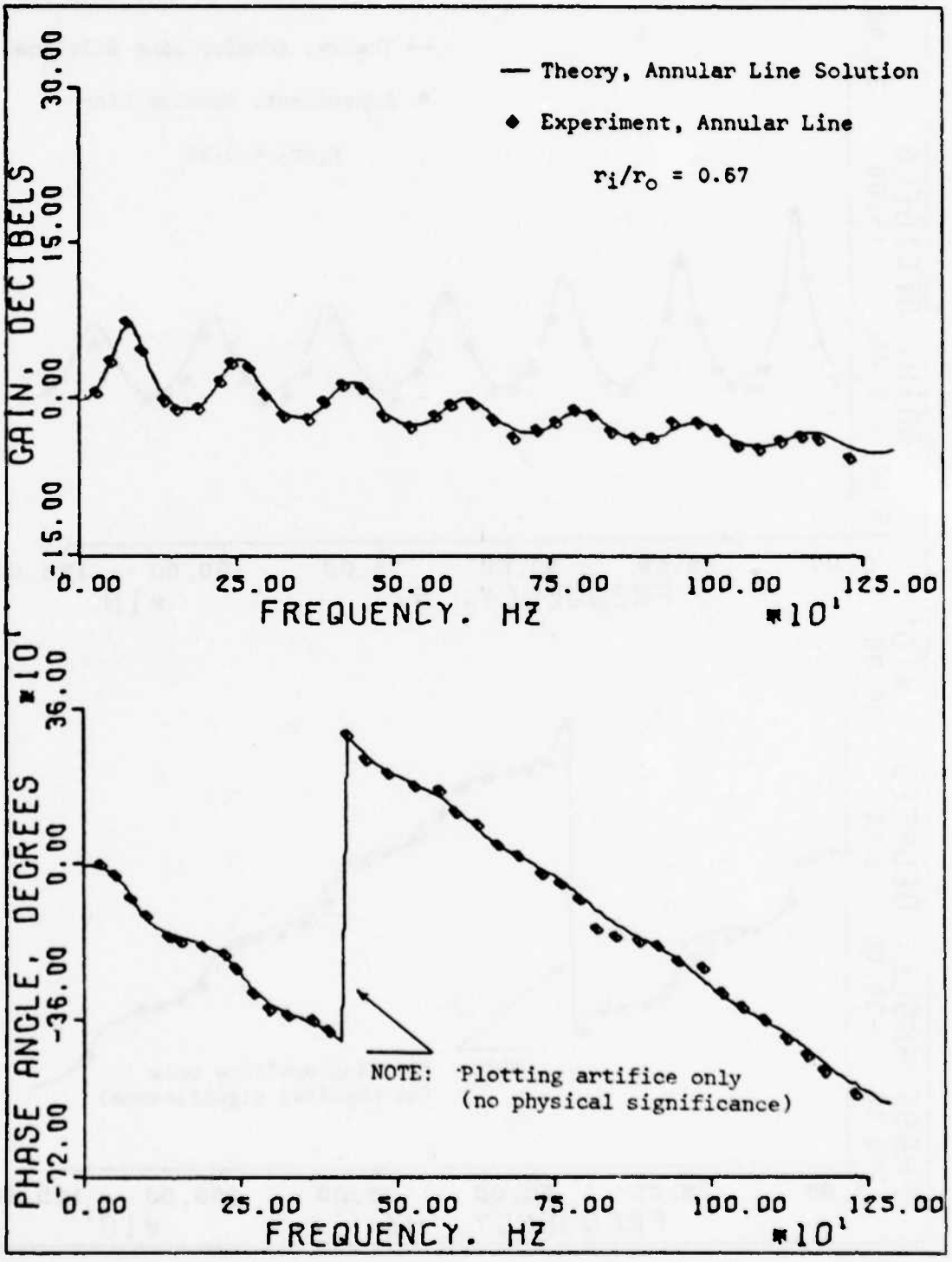

Figure 15. Correlation of Experimental Results with Annular Line Theory

of Farney is also plotted. The sharp increase in phase angle shown in the figures (approximately 720 degrees) is a plotting artifice to conserve space and has no other significance. The ambient test conditions at each radius ratio are given in Table II.

TABLE II

Ambient Test Conditions†

r^*	P(ambient) (psia)	$\overline{P}$(line) (psig)	$\overline{T}$ (°F)
0.07	14.50	5.01	79.0
0.23	14.44	5.01	80.0
0.67	14.20	5.01	80.0

†The tabulated values were used to determine the necessary mean properties of air.

As can be seen from the figures, the agreement between theory and experiment is excellent.

III. Correlation of the Linear Response of Circular and Noncircular Fluid Transmission Lines

In steady flow, it has been particularly useful to correlate the resistances of lines of noncircular cross sections with the resistance of circular lines through the classical hydraulic diameter. Similarly, in oscillatory flow, it would appear useful to be able to correlate the frequency response of noncircular lines to the response of circular lines. Besides the comparisons made between rectangular and circular lines [4] and between rectangular, annular and circular lines herein, other attempts have been made to predict the response of rectangular lines using the concept of the hydraulic diameter [13,14].

In this section, a dimensionless frequency is defined which leads to a generalized presentation of the frequency dependent response of lines of circular and noncircular cross section. The dimensionless frequency in turn leads to a characteristic radius for the noncircular line which is roughly analogous to the classical hydraulic radius used in steady developed flow for noncircular lines. It is shown that the frequency dependence of noncircular lines may be very closely approximated when the characteristic radius is used together with the circular line theory of Nichols [3]. The results are compared with those obtained by Healey and Carlson [13] for rectangular lines. In [13], the classical hydraulic radius together with Nichols' theory was used to predict the response of rectangular lines. The response predicted using the characteristic radius defined herein is shown to be clearly superior to the response predicted using the hydraulic radius. Results are presented for both rectangular and annular lines over a wide range

of aspect and radius ratio, respectively. In addition, an approach to impedance matching based on equivalent circular lines is presented.

Frequency Response Solutions

Several dimensionless frequencies (or frequency ratios) have been defined in order to present generalized frequency response solutions for circular lines. Nichols [3] showed that the frequency response of a circular line is a function of the dimensionless frequency ratio ω/ω_ν, where ω is the angular excitation frequency and ω_ν is a viscous characteristic frequency defined as

$$\omega_\nu = \frac{R_v}{L_a} \tag{65}$$

R_v is the laminar DC viscous resistance per unit line length and L_a is the adiabatic inertance per unit line length. For any line, R_v and L_a are defined as

$$R_v = \frac{1}{Q}\left[-\frac{dp}{dz}\right] \tag{66}$$

and

$$L_a = \frac{\rho^*}{A} \tag{67}$$

For a circular line, R_v and ω_ν become

$$R_{v_c} = \frac{8\pi\mu}{A_c^2} \tag{68}$$

and

$$\omega_{\nu_c} = \frac{8\pi\nu}{A_c} \tag{69}$$

Other formulations of the dimensionless frequency have also been defined for the circular line; for example, Brown et al. [15] used $\Omega = \omega r^2/\nu = 8\omega/\omega_{\nu_c}$, while Goldschmied [16] used $SN = 4\omega r^2/\nu = 32\ \omega/\omega_{\nu_c}$. In all of these cases, however, the dimensionless frequencies are proportional to $\omega A/\nu$.

Schaedel [4] showed that the response of rectangular lines of the same aspect ratio is a function of $\omega A/4\nu$, and it has been shown herein that the response of concentric annular lines of the same radius ratio is a function of $\omega A/8\pi\nu$. Typical results for the attenuation per line wavelength of rectangular and annular lines are plotted in Figures 16 and 17, respectively. Circular line results are included in Figure 17 as a special case of the annular line with the inside radius $r_i = 0$. The dependence on aspect ratio and radius ratio as well as signal frequency is clearly shown.

Generalized Response of Noncircular Lines

The $\alpha\lambda$ curves shown in Figures 16 and 17 for different aspect ratios and radius ratios all have the same general shape. Thus, it would seem possible that the results for different aspect or radius ratios could be generalized and related to a single curve. This can be accomplished approximately by using the dimensionless frequency defined by equation (65) with R_ν taken as the resistance of the particular cross section being considered.

A better approach is to include the inertance effects in the dimensionless frequency as well as the resistance effects and to present the results as a function of the dimensionless frequency ω/ω_c, where ω_c is the radian frequency defined by Nichols [3] as

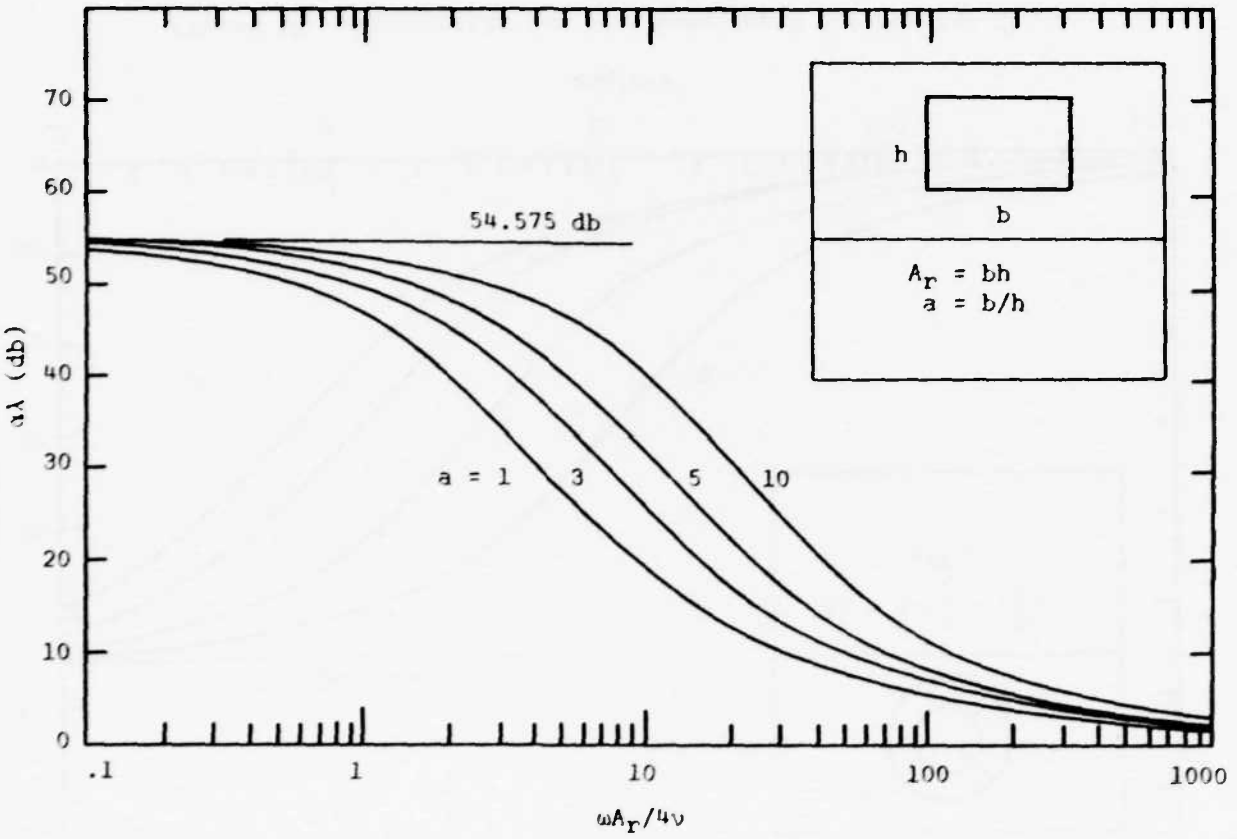

Figure 16. Attenuation Per Line Wavelength for Rectangular Lines

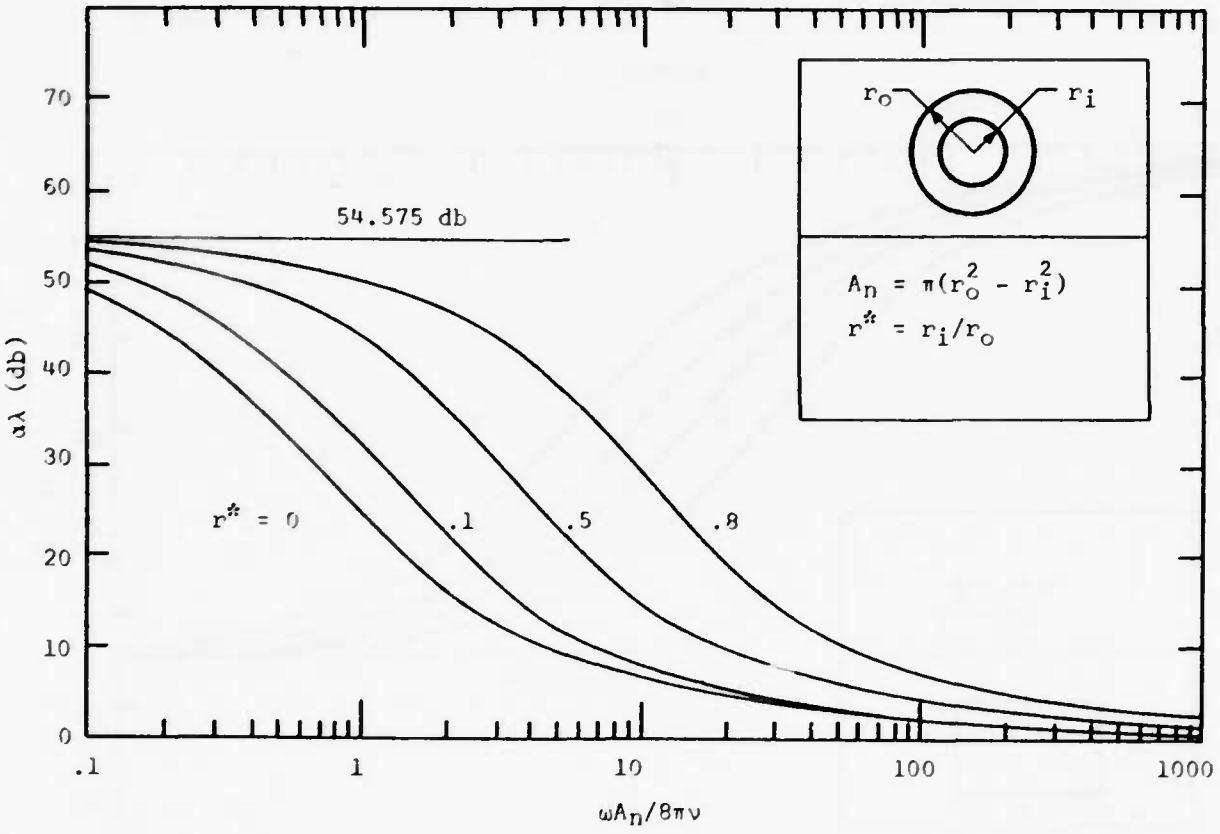

Figure 17. Attenuation Per Line Wavelength for Annular Lines

$$\omega_c = \frac{R_v}{L_v} \tag{70}$$

Here R_v is defined by equation (66), and L_v, the low-frequency or viscous inertance, is defined by

$$L_v = \left[\frac{1}{A}\int\left(\frac{u}{\bar{u}}\right)^2 dA\right] L_a = K_L \cdot L_a \tag{71}$$

where K_L depends on the laminar fully-developed velocity distribution.

The ratio ω/ω_c includes both viscous and inertial effects at low frequency. Consequently, this ratio more accurately represents the fluid line at low frequency ratios, and gives analytical results which are in closer agreement with both the theoretical and experimental results obtained for circular and noncircular lines.

The $\alpha\lambda$ results shown in Figures 16 and 17 are replotted in Figure 18 as a function of ω/ω_c. The families of curves for different aspect and radius ratios are now reduced approximately to a single curve. By incorporating the geometric dependence of aspect and radius ratio in ω_c, lines of different sizes and cross sections are shown to have approximately the same generalized frequency behavior. The circular line attenuation is also included in Figure 18, where ω_c for the circular line is the same as that given by Nichols [3]; i.e.,

$$\omega_{c_c} = \frac{R_{v_c}}{L_{v_c}} = \frac{\frac{8\pi\mu}{A_c^2}}{\frac{4}{3}L_{a_c}} = \frac{6\pi\nu}{A_c} = \frac{3}{4}\omega_{v_c} \tag{72}$$

Figure 18 shows $\alpha\lambda$, the attenuation per line wavelength. In order to obtain α, the attenuation per unit length, it is necessary to know λ the wavelength in the line for each ratio ω/ω_c. Curves of λ/λ_a vs $\omega A/4\nu$ for rectangular lines are given in [4], and are not reproduced herein. However, for annular lines curves of λ/λ_a vs $\omega A/8\pi\nu$ are given

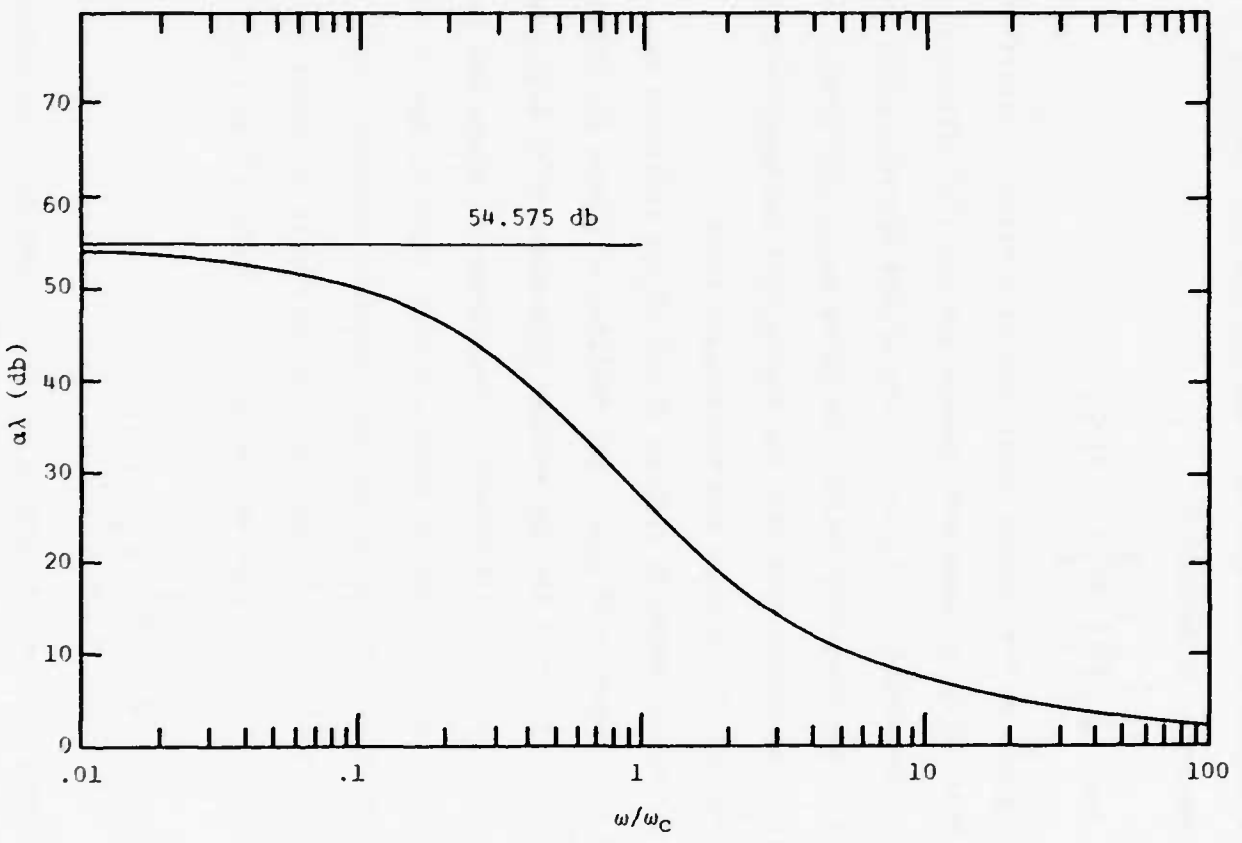

Figure 18. Attenuation Per Line Wavelength for Circular, Rectangular, and Annular Lines

in Figure 5. The dependence on radius ratio is clearly seen. Similar qualitative dependence on aspect ratio may be seen in [4] for rectangular lines. The families of curves depicting λ/λ_a reduce approximately to one curve representing circular, rectangular and annular lines when plotted against ω/ω_c as shown in Figure 19. The ratio λ/λ_a, equation (42), is also the ratio of the propagation or phase velocity in the line to the free sonic (adiabatic) velocity; i.e., $\lambda/\lambda_a = c/c_a$.

Numerical Results and Discussion

The results in Figures 16 through 19 were computed assuming standard properties of air at 80 F (Table I). The numerical differences in $\alpha\lambda$ in Figure 18 for the range of aspect or radius ratios shown in Figures 16 and 17 were small and are not plotted in Figure 18. The maximum difference in $\alpha\lambda$ between circular and rectangular lines was 1.05 db at $\omega/\omega_c = 6.0$ for $a = 10$. The maximum difference between annular and circular lines was 1.40 db at $\omega/\omega_c = 6.0$ for $r^* = 0.8$. For $\omega/\omega_c \leq 0.1$ the difference was less than 0.09 db, and for $\omega/\omega_c \geq 10$ the difference was less than 1.25 db.

The maximum difference in λ/λ_a between circular and rectangular lines was 0.035 at $\omega/\omega_c = 2.0$ and $a = 10$. The maximum difference between circular and annular lines was 0.046 at $\omega/\omega_c = 3.0$ and $r^* = 0.8$. For $\omega/\omega_c \leq 0.1$ the maximum difference for both rectangular and annular lines was less than 0.017 and for $\omega/\omega_c \geq 10$ the maximum difference was less than 0.025. The maximum departure of λ/λ_a from that predicted for the circular line for the range of aspect and radius ratios considered occurred for the annular line of radius ratio $r^* = 0.8$, as shown in Figure 19. All other configurations are nearer to the circular line results.

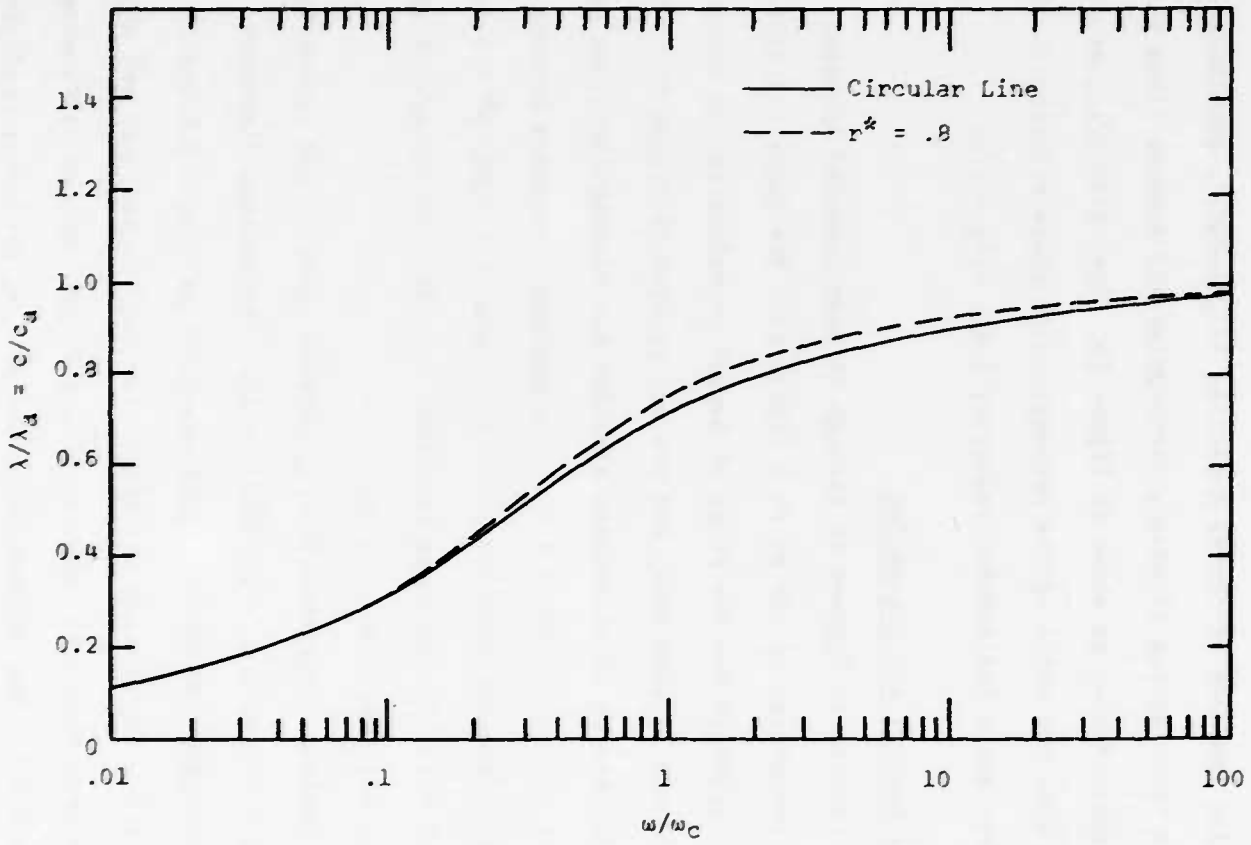

Figure 19. Wavelength Ratio for Circular, Rectangular, and Annular Lines

It is noted that whereas $\alpha\lambda$ vs ω/ω_c gives the tightest grouping of the $\alpha\lambda$ curves, λ/λ_a vs ω/ω_ν gives a slightly better grouping of the λ/λ_a curves, where ω_ν is defined by equation (65).

Determination of the Characteristic Frequency

The determination of values of ω_c for noncircular lines reduces essentially to obtaining values of R_v and L_v. Analytical expressions of R_v and L_v for circular, rectangular and annular lines are developed and discussed in Appendix A. A convenient method for obtaining R_v is to relate the R_v of the line with the noncircular cross section to that of a circular cross section; i.e.,

$$\frac{R_v}{R_{v_c}} = K_R \frac{A_c^2}{A^2} \tag{73}$$

where K_R for rectangular lines and annular lines depends on aspect ratio and radius ratio, respectively. Values of K_R have been calculated [4,17] and a few are given in Table III. The viscous inertance L_v is obtained from values of K_L, equation (71), for each geometric configuration. Values of K_L have also been calculated [4,17,18] and a few are given in Table III.

Starting with equation (70), a convenient equation for computing ω_c is easily derived as

$$\omega_c = \frac{K_R}{K_L} \frac{8\pi\nu}{A} \tag{74}$$

For circular lines: $K_{R_c} = 1$ and $K_{L_c} = 4/3$; thus $\omega_{c_c} = 6\pi\nu/A_c$. Values of ω_c for noncircular lines can easily be obtained using values from Table III or using the equations or data from the references [4,17,18].

TABLE III

Fully Developed Laminar Flow Parameters for Rectangular and Annular Lines

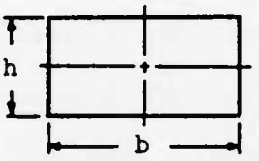

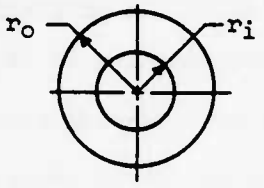

b/h	K_{R_r}	K_{L_r}	$f_r Re_r$	K_{G_r}	r_i/r_o	K_{R_n}	K_{L_n}	$f_n Re_n$	K_{G_n}
1	1.1322	1.3785	56.91	1.2733	0	1.0000	1.3333	64.00	1.0000
2	1.3920	1.3475	62.19	1.4324	0.1	1.7068	1.2298	89.37	1.2222
3	1.8133	1.3120	68.36	1.6977	0.2	2.1645	1.2168	92.35	1.5000
4	2.2671	1.2876	72.93	1.9895	0.3	2.7232	1.2101	93.85	1.8571
5	2.7317	1.2714	76.28	2.2918	0.5	4.4649	1.2035	95.25	3.0000
10	5.0959	1.2365	84.68	3.8515	0.8	13.4890	1.2004	95.92	9.0000
∞	∞	1.2000	96.00	∞	1.0	∞	1.2000	96.00	∞

The steady flow laminar resistance R_v does not depend on frequency; consequently, R_v may be expressed in terms of the classical steady-flow parameters:

$$R_v = fRe \frac{\mu}{2D_h^2 A} \tag{75}$$

where D_h is the conventional hydraulic diameter, f is the friction factor and Re is the Reynolds number. For a circular line, $D_h = D_c$ and $fRe = 64$; therefore,

$$R_{v_c} = 64 \frac{\mu}{2D_c^2 A_c} \tag{76}$$

Dividing equation (75) by equation (76)

$$\frac{R_v}{R_{v_c}} = \frac{fRe}{64} \frac{D_c^2}{D_h^2} \frac{A_c}{A} \tag{77}$$

where fRe, D_h, and A are determined for the noncircular cross section being considered. Selected values of fRe are given in Tab_e III for rectangular and annular cross sections. The relationship between K_R and fRe is obtained from equations (73) and (77)

$$K_R = \frac{fRe}{64} \frac{D_c^2}{D_h^2} \frac{A}{A_c} = \frac{fRe}{64} K_G \tag{78}$$

where K_G is a geometric shape factor defined as

$$K_G = \frac{D_c^2}{D_h^2} \frac{A}{A_c} = \frac{4A}{\pi D_h^2} = \frac{P_w^2}{4\pi A} \tag{79}$$

K_G is a constant for each geometric cross section. It is important to note that when $D_h = D_c$ the areas of the noncircular cross section A and equivalent diameter circle A_c are not equal and $K_G = A/A_c$. Likewise, when $A = A_c$ the hydraulic diameters are not equal and $K_G = D_c^2/D_h^2$. Expressions for K_G are given in Table IV for circular, rectangular and annular cross sections. Selected values of K_G are included in Table III for rectangular and annular cross sections.

TABLE IV

Geometric Cross Section Factor

Cross Section	K_G
circular	1
rectangular	$(a+1)^2/\pi a$
concentric annular	$1+r^*/1-r^*$

Use of the Hydraulic Diameter

Results based on hydraulic diameter can be used to predict line performance for small signal oscillatory flow. At a given signal frequency, Figure 18 shows that for the same attenuation on lines of different cross section, the ω_c must be the same. The use of equivalent hydraulic diameter for a noncircular line, however, leads to an ω_c that is, in general, not equal to ω_{c_c}. This will now be illustrated for a rectangular line.

From equation (74), the ratio $\omega_{c_r}/\omega_{c_c}$ is

$$\frac{\omega_{c_r}}{\omega_{c_c}} = \frac{4}{3} \frac{K_{R_r}}{K_{L_r}} \frac{A_c}{A_r} \tag{80}$$

By substituting for K_{R_r} from equation (78), the ratio becomes

$$\frac{\omega_{c_r}}{\omega_{c_c}} = \frac{4}{3} \frac{f_r Re_r}{64} \frac{1}{K_{L_r}} \frac{D_c^2}{D_{h_r}^2} \tag{81}$$

For $D_{h_r} = D_c$, equation (81) reduces to

$$\frac{\omega_{c_r}}{\omega_{c_c}} = \frac{4}{3K_{L_r}} \frac{f_r Re_r}{64} \tag{82}$$

Typical values of $\omega_{c_r}/\omega_{c_c}$ and $\sqrt{\omega_{c_r}/\omega_{c_c}}$ as a function of aspect ratio are shown in Table V using the values of $f_r Re_r$ and K_{L_r} from Table III.

TABLE V

Frequency Ratio Parameters for Rectangular Lines for $D_{h_r} = D_c$

b/h	$\omega_{c_r}/\omega_{c_c}$	$\sqrt{\omega_{c_r}/\omega_{c_c}}$
1	0.86	0.93
2	0.96	0.98
3	1.09	1.04
4	1.18	1.09
5	1.25	1.12
10	1.43	1.19

The ratio $\sqrt{\omega_{c_r}/\omega_{c_c}}$ can be interpreted approximately as the ratio of the viscous attenuation of rectangular to circular lines of the same hydraulic diameter at a given frequency. The values of $\sqrt{\omega_{c_r}/\omega_{c_c}}$ given in Table V confirm the attenuation results of Healey and Carlson [13] and explain the differences they found between the rectangular line solutions and circular line solutions of the same hydraulic diameter. When using circular line equations to predict rectangular line results, the differences can be avoided if the rectangular line friction factor ($f_r Re_r$) and inertance L_{v_r} are included in the calculations. This point will be made clearer in the next few paragraphs.

Determination of the Characteristic Radius

It is important to note that ω_c characterizes the frequency dependent line performance, and that to compute ω_c, only the kinematic viscosity, line geometry, and steady flow laminar velocity profile need be known. Presuming that $\omega_c = \omega_{c_x}$ is known for a line of arbitrary but constant axial cross section an equivalent circular line containing the same fluid is sought. The characteristic frequency of the circular line is

$$\omega_{c_c} = \frac{R_{v_c}}{L_{v_c}} = \frac{6\nu}{r_o^2} \tag{83}$$

Setting $\omega_{c_c} = \omega_{c_x}$, the radius of an equivalent circular line, called the characteristic radius, is easily found to be

$$r_c = \sqrt{6\nu/\omega_{c_x}} \tag{84}$$

Since no additional restrictions have been placed on the arbitrary line (i.e., neither the flow areas nor hydraulic diameters are assumed equal), equation (84) implies that for each arbitrary line there exists a unique equivalent circular line. The equivalent circular line will have approximately the same normalized frequency dependent behavior as the arbitrary line since the characteristic frequencies are equal. The characteristic radius is roughly analogous to the hydraulic radius used in steady flow problems.

Comparison of Characteristic and Hydraulic Radii

Healey and Carlson [13] used the classical hydraulic radius (based on the hydraulic diameter) for rectangular lines,

$$r_h = \frac{2A}{P_w} = \frac{bh}{b+h} = \frac{Dh}{2} \tag{85}$$

together with Nichols' equations for circular lines [3] to estimate the frequency response of blocked pneumatic lines of rectangular cross section. These results were then compared with the results predicted by the rectangular line theory of Schaedel [4] and with their own experimental data. The experimental data and predictions using Schaedel's theory were in excellent agreement for all aspect ratios tested (a=1,2,3,4,5). Using r_h and Nichols' equations for circular lines yielded good agreement with the data and with Schaedel's theory for aspect ratios of 2, 3, and 4; however, at a=1 and a=5 significant differences were observed between the predicted downstream amplitude response using r_h and the measured response.

Using the characteristic radius, equation (84), together with Nichols' theory, the normalized attenuation $\alpha\lambda$ vs ω was obtained for aspect ratios a = 1, 3, 5, and 10 and the results plotted in Figure 20. For comparison, predictions using r_h and Nichols' theory as in [13], and using Schaedel's theory are also plotted. The differences between Schaedel's results and those using r_c are so small that they cannot be seen on Figure 20. It may be concluded that the use of r_c gives much better agreement with Schaedel's theory and consequently with the experimental data of [13], than does the use of r_h. It can

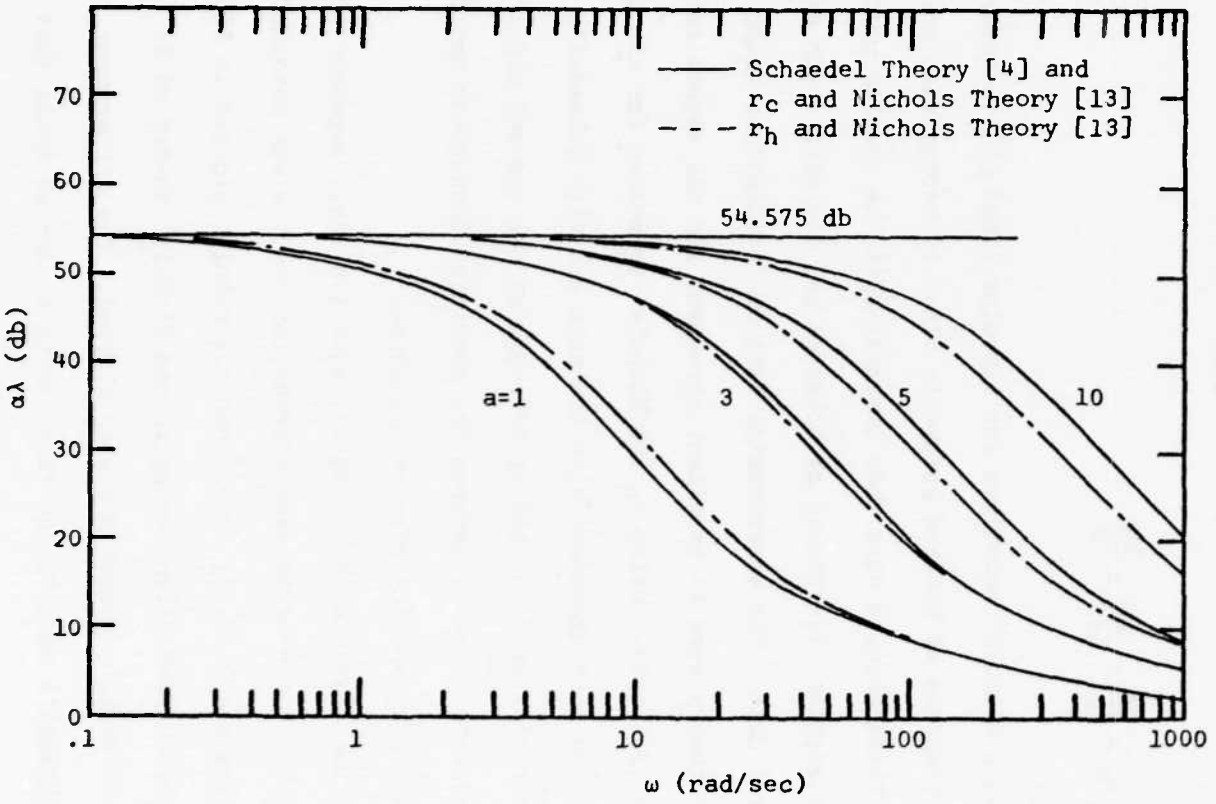

Figure 20. Comparison of Attenuation Per Line Wavelength of Rectangular Lines

also be seen that the use of hydraulic radius predicts too much attenuation per line wavelength for a=1 and not enough for a≥3. The difference increases with aspect ratio above a=3.

A similar comparison is presented for annular lines of $r^* = 0$, 0.1, 0.5, and 0.8 in Figure 21. At $r^*=0$, $r_c = r_h = r_o$ and Nichols' curve for circular lines is recovered. For $r^*>0$, the attenuation predicted using r_h and Nichols' theory is less than that predicted using either r_c and Nichols' theory or the exact annular theory given in Section II while the latter two approaches are in excellent agreement. The difference in predicted performance based on r_c and r_h continue to diverge with increasing radius ratio.

It is of interest to compare the hydraulic radius r_h and the characteristic radius r_c of a rectangular line, for a practical range of aspect ratio, Figure 22. The two approaches yield the same equivalent circular line at a=2.3 ($r_c=r_h$), and are nearly equal over the range $2 \leq a \leq 4$. However, the divergence of r_c and r_h away from a=2.3 is clearly seen. The circular radius required to give the same flow area, denoted r_A is defined as

$$r_A = \sqrt{A/\pi} \tag{86}$$

and is used to normalize both r_h and r_c. Similar results are plotted for annular lines in Figure 23. It can be seen that the ratio r_c/r_h decreases rapidly from unity, where $r^*=0$, and $r_c = r_h = r_A$. The area of the equivalent circular line using the characteristic radius is approximately 60% of that obtained using the hydraulic radius for $r_i^* \geq 0.2$.

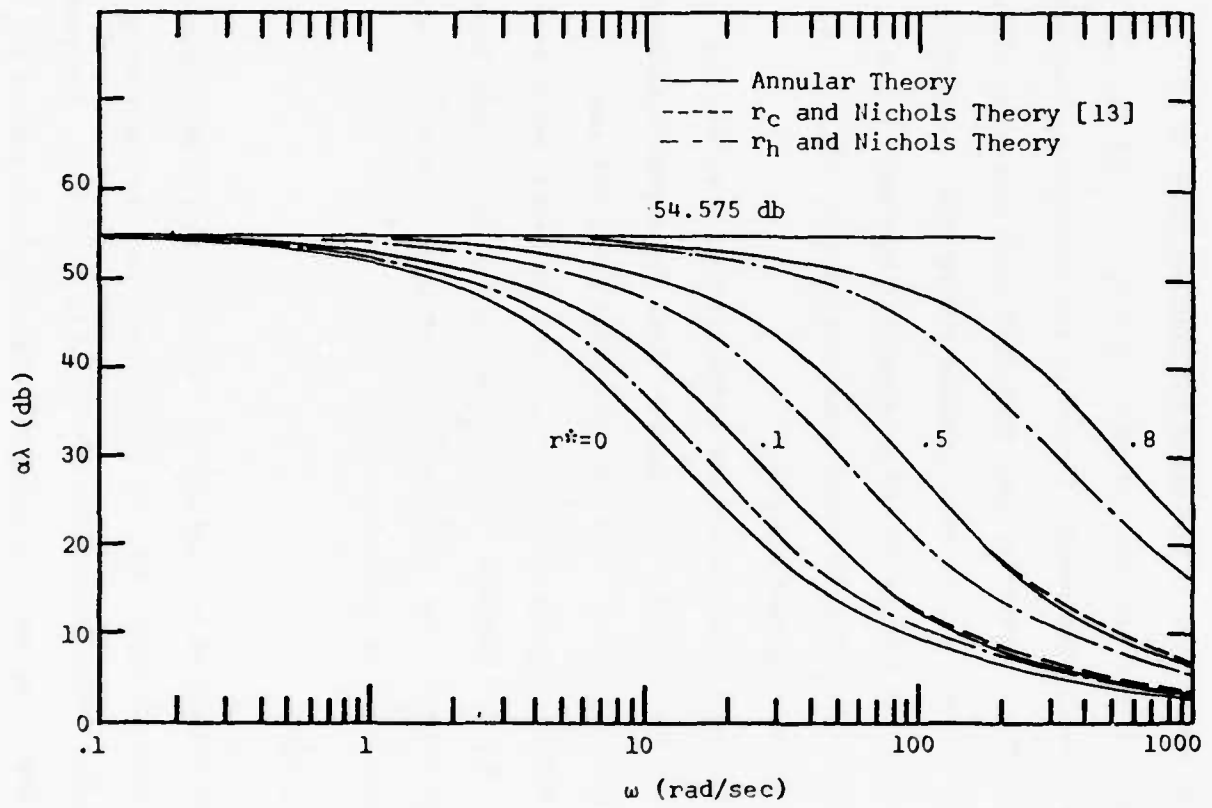

Figure 21. Comparison of Attenuation Per Line Wavelength of Annular Lines

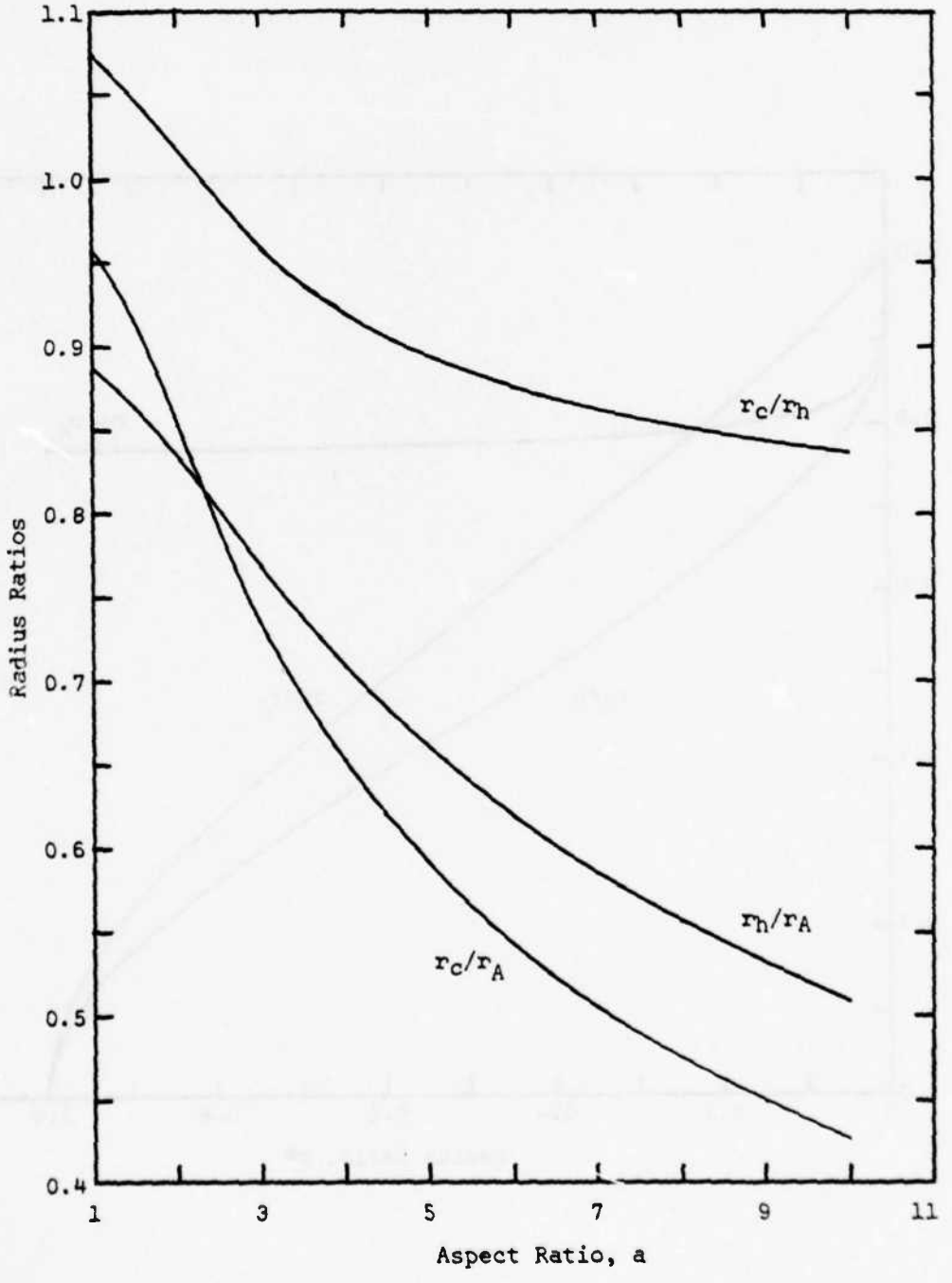

Figure 22. Radius Ratios of Rectangular Lines

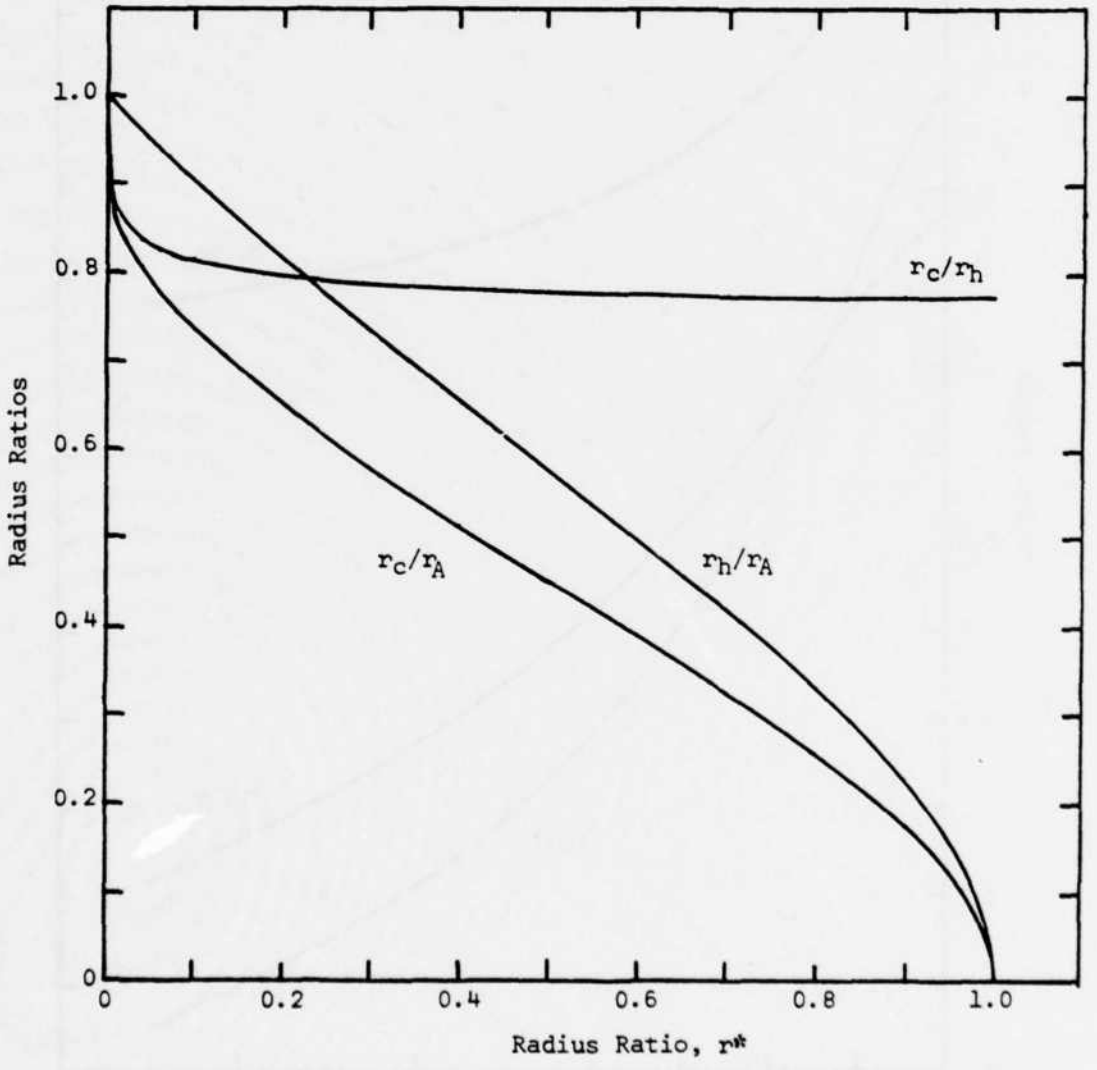

Figure 23. Radius Ratios of Annular Lines

In principle, if the frequency dependence of lines of arbitrary axial cross section may be correlated as above using ω_c, then an approximate impedance match may be found when it is necessary to join lines of different axial cross sections, as discussed in the next few paragraphs.

Impedance Matching

It is of practical importance to terminate a transmission line in its characteristic impedance or admittance since such a termination implies no reflections. Minimizing reflected signal strength is synonymous with increasing the efficiency of the line in transmitting the desired signal. Thus, it is appropriate to discuss impedance matching when lines of different axial cross section are to be joined. Such circumstances occur quite often in fluidic applications where circular lines feed fluidic components whose basic flow regions are rectangular due to laminate techniques in component fabrication. The joining of flow regions of different axial cross section may also be found in aircraft hydraulic systems.

If, for the present, we ignore the junction itself and concentrate on matching the characteristic impedance of transmission lines of different cross section, it would seem appropriate to require the characteristic frequencies to be matched.

The modulus and phase angle of the characteristic admittance ratio for circular, rectangular and annular lines versus ω/ω_c are plotted in Figures 24 and 25, respectively. Again it is seen that lines with the same ω_c exhibit approximately the same frequency dependence. The admittance ratio of rectangular lines is within 4% of that of circular

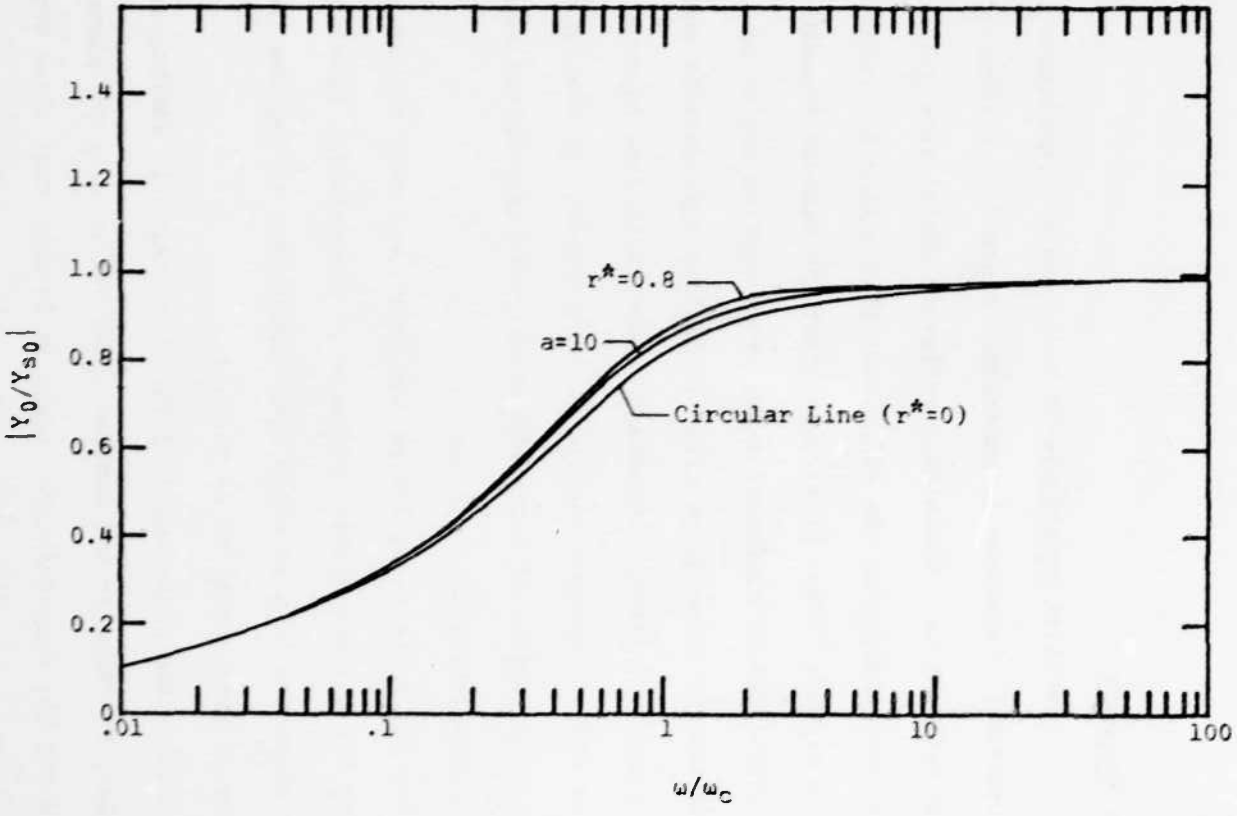

Figure 24. Characteristic Admittance Ratio for Circular, Rectangular and Annular Lines

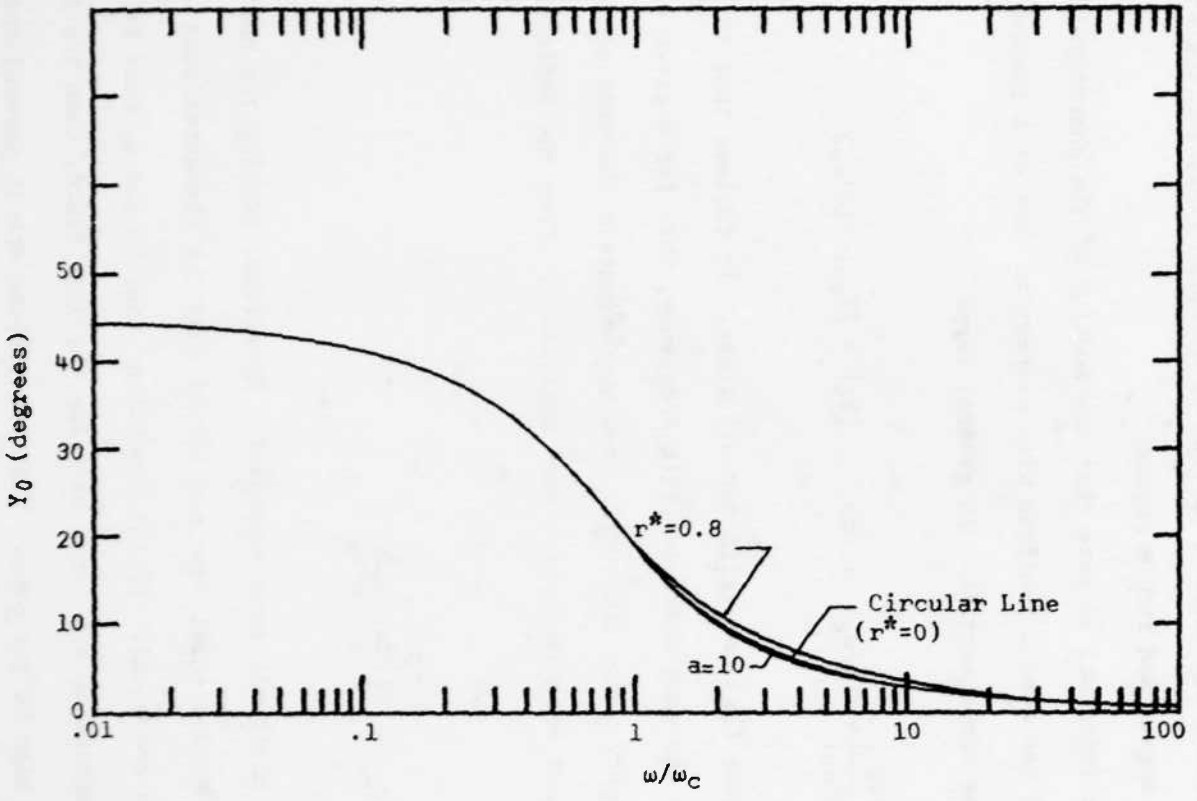

Figure 25. Phase Angle of Characteristic Admittance for Circular, Rectangular and Annular Lines

lines at aspect ratios $a \leq 10$, and the admittance ratio of annular lines is within 6% of that of circular lines for radius ratios $r^* \leq 0.8$. At lower aspect or radius ratios, these percentages decrease. The phase angle of the admittance vs ω/ω_c for both rectangular and annular lines is within 1.5 degrees of that of circular lines for the same ranges of aspect and radius ratios.

It is important to note that the modulus of the characteristic admittance has been normalized with respect to that of a lossless line of the same cross section. In general terms

$$\left|\frac{Y_0}{Y_{s0}}\right| \approx f(\omega/\omega_c) \qquad \text{or} \qquad |Y_0| \approx |Y_{s0}| \cdot f(\omega/\omega_c) \tag{87}$$

and equations (87) are valid for all lines. It follows that if two lines have the same characteristic frequency, then for a given excitation frequency ω the lines will have approximately the same admittance ratio but not necessarily the same admittance. From the definition of Y_{s0},

$$Y_{s0} = \sqrt{\frac{C_a}{L_a}} = \frac{A}{\rho^* c_a} \tag{36}$$

and Y_{s0} is obviously area dependent. Therefore, setting the characteristic frequencies equal does not insure that the characteristic admittances are equal. If the conditions that Y_0 and ω_c must be the same are imposed on two lines carrying the same fluid, then the flow areas must also be the same. These conditions are in general incompatible except for the special case when the two lines are identical. The

conditions amount to requiring that $r_A = r_c$ when lines of circular and noncircular cross section are to be joined. From Figure 23, it is seen that for annular lines $r_A = r_c$ only when $r^* = 0$; for rectangular lines, Figure 22, this condition is never achieved. It is concluded that the characteristic admittance (or impedance) of lines of different cross section carrying the same fluid cannot be matched at each and every physical frequency ω. The closest match to a circular line is obtained when $r_A \approx r_c$. ($r^* \to 0$ or $a \to 1$, for annular or rectangular lines.)

In practice, the most common constraint encountered is the specification of a steady mean flow through which the signals are to be transmitted. This constraint is equivalent to requiring that the flow continuity is maintained. It follows that for a given fluid two lines of the same flow area have the same lossless admittance. At a specified frequency ratio ω/ω_c, the two lines will also have approximately the same frequency dependent characteristic admittance. However, the characteristic frequencies are not the same and, consequently, neither are the physical frequencies for which the admittances are equal.

The characteristic frequency of noncircular lines will be higher than that of circular lines of the same cross-sectional area. For any excitation frequency ω, this implies that the characteristic admittance (impedance) of noncircular lines will be lower (higher) than for circular lines of the same area, and the designer is unfortunately faced with the resultant mismatch. Nevertheless, the characteristic frequency (or radius) of the noncircular line together with the circular line theory may be used in a simple procedure to predict the performance of the noncircular line at any desired frequency.

The ratios $\omega_{c_r}/\omega_{c_c}$ and $\omega_{c_n}/\omega_{c_c}$ are plotted in Figures 26 and 27 for rectangular and annular lines, respectively, assuming equal flow areas. Similar curves could be constructed for any noncircular line. The characteristic frequency of circular lines is easily determined ($\omega_{c_c} = 6\pi\nu/A_c$) and from curves similar to Figures 26 and 27 the characteristic frequency (ω_c) of the particular noncircular line is determined. For the physical frequency of interest, the frequency ratio ω/ω_c is computed and any desired performance parameter such as $\alpha\lambda$, Figure 19, or $|Y_0/Y_{s0}|$, Figure 24, is easily obtained from the circular line performance curves. It is emphasized that laminar mean flow is assumed; combined turbulent mean flow and laminar oscillatory flow is discussed in Section V.

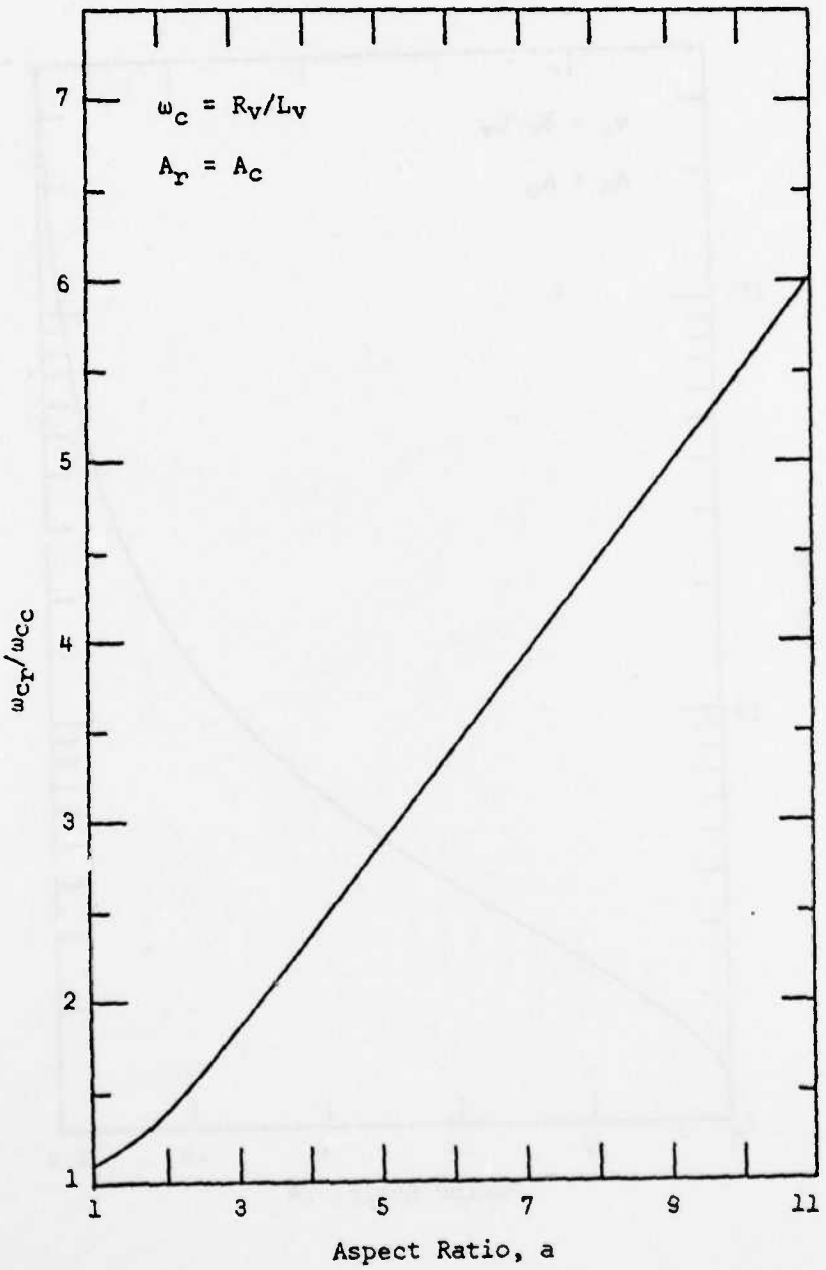

Figure 26. Ratio of Characteristic Frequencies of Rectangular to Circular Lines

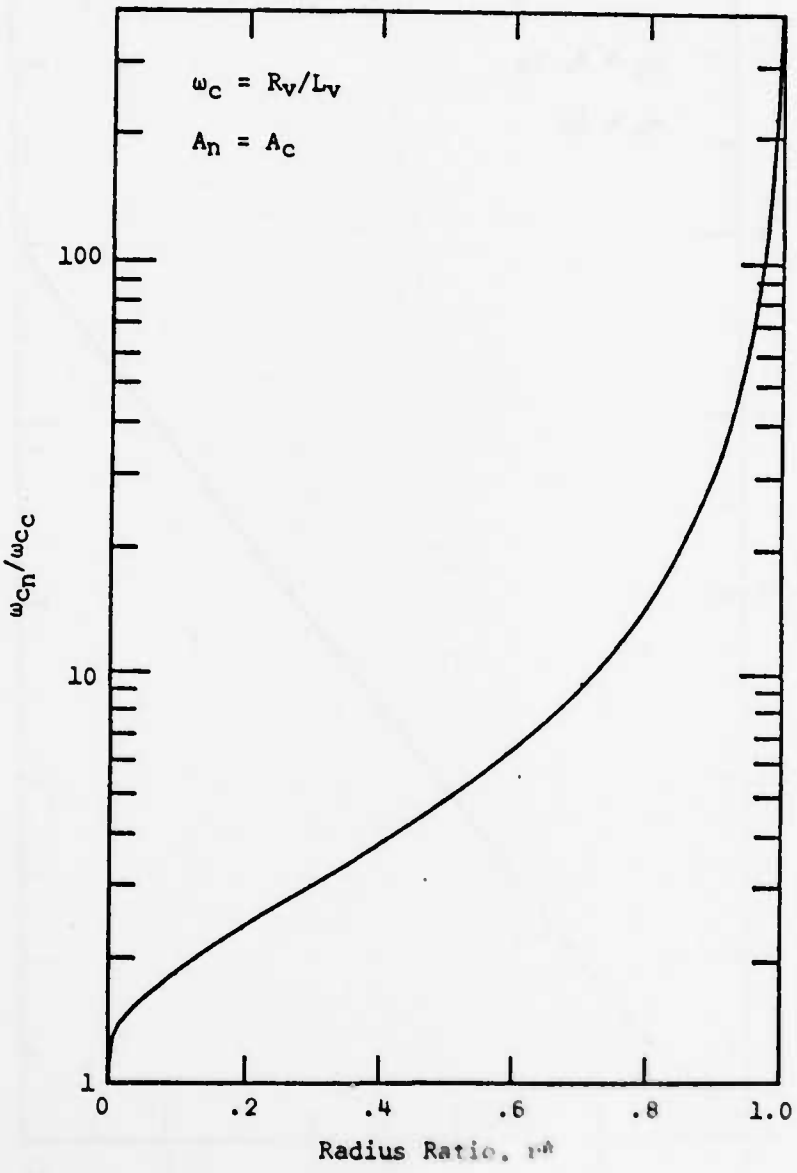

Figure 27. Ratio of Characteristic Frequencies of Annular to Circular Lines

IV. The Transient Response of Noncircular Fluid Transmission Lines

The transient response of fluid transmission lines of circular cross section was obtained by Brown [2], who derived the propagation operator and characteristic impedance of an infinitely long uniform rigid line in the Laplace domain for both compressible and incompressible fluids. Brown's solution is identical to that of Iberall [1] and Nichols [3] frequency domain models for the special case of sinusoidal excitation of the circular line. Subsequently, Karam [19,20] developed a simplified solution for the transient response of circular lines after transforming approximate high and low frequency domain models into the time domain and then observing a basic similarity between the transformed solutions. Karam's solution is more easily applied than that of Brown [2], and may be used to obtain the impulse and step responses of semi-infinite fluid-filled circular lines with good accuracy and without the aid of a computer.

In Section III, a method of expressing the frequency dependence of noncircular lines entirely in terms of equivalent circular lines was presented, and results were obtained for rectangular and annular lines over a wide range of aspect and radius ratio. The primary purpose of this section is to present a method of transforming the frequency response of noncircular lines into the time domain. The analytical approach essentially combines the approaches of [2,3,20] and that of the previous section, and results in a simple but complete solution of the step response of noncircular lines.

Frequency Domain Equations

The exact analytical expressions for the parameters Z, Y, Γ, and Y_0 which characterize the performance of a fluid transmission line are relatively cumbersome to use in the frequency or Laplace domain. Furthermore, it has been observed that the time transforms associated with these parameters have not yielded closed form analytical expressions over any of the frequency or Laplace domain, even for the simple case of circular transmission lines. The mathematical difficulties may be traced directly to the underlying frequency or Laplace domain solutions, which contain ratios of Bessel functions. These ratios are not thus far expressible in a form amenable to transformation into the time domain. Further, according to Sneddon [21], it is unlikely that the Bessel solutions will ever be totally transformed. Instead, high and low frequency approximations are made, and these approximations are then transformed into the time domain. In the mid-frequency range, very complicated numerical techniques have been used to accomplish the transformation [22]. Alternately, the transient response in the mid-frequency range may be approximated in the time domain itself, as was done by Karam [20].

The general approach taken herein will be to partition the frequency domain into three regions, to analyze the equivalent electrical circuit of a general transmission line in each of these regions, and then to express the results in the time domain. In this approach, the text by Weber [11] is especially useful.

The three frequency regions are defined with reference to the characteristic frequency, $\omega_c = R_v/L_v$, as follows: low frequency

($\omega << \omega_c$), mid-frequency ($\omega = \omega_c$), and high frequency ($\omega >> \omega_c$). The characteristic frequency ratio $\omega/\omega_c = \omega L_v/R_v$ may be thought of as a frequency dependent (AC) Reynolds number. At low frequency ratios viscous flow effects are prevalent while at high frequency ratios inertial effects prevail. In the mid-frequency range viscous and inertial effects are of the same order of magnitude. Similarly, the thermal characteristic frequency $\omega_T = \omega_c/\sigma^2$ roughly divides the heat transfer effects into regions of isothermal behavior, $\omega << \omega_T$ and adiabatic behavior, $\omega >> \omega_T$. Since the Prandtl number (σ^2) is near unity for air (and many other gases) either ω_c or ω_T will suffice as the overall behavioral index, and ω_c has been chosen for this work. For liquids ($\gamma = 1$), there is essentially no dependence on the Prandtl number, since terms in the energy equation containing the Prandtl number are premultiplied by the quantity $(1-\gamma)$. [See, for example, equation (26).]

At low frequencies, the equivalent circuit, Figure 2, is comprised of essentially constant value elements of R, L, and C with G = 0. These values are $R = R_v$, $L = L_v$, and $C = C_i = \gamma C_a$, for any line of constant axial cross section. Using these values in the defining equations of the series impedance and shunt admittance [equations (28) and (29)], together with equations (32) and (34), the low frequency characteristic impedance and propagation operator are easily determined:

$$Y_{0_L} = \sqrt{\frac{Y_L}{Z_L}} \simeq \sqrt{\frac{\gamma C_a \omega}{2R_v}}\,(1+j) = Y_{s_0}\sqrt{\frac{\gamma}{2K_L}}\sqrt{\frac{\omega}{\omega_c}}\,(1+j) \qquad (88)$$

$$\Gamma_L = \sqrt{Z_L Y_L} = \alpha_L + j\beta_L \simeq \sqrt{\frac{\gamma R_v C_a \omega}{2}}\,(1+j) \qquad (89)$$

Therefore, the low frequency attenuation, α_L, and phase angle increase, β_L, are

$$\alpha_L = \sqrt{\frac{\gamma}{2}} \cdot \sqrt{R_v C_a \omega} = \frac{1}{c_a} \cdot \sqrt{\frac{\gamma}{2} K_L} \cdot \sqrt{\omega \omega_c} \tag{90}$$

$$\beta_L = \alpha_L \tag{91}$$

At high frequencies, the inductance and capacitance approach their adiabatic values. However, the resistance and conductance are frequency dependent and become large with frequency. Karam and Franke [9] have developed approximations for the high frequency circuit components, which are rewritten in terms of ω_c as follows:

$$R_H = \frac{1}{2} L_a \sqrt{K_L \omega \omega_c} \tag{92}$$

$$L_H = L_a = \rho^*/A \tag{93}$$

$$G_H = \frac{\gamma - 1}{2\sigma} C_a \sqrt{K_L \omega \omega_c} \tag{94}$$

$$C_H = C_a = A/\gamma p^* \tag{95}$$

In the high frequency region $R \ll \omega L$ and $G \ll \omega C$. Using these inequalities, the high frequency attenuation per unit length, α_H, and phase angle increase per unit length, β_H, are approximately [11]:

$$\alpha_H = \frac{L_H G_H + R_H C_H}{2\sqrt{L_H C_H}} \tag{96}$$

$$\beta_H = \omega \sqrt{L_H C_H} \tag{97}$$

Substituting equations (92) through (95) into equations (96) and (97),

$$\alpha_H = \frac{1}{4}\left[1 + \frac{\gamma-1}{\sigma}\right]\sqrt{R_v C_a \omega} = \frac{1}{4c_a}\left[1 + \frac{\gamma-1}{\sigma}\right]\sqrt{K_L \omega \omega_c} \tag{98}$$

$$\beta_H = \omega\sqrt{L_a C_a} = \frac{\omega}{c_a} \tag{99}$$

It is important to note that the foregoing development is applicable to any fluid transmission line of arbitrary but constant axial cross section.

From equations (90) and (96), it is seen that both α_L and α_H are of the form $\alpha = K\sqrt{\omega}$, where K is constant, and such a line has a rather simple time domain solution.

Time Domain Equations

The characteristic time t_c is defined as the inverse of the characteristic frequency ($t_c = 1/\omega_c$), and the time domain is divided into three regions corresponding to the previously defined frequency regions. Thus, the short time region ($t << t_c$) corresponds to the high frequency region ($\omega >> \omega_c$) and the long time region ($t >> t_c$) corresponds to the low frequency region ($\omega << \omega_c$).

Metzger and Vabre [23] have shown that when the high frequency attenuation is of the form $\alpha_H = K\sqrt{\omega}$, the step response P_{r_H} to a step input U(t) at ℓ inches down a semi-infinite line is

$$P_{r_H} = \text{erfc}\left[\frac{1}{2}\left(\frac{\alpha_H^2 \ell^2}{\pi f(t-T)}\right)^{1/2}\right] U(t-T) \tag{100}$$

where $U(t) = |P_s|u(t)$, $u(t)$ is a unit step input, $T = \ell/c_a$ is the adiabatic delay time, and f is the signal frequency. For long times, Karam [20] has shown that the unit step response may be written as

$$P_{r_L} = \text{erfc}\left[\frac{1}{2}\left(\frac{\alpha_L^2 \ell^2}{\pi f t}\right)^{1/2}\right] U(t) \tag{101}$$

Since for long times $t \simeq t-T$, evidently the unit step responses for long and short times are governed by the same relation. It seems reasonable to assume that the step response will retain the same form in the mid-frequency range. Thus, in general

$$P_r = \text{erfc}\left[\frac{1}{2}\left(\frac{\alpha^2 \ell^2}{\pi f(t-T)}\right)^{1/2}\right] U(t-T) \tag{102}$$

It is noted that this assumption avoids the transformation of the mid-frequency region into the time domain. Brown and Nelson [22] achieved some success in the mid-frequency range for liquid-filled circular lines, but the method was numerical and was reportedly quite complex and sensitive. The assumption that the attenuation is of the form $\alpha = K\sqrt{\omega}$ in the mid-frequency range is a convenience which allows the entire time domain solution to be expressed as a single complementary error function. The "constant" K is actually frequency-dependent in the mid-range. Karam [20] used the time transform of the known low and high frequency asymptotes obtained from the equivalent circuit approximations and connected these with a logarithmic straight line of the form $\log_{10}(\alpha/\alpha_H) = A + B \log_{10} \tau'$, where $\tau' = tv/r_o^2$. This straight line patch is therefore made in the time domain and any correspondence with the

frequency domain is lost in the mid-frequency range. Karam approximated the transient behavior of α/α_H for circular lines as [20]:

$$\frac{\alpha}{\alpha_H} = \begin{cases} 1 & \text{for } \tau' \leq 0.0125 \\ K(\tau')^m & \text{for } 0.0125 \leq \tau \leq 1.25 \\ \dfrac{\sqrt{8\gamma}}{1 + \dfrac{\gamma-1}{\sigma}} & \text{for } \tau' \geq 1.25 \end{cases} \tag{103}$$

where

$$m = \frac{1}{2} \log_{10} \left[\frac{\sqrt{8\gamma}}{1 + \dfrac{\gamma-1}{\sigma}} \right] \quad \text{and} \quad K = (0.0125)^{-m}$$

A qualitative plot of α/α_H versus τ is given in Figure 28, along with a representation of Nichols' transformed solution. It is emphasized that the dotted line of Figure 28 representing Nichols' solution is only qualitative; if the exact transform of Nichols' solution were known, there would be no need for the straight line approximation. Karam defines $\tau_0' = Tv/r_o^2$ and expresses the unit step response as

$$P_r = \text{erfc} \left\{ \frac{\frac{1}{2}\left[1 + \dfrac{\gamma-1}{\sigma}\right]\left[\dfrac{\alpha}{\alpha_H}\right]\tau_0'}{\sqrt{\tau'-\tau_0'}} \right\} U(\tau'-\tau_0') \tag{104}$$

This solution gives one of the simplest representations of the step response of circular lines and shows very good agreement with the much more complicated analytical and numerical solution of Brown and Nelson [22] for liquid lines. Karam's solution is also in good agreement with his own experimental data and that of Kantola [24] for air-filled lines. The pressure step response of liquid-filled lines obtained using the

AD-A055 854 AIR FORCE FLIGHT DYNAMICS LAB WRIGHT-PATTERSON AFB OHIO F/G 17/2
THE SMALL SIGNAL RESPONSE OF FLUID TRANSMISSION LINES, INCLUDIN--ETC(U)
MAR 78 E F MOORE

UNCLASSIFIED AFFDL-TR-78-12 NL

2 OF 2
AD A055 854

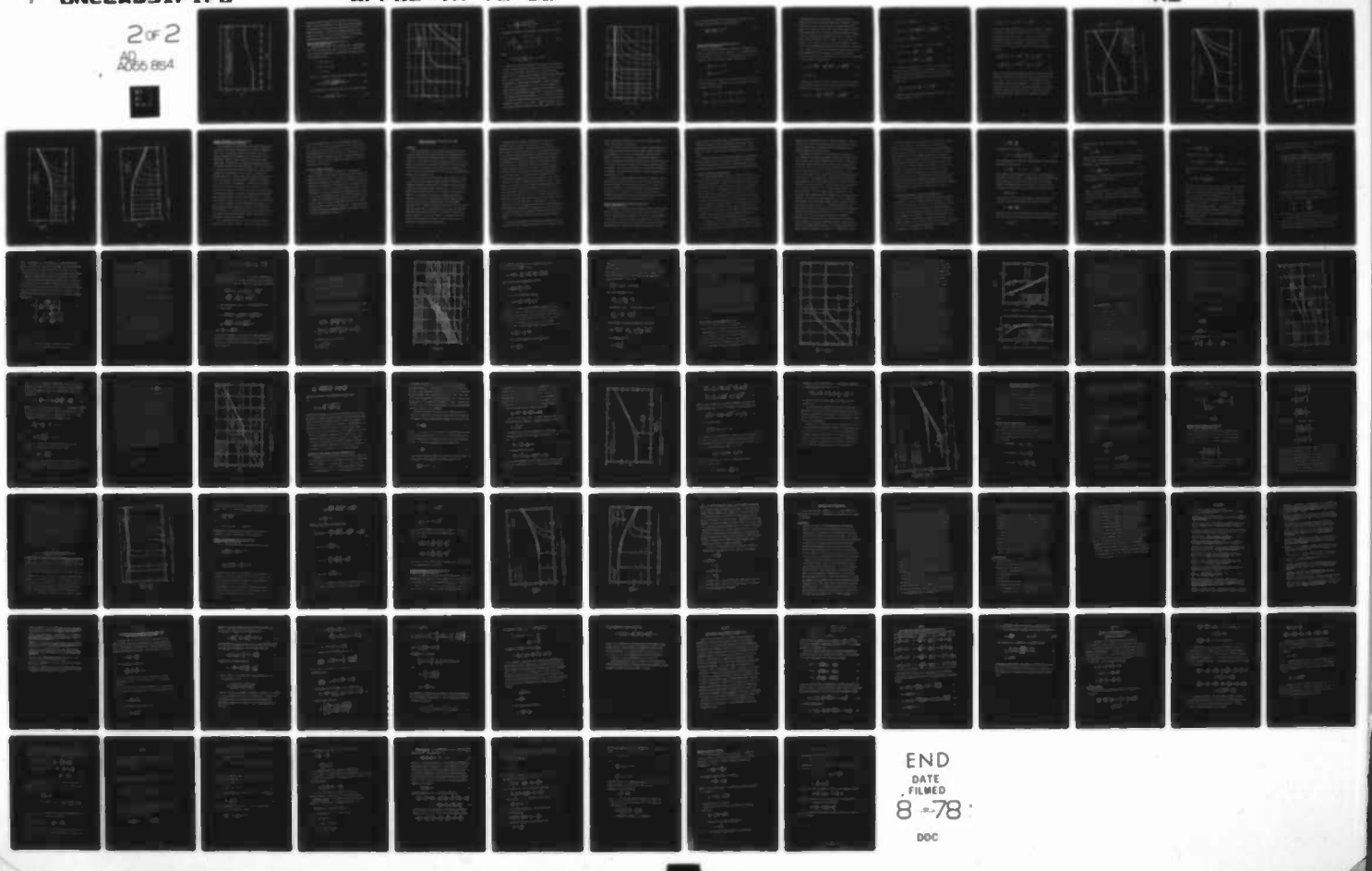

END
DATE FILMED
8-78
DDC

2 OF 2

AD
A055 854

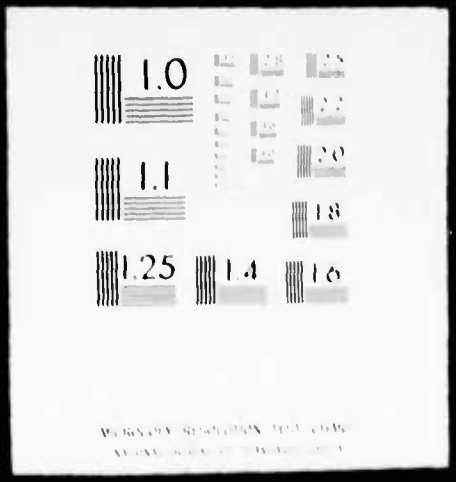

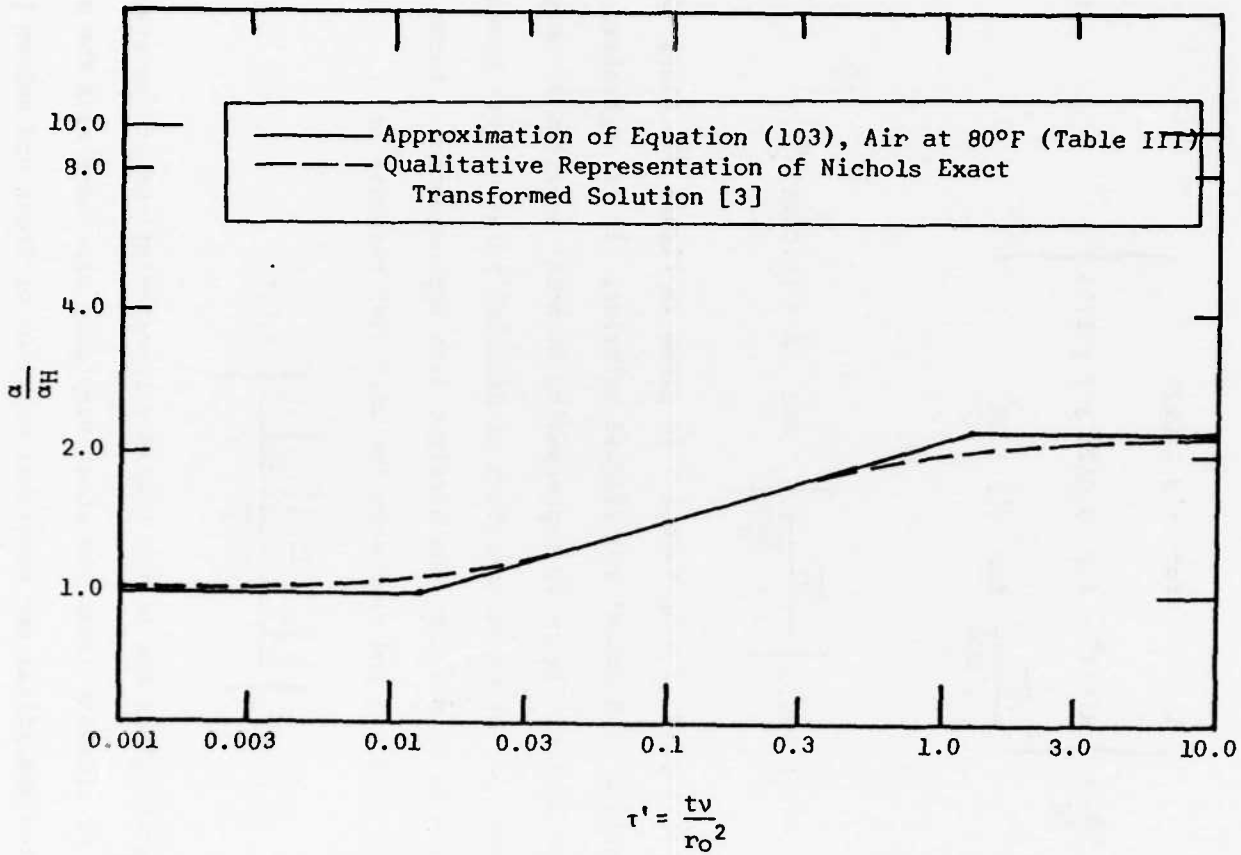

Figure 28. Logarithmic Approximation of Attenuation Ratio for Circular Lines

results of Brown and Nelson [22] and of Karam [20] are plotted in Figure 29 for selected values of τ_0'. Karam's results are applicable to liquids when γ is unity and the fluid bulk modulus K_B is used to compute the celerity. In [22,24], the nondimensional time is also defined as $\tau' = t\nu/r_o^2$. It is seen from Figure 29 that the predicted responses are in good agreement over a wide range of τ_0'.

Pressure (Flow) Response of Noncircular Lines to a Step Input of Pressure (Flow)

Whereas Karam and others used the quantity ν/r_o^2 to nondimensionalize time, the characteristic time, $t_c = 1/\omega_c$, will be used herein. Thus, τ' and τ_0' are redefined and a characteristic time equal to unity is introduced as follows:

$$\begin{aligned} \tau &= \omega_c t = t/t_c = 6\tau' \\ \tau_0 &= \omega_c T = T/t_c = 6\tau_0' \\ 1 &= \omega_c t_c = t_c/t_c \end{aligned} \tag{105}$$

In terms of the redefined nondimensional times, equation (104) becomes

$$P_r = \operatorname{erfc}\left\{\frac{\frac{1}{2}\left[1 + \frac{\gamma-1}{\sigma}\right]\left[\frac{\alpha}{\alpha_H}\right]\tau_0}{\sqrt{6(\tau-\tau_0)}}\right\} U(\tau-\tau_0) \tag{106}$$

and the expression for the long and short time step responses become

$$P_{r_L} = \operatorname{erfc}\left\{\frac{1}{2}\left(\frac{\gamma\tau_0^2}{\tau-\tau_0}\right)^{1/2}\right\} U(\tau-\tau_0) \tag{107}$$

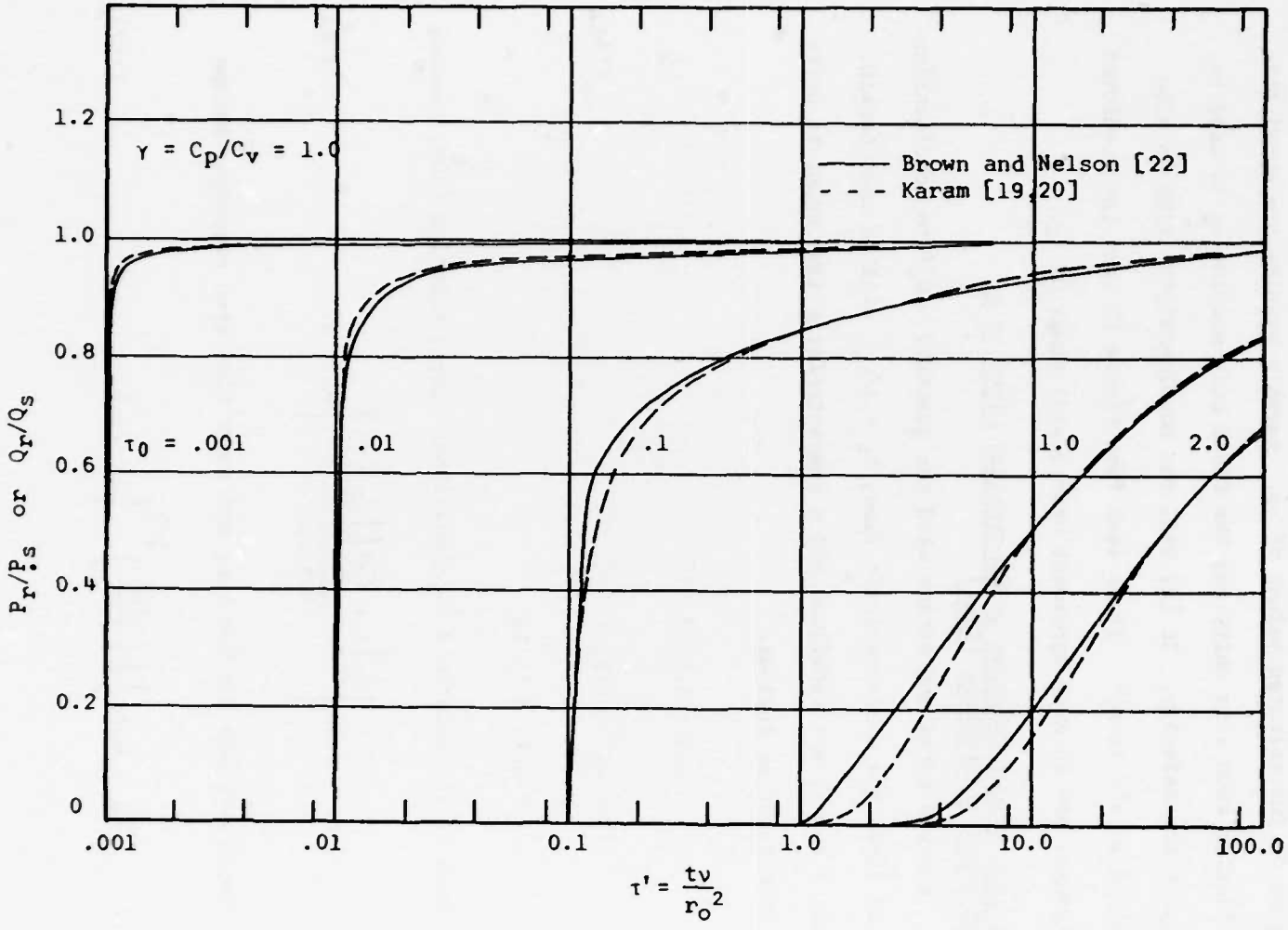

Figure 29. Comparison of Pressure (Flow) Response to a Unit Step Input of Pressure (Flow) for Liquid-Filled Circular Lines

$$P_{r_H} = \operatorname{erfc}\left\{\frac{1}{2}\left[\frac{\left(1 + \frac{\gamma-1}{\sigma}\right)^2 \tau_0^2}{6(\tau-\tau_0)}\right]^{1/2}\right\} U(\tau-\tau_0) \qquad (108)$$

The logarithmic straight line approximation may be rewritten as follows:

$$\frac{\alpha}{\alpha_H} = \begin{cases} 1 & \text{for } \tau \leq 0.1 \\ K\tau^m & \text{for } 0.1 \leq \tau \leq 10 \\ \dfrac{\sqrt{8\gamma}}{1 + \frac{\gamma-1}{\sigma}} & \text{for } \tau \geq 10 \end{cases} \qquad (109)$$

where

$$m = \frac{1}{2} \log_{10}\left(\frac{\sqrt{8\gamma}}{1 + \frac{\gamma-1}{\sigma}}\right) \quad \text{and} \quad K = (0.1)^{-m}$$

Equations (106) and (109) approximately describe the step response of lines of constant axial cross section, either circular or noncircular. The key point is the definition and use of ω_c, since the ratio ω/ω_c (hence, $\tau = t/t_c$) characterizes the response of the selected transmission line. For long times, say one decade or more above t_c ($\tau \geq 10$), the line response is characterized by predominantly viscous, isothermal behavior. At one decade below t_c ($\tau \leq 0.1$) the line performance is nearly inertial and adiabatic. Furthermore, the step response of all lines of the same nondimensional delay time $\tau_0 = \omega_c T$ may be represented by a single curve when plotted against $\tau = \omega_c t$. Equation (106) versus τ is plotted in Figure 30 for several values of τ_0. The fluid has been assumed to be air at 80 F ($\gamma = 1.4017$). Figure 30 represents either the pressure response downstream to an upstream pressure step input or

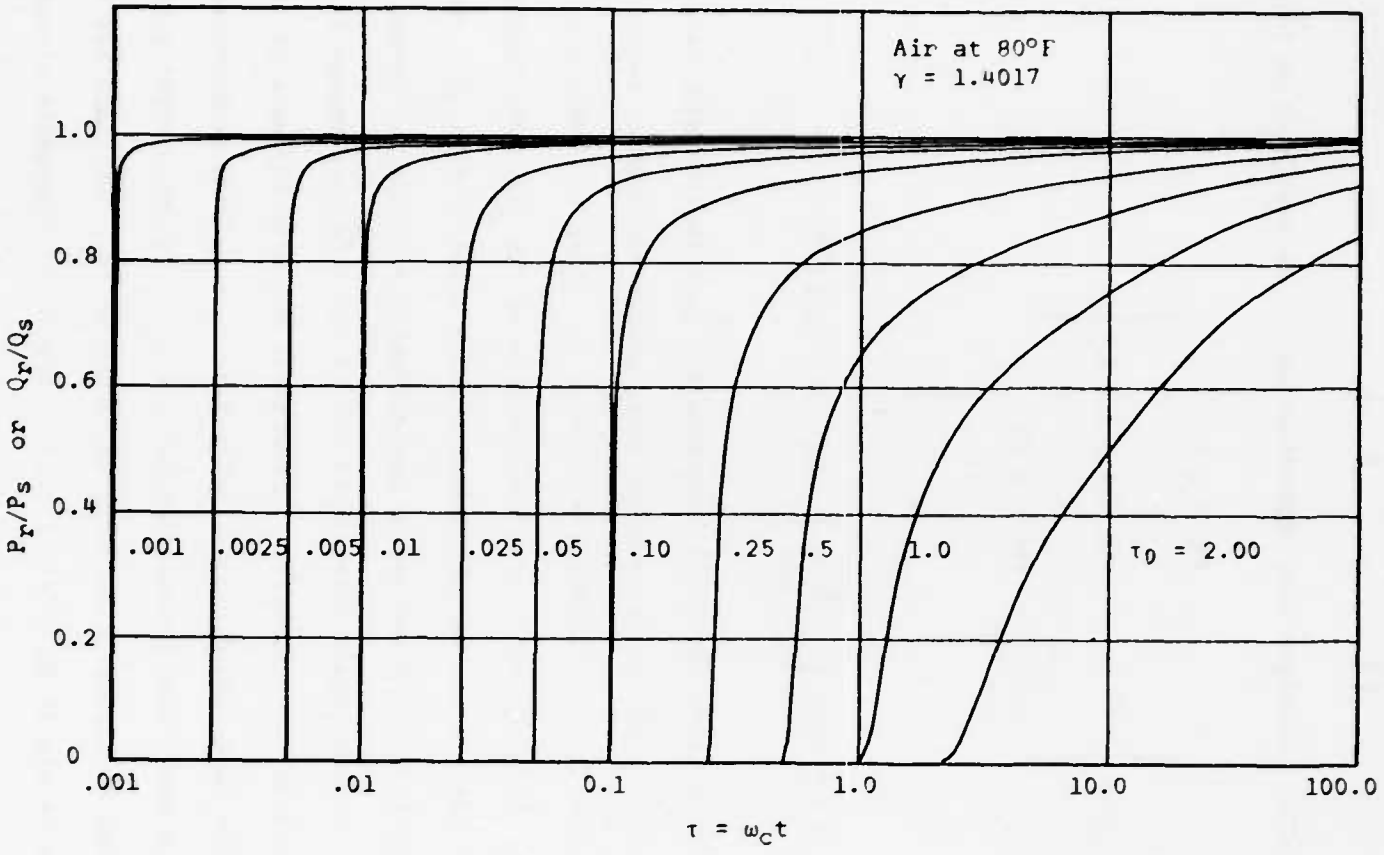

Figure 30. Pressure (Flow) Response to a Step Input of Pressure (Flow) for Air-Filled Lines of Arbitrary Cross Section

the flow response downstream to an upstream flow step input, i.e., the equivalent transfer function in the Laplace domain is

$$\frac{P_r(s)}{P_s(s)} = \frac{Q_r(s)}{Q_s(s)} = \frac{1}{s} e^{-\ell\Gamma(s)} \tag{110}$$

Pressure (Flow) Response of Noncircular Lines to a Step Input of Flow (Pressure)

Two other transfer functions are of interest in determining the response of semi-infinite lines. These are: (1) the pressure response to a step input of flow, and (2) the flow response to a step input of pressure. The respective Laplace transfer functions are:

$$\frac{P_r(s)}{Q_s(s)} = \frac{1}{s} Z_o(s) e^{-\ell\Gamma(s)} \tag{111}$$

$$\frac{Q_r(s)}{P_s(s)} = \frac{1}{s} Y_o(s) e^{-\ell\Gamma(s)} \tag{112}$$

and it is noted that a convolution integral may be used to solve for the time domain response. Karam [20] has used the following equations to approximate these responses:

$$\frac{P_r}{Q_s}(\tau) = \int_0^\tau Z_o(\lambda) \frac{P_r}{P_s}(\tau-\lambda)d\lambda \cong \frac{P_r}{P_s}(\tau) \int_0^\tau Z_o(\lambda)d\lambda \tag{113}$$

$$\frac{Q_r}{P_s}(\tau) = \int_0^\tau Y_o(\lambda) \frac{P_r}{P_s}(\tau-\lambda)d\lambda \cong \frac{P_r}{P_s}(\tau) \int_0^\tau Y_o(\lambda)d\lambda \tag{114}$$

The approximations given by the terms on the right hand side of equations (113) and (114) are made to simplify the results by avoiding computations of the convolution integral. These approximations are based on the observation that $P_r/P_s(\tau)$ rises fairly rapidly after the nominal time delay T and is essentially constant thereafter, especially for small τ, whereas $Z_o(Y_o)$ is essentially constant for small τ, and varies inversely (directly) as $\sqrt{\tau}$ for large τ. It can be seen in Figure 30 that for large τ_0, $P_r/P_s(\tau)$ does not rise rapidly. Thus the validity of the approximations decreases with increasing τ_0. Fortunately, lines of large τ_0 are not practical transmission lines; this conclusion will be substantiated and illustrated in a subsequent discussion. Using the large and small s approximations of $Z_o(s)$ and $Y_o(s)$, corresponding to short and long time, respectively,

$$Z_{o_L} = \frac{1}{Y_{o_L}} = \sqrt{\frac{Rv}{C_i s}} = \sqrt{\frac{La}{C_a} \cdot \frac{Rv}{\gamma La \cdot s}} = Z_{s_o} \sqrt{\frac{K_L \cdot \omega_c}{\gamma s}} \qquad (115)$$

$$Z_{o_H} = \frac{1}{Y_{o_H}} = Z_{so} \qquad (116)$$

The integrals on the right hand side of equations (113) and (114) may be easily evaluated using the inverse Laplace transform [$\mathcal{L}^{-1}$] and the approximations of equations (115) and (116). Thus

$$\int_0^t Z_{o_L}(\lambda)d\lambda = \mathcal{L}^{-1}\left[\frac{Z_{so}}{s} \cdot \sqrt{\frac{K_L \cdot \omega_c}{\gamma s}}\right] = 2Z_{so} \sqrt{\frac{K_L \cdot \omega_c \cdot t}{\gamma \pi}} \qquad (117)$$

$$\int_0^t Z_{o_H}(\lambda)d\lambda = \mathcal{L}^{-1}\left[\frac{Z_{so}}{s}\right] = Z_{so} \tag{118}$$

$$\int_0^t Y_{o_L}(\lambda)d\lambda = \mathcal{L}^{-1}\left[\frac{Y_{so}}{s}\sqrt{\frac{\gamma s}{k_L \cdot \omega_c}}\right] = Y_{so}\sqrt{\frac{\gamma}{k_L \cdot \omega_c \cdot \pi\tau}} \tag{119}$$

$$\int_0^t Y_{o_H}(\lambda)d\lambda = \mathcal{L}^{-1}\left[\frac{Y_{so}}{s}\right] = Y_{so} \tag{120}$$

For $\tau' = tv/r_o^2$ and $\tau = \omega_c t$ equations (117) and (119) become

$$\int_0^t Z_{o_L}(\lambda)d\lambda = Z_{so}\sqrt{\frac{32\tau'}{\gamma\pi}} = Z_{so}\sqrt{\frac{4k_L\tau}{\gamma\pi}} \tag{121}$$

$$\int_0^t Y_{o_L}(\lambda)d\lambda = Y_{so}\sqrt{\frac{\gamma}{8\pi\tau'}} = Y_{so}\sqrt{\frac{\gamma}{\pi k_L \tau}} \tag{122}$$

It is convenient and more realistic to construct a single continuous function to describe the behavior of the integrals of Z_o and Y_o. Karam [20] has found that equations (118) and (121) may be combined as follows to give a closer approximation of the overall behavior of the integral of Z_o.

$$\frac{1}{Z_{so}}\int_0^t Z_o(\lambda)d\lambda = \left(1 + \frac{32\tau'}{\pi\gamma}\right)^{1/2} = \left(1 + \frac{4k_L\tau}{\gamma\pi}\right)^{1/2} \tag{123}$$

Similarly a continuous function approximating the integral of Y_o is obtained in terms of τ' and τ as

$$\frac{1}{Y_{so}} \int_0^{\tau} Y_o(\lambda)d\lambda = \left(1 + \frac{8\pi\tau'}{\gamma}\right)^{-1/2} = \left(1 + \frac{K_L\pi\tau}{\gamma}\right)^{-1/2} \qquad (124)$$

Equations (123) and (124) versus τ' are plotted in Figure 31, along with the asymptotic limits given by equations (118), (120), (121), and (122), for air-filled circular lines with $\gamma = 1.4017$. It is seen that the two continuous functions of equations (123) and (124) are properly bounded by the respective asymptotes. Using equations (113), (114), (123), and (124) the desired step responses are obtained in dimensionless form as

$$\frac{1}{Z_{so}}\left(\frac{P_r}{Q_s}\right) = \frac{P_r}{P_s}(\tau')\left(1 + \frac{32\tau'}{\pi\gamma}\right)^{1/2} = \frac{P_r}{P_s}(\tau)\left(1 + \frac{4K_L\tau}{\gamma\pi}\right)^{1/2} \qquad (125)$$

$$Z_{so}\left(\frac{Q_r}{P_s}\right) = \frac{P_r}{P_s}(\tau')\left(1 + \frac{8\pi\tau'}{\gamma}\right)^{-1/2} = \frac{P_r}{P_s}(\tau)\left(1 + \frac{K_L\pi\tau}{\gamma}\right)^{-1/2} \qquad (126)$$

Equations (125) and (126) are plotted in Figures 32 and 33, respectively, along with the results of Brown and Nelson [22] for liquid-filled lines ($\gamma = 1$) and $\tau' = t\nu/r_o^2$. It is seen that the two approaches are in good agreement over a practical range of τ'. The above step responses are adapted to non-circular air-filled lines as was done for P_r/P_s, and the results are shown in Figures 34 and 35. In these latter figures, the dimensionless times are based on the characteristic frequency, i.e., $\tau = \omega_c t$.

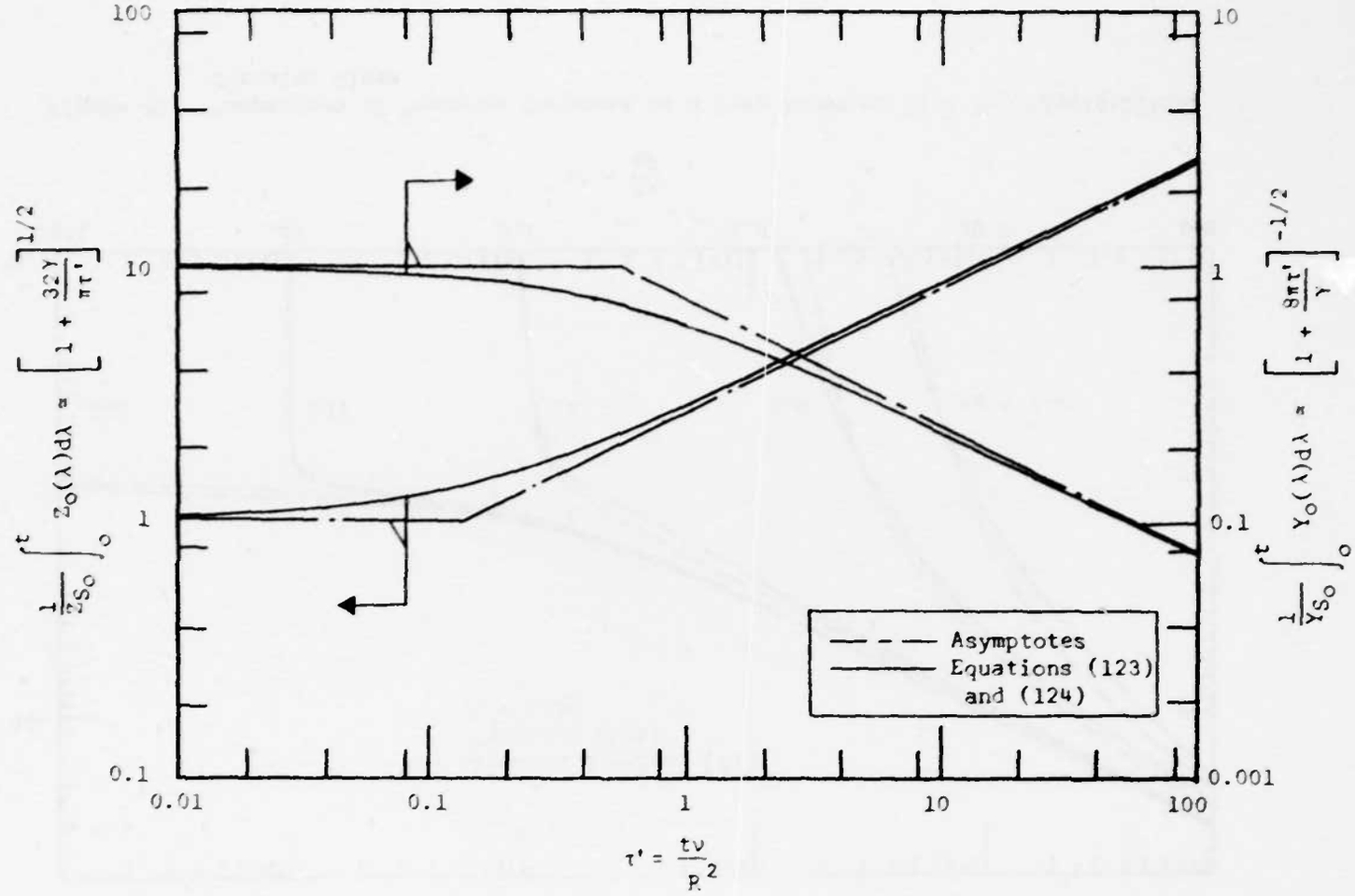

Figure 31. Normalized Approximations of the Integrals of Characteristic Impedance and Admittance

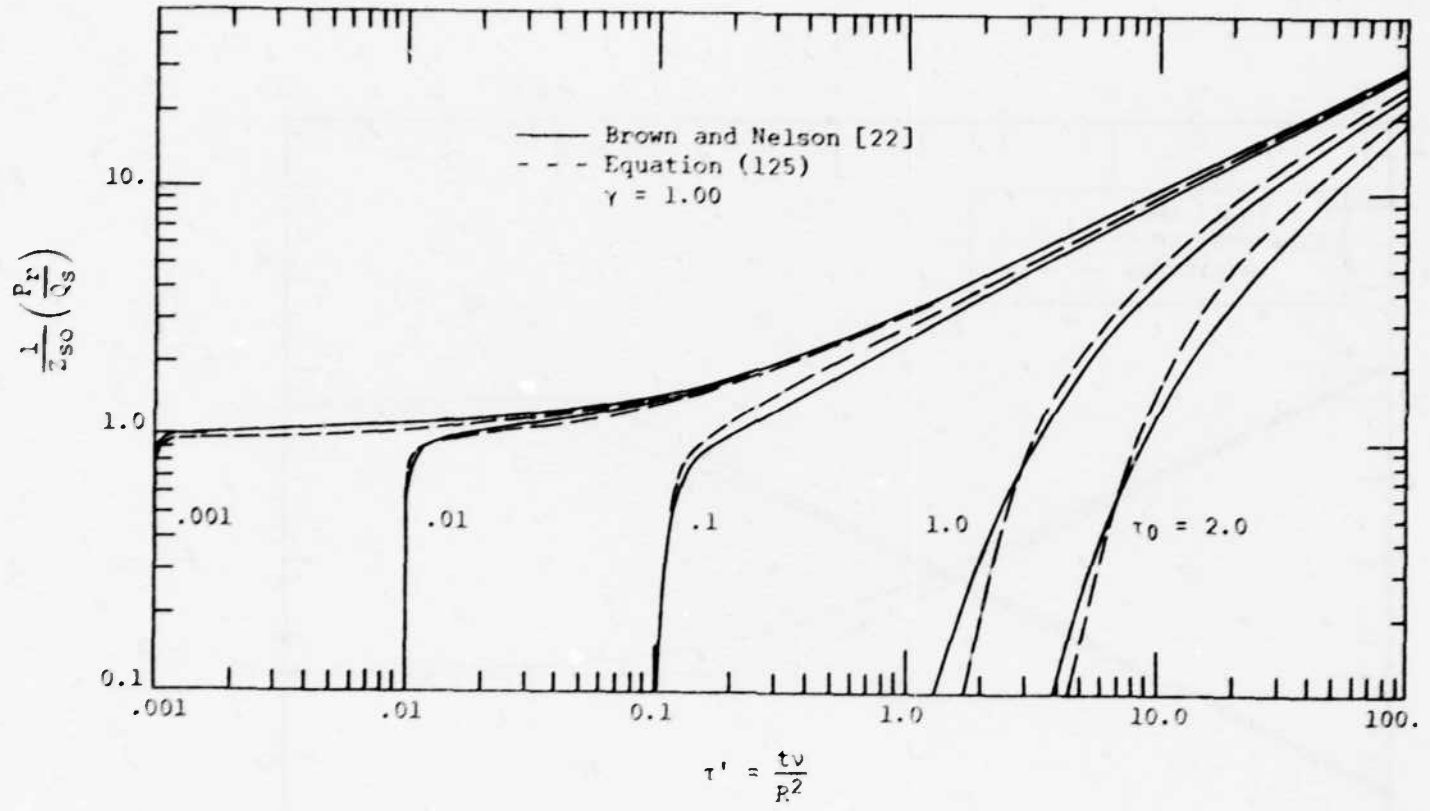

Figure 32. Comparison of Pressure Response to a Step Input of Flow for Liquid-Filled Circular Lines

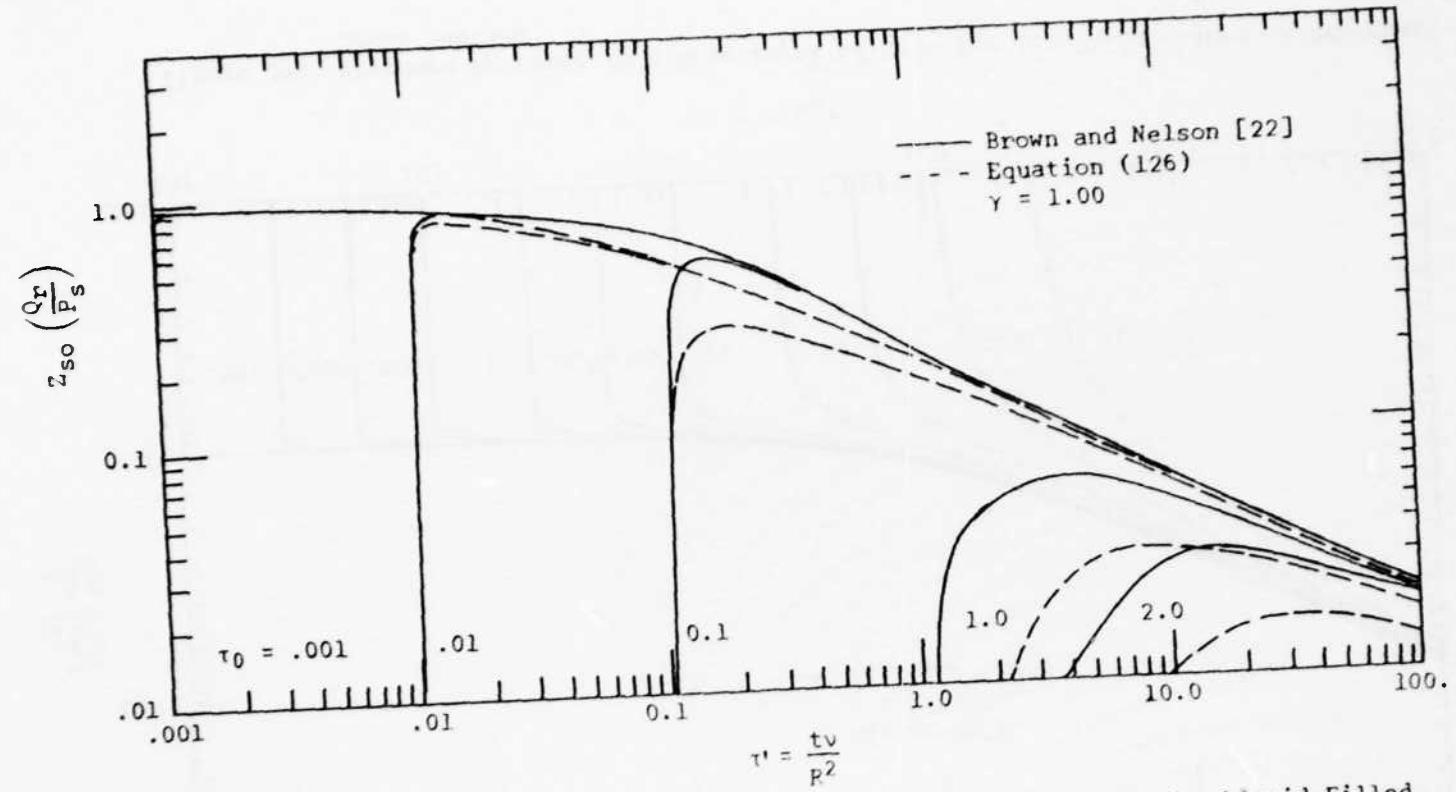

Figure 33. Comparison of Flow Response to a Step Input of Pressure for Liquid-Filled Circular Lines

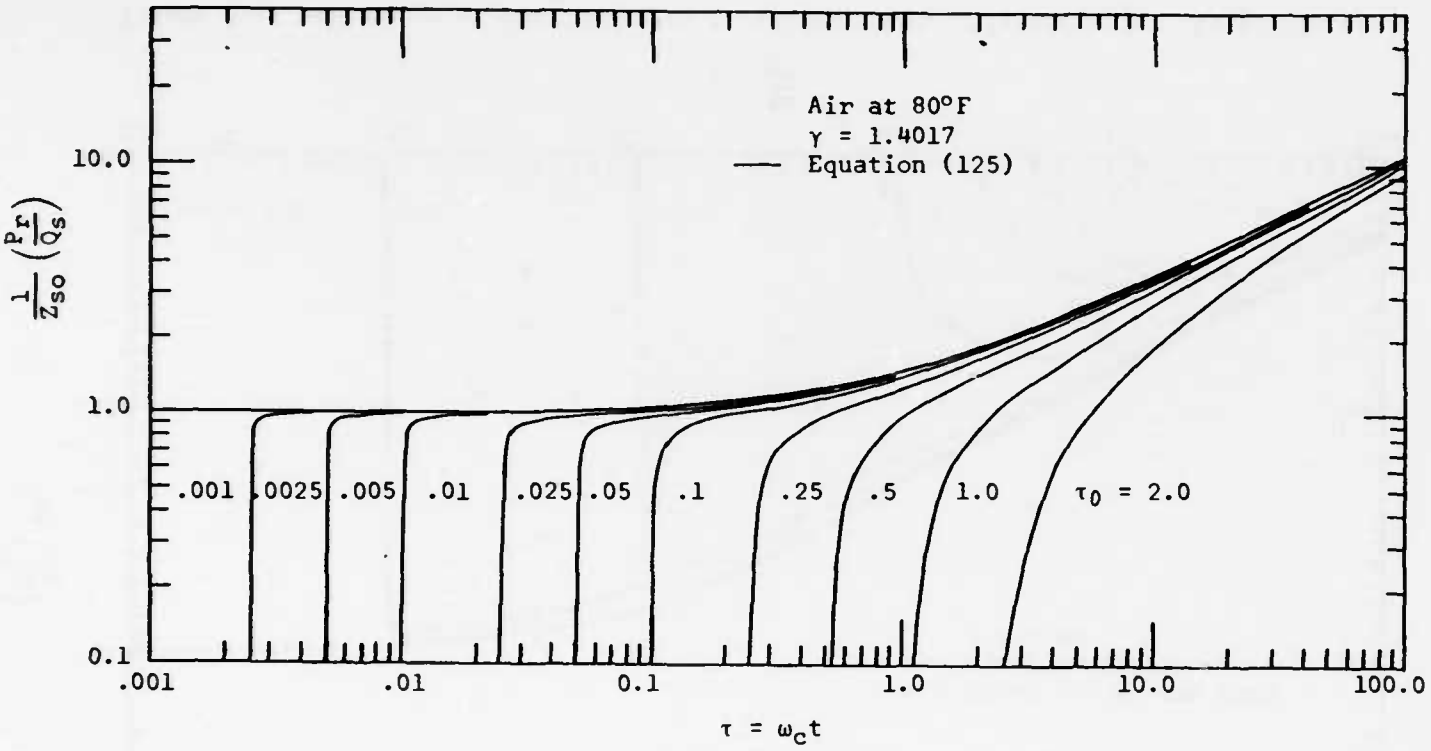

Figure 34. Pressure Response to a Step Input of Flow for Air-Filled Lines of Arbitrary Cross Section

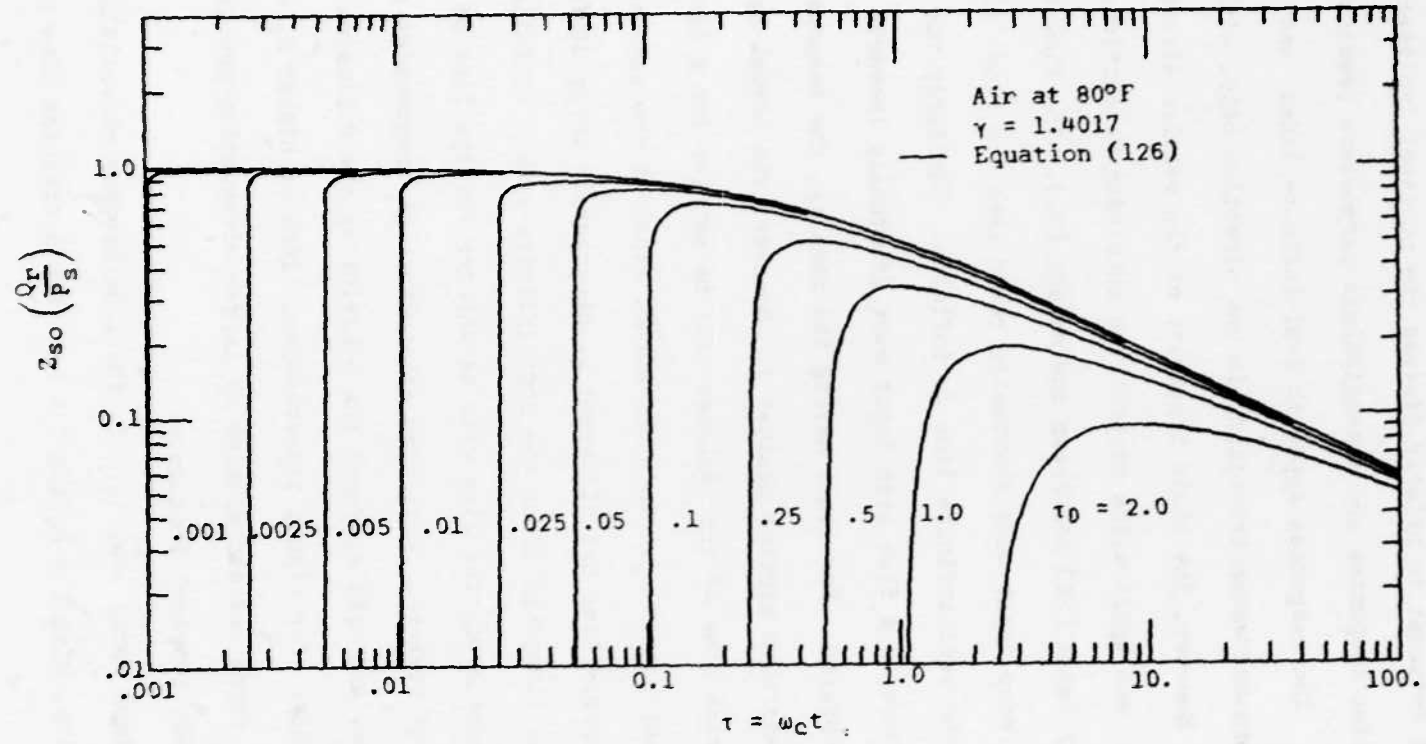

Figure 35. Flow Response to a Step Input of Pressure for Air-Filled Lines of Arbitrary Cross Section

Physical Implications of the Fluid Line Step Responses and Dimensionless Parameters

It is of interest to briefly discuss the physical implications of the various step responses and dimensionless parameters presented in this section. The responses apply to semi-infinite lines, and therefore represent waves travelling in one direction only, with no reflections. However, the basic linearity of the results allows superposition and application to problems involving reflections, as illustrated by Karam [20] and Brown and Nelson [22]. The flow response to a pressure step input must eventually reach zero (no flow) since the impedance of the semi-infinite line is infinite. Similarly the pressure response to a flow step input must eventually increase until the line is ruptured. For lines having the same τ_0, the responses will be the same when plotted against τ. However, the actual delay time, T, and rise time of the response will be shorter for a line cross section of higher ω_c. In other words, lines of the same τ_0 and working fluid properties but different ω_c necessarily imply different axial locations (lengths) along the semi-infinite line. It follows that the distance along the line will be shorter for the line of higher ω_c. The line of higher ω_c will also attenuate high frequencies at a more rapid rate, and will approach the behavior of the diffusive RC line more rapidly. For signal transmission, lines of higher ω_c should be avoided, as these are accompanied by larger attenuation per line wavelength at any physical frequency.

As τ_0 becomes large, say $\tau_0 \geq 1$, the line becomes essentially a diffusive RC line, with $R = R_v$ and $C = C_i$. For a circular line of

1/8 inch inside radius filled with air at 80°F (Table I properties) and $\tau_0 = \omega_c T = 1$, the corresponding length is 122 ft and T is 0.107 sec. For the same line cross section and τ_0, but filled with water at 80°F, the corresponding length is 9,576 feet and T is 1.945 seconds. It is unlikely that signal transmission would be of interest over such long fluid lines. For such lines, treatment as a lumped RC line would be sufficient for most purposes.

Summary of Transient Responses

In this section a method was presented for determining the transient response of semi-infinite fluid-filled lines of arbitrary but constant axial cross section. The results were presented in terms of a characteristic frequency which depends only on the laminar steady flow resistance and conductance of the arbitrary line. Equivalent circuit parameters (R, G, L and C) were developed and used to obtain the time transforms of the various combinations of pressure and flow responses to step inputs of pressure and flow. Results were compared with those of others for both compressible and incompressible fluids. For non-circular lines the results are shown for air at 80°F. It is noted that the results are restricted to laminar flow. Similar results for the various step inputs propagating through fully developed turbulent mean flow are presented in Section VI.

V. Laminar Oscillatory Flow Combined with Steady Developed Mean Flow

Background

Several investigations have been completed concerning the transmission of small oscillatory signals through fully developed mean flow. A majority of these have been directed toward the superposition of laminar oscillatory signals on fully developed laminar mean flow [2,3,4]. Recently, investigations concerning the behavior of oscillatory signals combined with fully developed turbulent flow have been completed [15, 25,27]. Most of the recent efforts have been restricted to incompressible adiabatic flow in circular lines.

Nichols [3] obtained the small-signal frequency response of fluid-filled circular lines including frequency dependent dispersion of the propagation speed and distortion of the oscillatory signal wave shape. In addition, heat transfer effects were included. In essence, Nichols separated the steady and oscillatory fluid parameters (as was done in Appendix C) and subsequently solved the oscillatory flow problem; nevertheless, his solution is applicable to flows combining steady developed laminar mean flow (Hagen-Poiseuille flow) and laminar oscillatory flow. Holmboe and Rouleau [28] have shown that if the initial conditions are assumed to be Hagen-Poiseuille flow then the governing differential equations may be placed in a form which is identical to Nichols' equations. The results of Brown [2], expressed in both the Laplace and time domains, are identical to those of Nichols for the special case of sinusoidal excitation signals.

More recently Brown, Margolis and Shaw [15] have obtained the frequency response of liquid-filled circular lines carrying fully developed turbulent mean flow. The authors developed two and three region viscosity profiles which resulted in fairly complicated solutions. It is noted that at high Reynolds numbers and dimensionless frequencies there were significant gaps in the frequency domain solutions wherein the attenuation of the oscillatory signals was not predicted by any of the authors' models. Recently Funk and Wood [25] developed a single boundary layer model to account for the transient viscous effects and applied this model to small amplitude sinusoidally disturbed turbulent flow in circular lines. The authors developed a transfer function relating the local boundary layer velocity gradient to the core velocity of the flow. The model is comparatively much simpler than that of Brown, et al. [15]; nevertheless it gives values of frequency dependent signal attenuation which are in excellent agreement with the theory and the experimental data of Reference [15]. It is noted that the utility of the model given in Reference [25] is limited to the high frequency regime and constant phase velocity; Funk and Wood suggest the use of a quasi-steady model (i.e., a constant LRC model) at low frequencies. It will be subsequently shown that the model of Funk and Wood is closely related to the high frequency approximations developed by Nichols [3] and Karam [20] for laminar oscillatory flow combined with laminar steady flow, and to the concept of a characteristic frequency and radius previously developed herein.

Trikha [29] has suggested that the frequency dependent part of the friction in turbulent flow may be approximated as the frequency dependent

part of the friction in laminar flow for a limited range of Reynolds number (in this matter, see also [7]).

In this section a simplified model of combined steady turbulent and small signal oscillatory flow is developed which is based on analysis of the components R, G, L, and C of the equivalent electrical circuit, Figure 2, and also on the concept of a characteristic frequency. A method of determining the frequency response of lines of either circular or noncircular cross section carrying fully developed turbulent mean flow is developed. The results are presented for a dimensionless attenuation and frequency. For the circular line model, results are compared with those given in [15,25].

In Section VI, Karam's approximate method [19] is adapted to lines of both circular and noncircular cross section carrying turbulent mean flow and the pressure and flow transient responses of the lines to step inputs are estimated. Before proceeding with the broader purposes of this section, it is instructive to review the physical aspects of combined oscillatory flow and steady, developed mean flow of compressible or incompressible fluids in a semi-infinite circular line.

Physical Considerations of Combined Oscillatory and Steady Developed Mean Flow

A large body of literature exists concerning steady, fully developed, laminar or turbulent flow in circular lines, from which one may select flow relationships ranging in complexity from relatively straightforward to very complex. For turbulent mean flow, elegant theoretical flow descriptions involving statistical approaches and correlation techniques have been proposed. However, these descriptions have failed to yield

solutions except in the simplest cases. The approach taken herein is to develop the necessary steady flow parameters from the more useful phenomenological descriptions of steady turbulent mean flow. In this approach, the texts of Schlichting [30] and Hinze [31] are particularly useful.

For small signal excitation of developed turbulent flow, the steady flow velocity profile will not be greatly altered by the superimposed oscillatory signal provided the steady flow Reynolds number is sufficiently large, and the oscillatory signal amplitude is relatively small.

Steady and Oscillatory Boundary Layers

For steady developed laminar flow in a circular line or duct the boundary layer is presumed to extend from the wall to the centerline of the circular cross section. Thus the steady flow laminar boundary layer thickness denoted $\delta_{v\ell}$, is always equal to the radius of the circular line ($\delta_{v\ell} = r_o$), and is not dependent on the laminar flow Reynolds number. The classical Hagen-Poiseuille velocity profile is obtained for all laminar flow in circular lines. However, for steady developed turbulent flow the associated velocity profile and boundary layer thickness will depend on the Reynolds number. As the turbulent flow Reynolds number increases, the associated velocity profile changes shape and approaches a plug-flow profile. Simultaneously the associated turbulent boundary layer thickness δ_{vt} decreases, indicating large velocity gradients at or near the wall and large resistive losses.

For laminar oscillatory flow, the dynamic boundary layer thickness will vary with frequency. Nichols [3] proposed a boundary layer thickness, $\delta_\omega = \sqrt{2\nu/\omega}$, for circular lines; and it is seen that the oscillatory

boundary layer thickness decreases with increasing frequency. Similar effects occur in electrical conductors where δ_ω is called the skin depth. At low frequencies the oscillatory velocity profile approaches the classical Hagen-Poiseuille distribution.

When laminar oscillatory flow is combined with steady mean flow, it is assumed that an interaction between the steady flow boundary layer and the dynamic (oscillatory) boundary layer will occur. If the steady flow boundary layer thickness is less than that of the oscillatory flow (i.e., $\delta_{v_\ell} < \delta_\omega$ or $\delta_{v_t} < \delta_\omega$) then the oscillatory flow will be dependent upon the steady flow profile. On the other hand, when $\delta_\omega < \delta_{v_\ell}$ (or $\delta_\omega < \delta_{v_t}$) the behavior of the oscillatory flow tends to become independent of the mean flow. This observation is substantiated both analytically and experimentally by the work of Brown, et al. [15], Franke, Karam and Lymburner [14], and others [9,25]. Stated in other terms, the behavior of the oscillatory signal in the low frequency region depends on the mean flow whereas in the high frequency region the behavior of the oscillatory signal becomes essentially independent of the mean flow and dependent on the oscillatory signal frequency (ω). For the experimental data available, the high frequency behavior appears to approach laminar oscillatory flow behavior [15,27]. It is further assumed that for any steady flow there exists a frequency at which the dynamic and steady flow boundary layer thicknesses are comparable ($\delta_\omega \approx \delta_v$). In this region, a transition from essentially steady flow dependence to frequency dependence takes place, or vice versa. Similar qualitative behavior would be expected concerning the temperature profiles, particularly for fluids with a Prandtl number near unity. For circular lines Nichols [3] defines a thermal nonadiabatic skin depth as $\delta_T = \sqrt{2\nu_T/\omega}$ which is seen

to be frequency dependent. At low frequencies the heat transfer behavior of the oscillatory flow will depend essentially on the mean flow, whereas at high frequencies the heat transfer will depend essentially upon the oscillatory frequency. Much of the discussion of the frequency domain equations in Section IV applies qualitatively to the above discussion. It is not intended to extend the discussion of the various boundary layers any further, since ultimately a model for circular and noncircular lines with mean turbulent flow is sought. For certain non-circular lines, more than one δ_ω or δ_ν is involved and it is more convenient to eliminate the dependence of the flow on the geometric cross section of the line. By integrating the various parameters over the appropriate cross section, geometry dependence may be essentially removed, as was previously done in developing the characteristic frequency and components of the equivalent electrical circuit for laminar oscillatory flow.

A Mean Flow Characteristic Frequency for Circular Lines

The concept of a characteristic frequency which divides the flow into regions of viscous, isothermal behavior, and inertial, adiabatic behavior has been discussed in Section III for circular and noncircular lines. It is desired to extend this concept to lines of arbitrary cross section, carrying combined oscillatory and steady turbulent mean flow. Returning to the equivalent electrical circuit, Figure 2, and keeping in mind that the underlying steady flow determines the low frequency behavior of the oscillatory signal, it is necessary to determine R, L, G, and C for the underlying steady flow. The low frequency resistance, R_v, is dependent on the mean flow,

$$R_v = \frac{\frac{-\partial p}{\partial z}}{Q} = \frac{\frac{-\partial p}{\partial z}}{A\bar{u}} \tag{127}$$

and similarly for the inertance,

$$L_v = K_L \cdot L_a = \left[\frac{1}{A}\int_A \left(\frac{u}{\bar{u}}\right)^2 dA\right] \cdot L_a \tag{128}$$

If the underlying mean flow is fully developed laminar, it was previously shown that for circular lines

$$R_{v\ell} = \frac{8\pi\mu}{A^2} \quad , \quad L_{v\ell} = \frac{4}{3} L_a \quad , \quad \omega_{c\ell} = \frac{6\nu}{r_o^2}$$

where subscript ℓ denotes laminar flow conditions. These parameters do not depend on Reynolds number. For turbulent mean flow, the shape of the velocity profile is a function of the friction factor and Reynolds number. The defining relation for the steady flow friction factor, f, for laminar or turbulent mean flow in circular or noncircular lines, is

$$\frac{-\partial p}{\partial z} = \frac{f}{D_h} \frac{1}{2} \rho \bar{u}^2 \tag{129}$$

From equations (127) and (129), the laminar or turbulent steady flow resistance of any line of arbitrary but constant cross section is

$$R_v = \frac{f\rho\bar{u}}{2AD_h} = \frac{(fRe)\mu}{2AD_h^2} \tag{130}$$

The simplest form of the relation between f and Re for developed turbulent flow in both circular and noncircular lines is the Blasius relation,

$$f = 0.3164/Re^{1/4} \tag{131}$$

where the Reynolds number, Re is defined in terms of the hydraulic diameter:

$$Re = \frac{\rho \bar{u} D_h}{\mu} \tag{132}$$

Equation (131) gives good accuracy up to $Re \leq 5 \times 10^5$ [30], and is used to compute f herein. Using Equations (130) and (131) the turbulent viscous resistance of lines of arbitrary cross section, R_{v_t}, becomes

$$R_{v_t} = \frac{0.3164\mu}{2AD_h^2} (Re)^{3/4} \tag{133}$$

From Hinze [31], the steady turbulent velocity profile in circular lines may be expressed as a simple power law,

$$\frac{u}{u_{max}} = \left(\frac{y}{r_o}\right)^{1/n} \tag{134}$$

where n is a function of Re, $y = r_o - r$, and u_{max} is the maximum (centerline) velocity. Further, the work of Nunner as presented by Hinze [31] shows that the exponent n may be expressed as a function of f only,

$$\frac{1}{n} = \sqrt{f} \tag{135}$$

Equation (135) is shown to be in good agreement with the experimental data of Nunner, Nikuradse, and Laufer, for both smooth and rough circular lines [31]. From Schlichting [30],

$$\frac{\bar{u}}{u_{max}} = \frac{2n^2}{(n+1)(2n+1)} \tag{136}$$

Thus

$$\frac{u}{\bar{u}} = \frac{(n+1)(2n+1)}{2n^2}\left[\frac{y}{r_o}\right]^{1/n} \tag{137}$$

The turbulent viscous inertance, L_{v_t}, becomes

$$L_{v_t} = \frac{1}{A}\int_A \left[\frac{u}{\bar{u}}\right]^2 dA \cdot L_a = \frac{(n+1)(2n+1)^2}{4n^2(n+2)} \cdot L_a = K_{L_t} \cdot L_a \tag{138}$$

and K_{L_t} is seen to be a simple expression. In terms of the friction factor

$$K_{L_t} = \frac{L_{v_t}}{L_a} = \frac{(\sqrt{f}+1)(\sqrt{f}+2)^2}{4(2\sqrt{f}+1)} \tag{139}$$

The value of K_{L_t} will be near unity since the steady turbulent velocity profiles are similar to inertial or plug flow profiles. As Re becomes large, it can be seen that $u/\bar{u}$ and K_{L_t} approach unity, while $n \to \infty$ and $f \to 0$. It is further noted that K_{L_t} near unity implies that L_{v_t} does not differ much from L_a, and the assumption that the frequency dependent inertia is in fact constant ($L = L_a$, or $L = L_{v_t}$) is a good approximation, particularly at high Reynolds numbers. The approximation $L_{v_t} = L_a$ is particularly useful in dealing with lines of arbitrary cross section carrying turbulent through flow, where expressions for $u/\bar{u}$ are either very complex or unknown.

A broad range of values of K_{L_t} for circular lines, together with closely related parameters, were obtained using equations (131), (135)

and (139), and are included in Table VI. It is seen that the tabulated data is consistent with the preceding discussion of K_{L_t}.

TABLE VI

Turbulent Steady Flow Inertance Factor (K_{L_t}) for Circular Lines

Re	f	fRe	n	K_{L_t}
1,000	0.056265	56.3	4.2158	1.0500
5,000	0.037627	188.1	5.1553	1.0352
10,000	0.031640	316.4	5.6219	1.0302
50,000	0.021159	1,057.9	6.8747	1.0211
100,000	0.017792	1,779.2	7.4969	1.0180
500,000	0.011899	5,949.3	9.1675	1.0125
1,000,000	0.010005	10,005.0	9.9973	1.0106

Characteristic Frequency and Radius - Turbulent Mean Flow

Proceeding as in Section III, a set of characteristic frequencies and radii based on turbulent mean flow quantities are defined as

$$\omega_{c_t} = \frac{R_{v_t}}{L_{v_t}} \quad ; \quad r_{c_t} = \sqrt{\frac{6\nu}{\omega_{c_t}}} \tag{140}$$

$$\omega_{v_t} = \frac{R_{v_t}}{L_a} \quad ; \quad r_{v_t} = \sqrt{\frac{8\nu}{\omega_{v_t}}} \tag{141}$$

where subscript t denotes turbulent mean quantities.

It is more convenient to use the characteristic quantities defined in equation (141), since these quantities (i.e., adiabatic inertance) are more easily determined, and are consistent with the previous discussion and other publications on the subject [3,25]. Both ω_{c_t}

and ω_{ν_t} are dependent on the turbulent friction factor and Reynolds number. In essence, the circular line carrying fully developed turbulent flow is replaced by an equivalent smaller line of radius r_{ν_t} or r_{c_t} carrying fully developed laminar flow, of the same characteristic frequency.

Nichols' frequency domain solutions [3], applicable to circular fluid lines carrying either developed laminar mean flow or no mean flow, are to be used to solve the normalized frequency-dependent performance of both circular and noncircular lines carrying fully developed turbulent flow, and are repeated herein for the convenience of the reader. The impedance, admittance, propagation operator and characteristic impedance/admittance are

$$Z = j\omega L_a \left[1 - \frac{2J_1\left(\sqrt{\frac{\omega}{\nu}}\, r_o j^{3/2}\right)}{\sqrt{\frac{\omega}{\nu}}\, r_o j^{3/2}\, J_o\left(\sqrt{\frac{\omega}{\nu}}\, r_o j^{3/2}\right)} \right]^{-1} \tag{142}$$

$$Y = j\omega C_a \left[1 + \frac{2(\gamma-1)\, J_1\left(\sqrt{\frac{\omega}{\nu_T}}\, r_o j^{3/2}\right)}{\sqrt{\frac{\omega}{\nu_T}}\, r_o j^{3/2}\, J_o\left(\sqrt{\frac{\omega}{\nu_T}}\, r_o j^{3/2}\right)} \right] \tag{143}$$

$$\Gamma = \sqrt{ZY} = \alpha + j\beta \tag{144}$$

$$Z_0 = \sqrt{Z/Y} = 1/Y_0 \tag{145}$$

To use the above solutions as stated, the radius r_o is replaced by one of the characteristic radii, equations (140) or (141), and for

turbulent flow the further assumption $\nu_T = \nu$ is made. This assumption implies a Prandtl number of unity which is thought to be more representative of turbulent processes [30,31]. The adiabatic inertance and capacitance (L_a, C_a) are computed from the actual line properties. Equations (141) through (144) are the same equations which were used to closely approximate the normalized frequency dependence of both circular and noncircular lines, carrying either laminar or no mean flow, and the results were shown in Figures 18, 19, 24, and 25. These normalized results will remain the same, when plotted against the characteristic frequency ratio, ω/ω_{ν_t}.

As mentioned in Section III, for a given value of the argument of the Bessel functions, $\sqrt{\omega/\nu}\,r$ (or equivalently, ω/ω_c or ω/ω_ν), the normalized frequency dependence will be the same when plotted against this argument. Since it now is intended to apply the above modeling approach to circular and noncircular lines carrying turbulent through flow, it is necessary to closely examine the range of validity and application of this approach. The following development will address the low, mid, and high frequency domains relative to the turbulent viscous characteristic frequency, ω_{ν_t}, and Nichols' solutions.

Low Frequency Domain - Turbulent Mean Flow. For $\omega << \omega_{\nu_t}$ a quasi-steady constant LRC model is the simplest approach, as suggested by Brown, et al. [15] and Funk and Wood [25]. The equivalent electrical circuit is comprised of the constant value elements, $R = R_{\nu_t}$, $L = L_a (= L_{\nu_t})$, $G = 0$, and $C = C_i = \gamma C_a$. The low frequency series impedance and shunt admittance are

$$Z_{L_t} = R_{v_t} + j\omega L_a = R_{v_t}\left[1 + j\frac{\omega}{\omega_{\nu_t}}\right] = j\omega L_a\left[1 - j\frac{\omega_{\nu_t}}{\omega}\right] \tag{146}$$

$$Y_{L_t} = G + j\omega C_i = j\omega\gamma C_a \tag{147}$$

From equations (141) and (146), it is seen that as ω approaches zero, Z_{L_t} approaches the steady turbulent DC resistance, R_{v_t}, equation (133). The low frequency propagation operator and characteristic impedance are

$$\Gamma_{L_t} = \sqrt{Z_{L_t}Y_{L_t}} = \alpha_{L_t} + j\beta_{L_t} = \frac{j\omega}{c_a}\left[\gamma\left(1 - j\frac{\omega_{\nu_t}}{\omega}\right)\right]^{1/2} \tag{148}$$

$$Z_{0_{L_t}} = \sqrt{\frac{Z_{L_t}}{Y_{L_t}}} = \rho\frac{c_a}{A}\left[\frac{1}{\gamma}\left(1 - j\frac{\omega_{\nu_t}}{\omega}\right)\right]^{1/2} \tag{149}$$

For very low frequencies, $\omega/\omega_{\nu_t} << 1$, the above expressions may be further simplified:

$$\Gamma_{L_t} \approx \sqrt{j\gamma R_{v_t}C_a\omega} = \frac{1}{c_a}\sqrt{j\gamma\omega_{\nu_t}\omega} = \frac{\omega_{\nu_t}}{c_a}\sqrt{\frac{\gamma}{2}\frac{\omega}{\omega_{\nu_t}}}(1+j) \tag{150}$$

$$Z_{0_{L_t}} \approx \sqrt{\frac{R_{v_t}}{j\gamma\omega C_a}} = \rho\frac{c_a}{A}\frac{\omega_{\nu_t}}{\omega}\sqrt{\frac{\omega}{2\gamma\omega_{\nu_t}}}(1-j) \tag{151}$$

where $\rho\frac{c_a}{A} = Z_{s_0} = \sqrt{L_a/C_a}$.

To facilitate discussion of the constant LRC model and comparison with recent work, the dimensionless frequency, Ω, and normalized attenuation, α_{B_r}, for circular lines introduced by Brown, et al. [15] will be used. These are

$$\Omega = \frac{r_o^2 \omega}{\nu} \tag{152}$$

$$\alpha_{Br} = \frac{r_o^2 c_a}{\nu} \alpha \tag{153}$$

Using the constant LRC model, equation (148), and the above parameters, it can be seen in Figure 36 that a principal effect of increasing the steady turbulent Reynolds number is to increase the attenuation at all frequencies, up to the laminar reference curve. Figure 36 shows the extension of the constant LRC curves beyond the laminar limit, and also indicates that for a given Reynolds number a plateau is reached, after which the LRC model fails to predict further increases in attenuation.

To obtain the limiting value of α, denoted α_M, for the constant LRC model and large values of ω, Γ_{L_t} is first rewritten using equations (146) and (147), and then expressed in terms of its modulus and phase angle,

$$\Gamma_{L_t} = \sqrt{Z_{L_t} Y_{L_t}} = \sqrt{\frac{-\omega^2 R_{\nu_t} C_i}{\omega \nu_t}} \sqrt{1 - j \frac{\omega \nu_t}{\omega}} \tag{154}$$

$$\Gamma_{L_t} = \left| \omega \sqrt{L_a C_i} \left[1 + \left(\frac{\omega \nu_t}{\omega} \right)^2 \right]^{1/4} \right| \angle \frac{1}{2} \left[\pi - \arctan \frac{\omega \nu_t}{\omega} \right] \tag{155}$$

For large values of ω/ω_{ν_t}, or small ω_{ν_t}/ω,

$$\left[1 + \left(\frac{\omega \nu_t}{\omega} \right)^2 \right]^{1/4} \approx 1$$

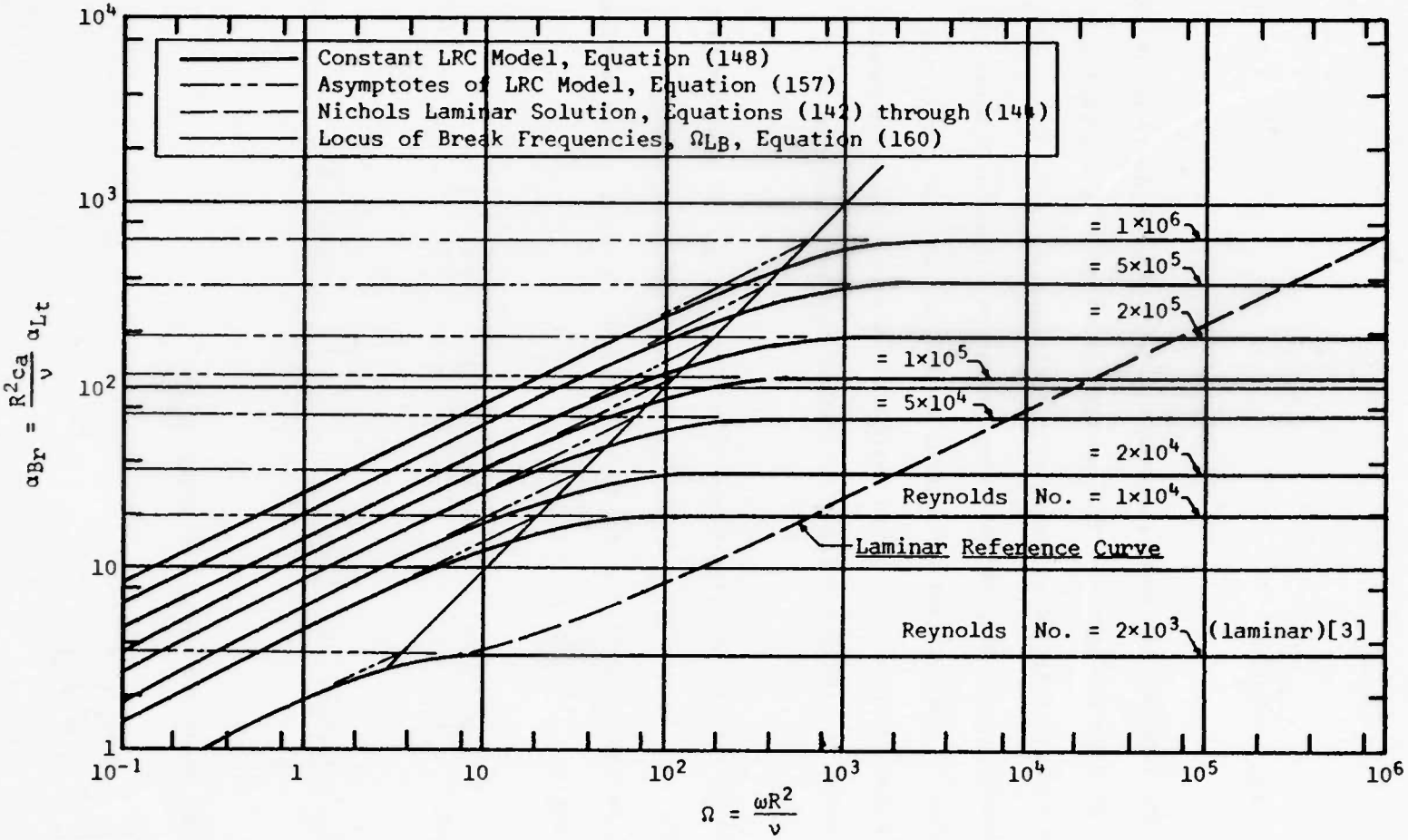

Figure 36. Variation of Low Frequency Attenuation with Reynolds Number in Circular Lines

Taking α_M as the real part of Γ_{L_t}, and using the relations $R_{v_t} = \omega_{v_t} L_a$, $C_i = \gamma C_a$, and $\sqrt{C_a L_a} = 1/c_a$;

$$\alpha_M = \omega\sqrt{\gamma C_a L_a} \cos\left[\frac{\pi}{2} - \frac{1}{2}\frac{\omega_{vt}}{\omega}\right] = \frac{\omega\sqrt{\gamma}}{c_a} \sin\left[\frac{1}{2}\frac{\omega_{vt}}{\omega}\right] \tag{156}$$

Using the small angle approximation, $\sin\theta \approx \theta$,

$$\alpha_M \approx \frac{\omega\sqrt{\gamma}}{c_a}\left[\frac{1}{2}\frac{\omega_{vt}}{\omega}\right] = \frac{1}{2}\frac{\omega_{vt}}{c_a}\sqrt{\gamma} \tag{157}$$

Similarly, for the plateau phase lag, β_M,

$$\beta_M = \frac{\omega}{c_a}\sqrt{\gamma} \sin\left[\frac{\pi}{2} - \frac{1}{2}\frac{\omega_{vt}}{\omega}\right] \approx \frac{\omega}{c_a}\sqrt{\gamma} \tag{158}$$

The asymptotes of value α_M for each Reynolds number are also plotted in Figure 36, and it is seen that α_M is an accurate representation of the constant LRC attenuation in the mid-frequency range. Equating the expressions for α given by equations (150) and (157), the low frequency corner, or break frequency ratio, $\omega/\omega_{v_t} = 1/2$, is obtained.

To convert to Brown's dimensionless frequency, used in Figure 36,

$$\Omega = 8\left(\frac{R}{r_{v_t}}\right)^2 \cdot \frac{\omega}{\omega_{v_t}} = \frac{R^2\omega}{\nu} \tag{159}$$

The locus of break frequency ratios in terms of Ω is

$$\Omega_{LB} = 4\left(\frac{R}{r_{v_t}}\right)^2 \tag{160}$$

This locus is also plotted in Figure 36. An expression for the dimensionless frequency Ω at which the α_M asymptote intersects Nichols' laminar reference curve, Figure 36, is obtained by equating α_M and α_H, equations (157) and (98), respectively. Equation (98) was derived from laminar theory, and contains developed laminar flow quantities, denoted by subscript ℓ.

$$\frac{1}{2}\frac{\omega\nu_t}{C_a}\sqrt{\gamma} = \frac{1}{4c_a}\left[1 + \frac{\gamma-1}{\sigma}\right]\sqrt{\omega\omega\nu_\ell} \tag{161}$$

which can be rearranged to give

$$\left.\frac{\omega}{\omega\nu_t}\right|_{H_B} = \frac{4\gamma}{\left[1 + \frac{\gamma-1}{\sigma}\right]^2} \cdot \frac{\omega\nu_t}{\omega\nu_\ell} \tag{162}$$

For incompressible flow, $\gamma = 1$, and equation (162) becomes

$$\left.\frac{\omega}{\omega\nu_t}\right|_{H_B} = 4\,\frac{\omega\nu_t}{\omega\nu_\ell} = 4\left[\frac{R}{r\nu_t}\right]^2 \tag{163}$$

In terms of Brown's dimensionless frequency, see Figure 36,

$$\Omega_{H_B} = 8\left[\frac{R}{r\nu_t}\right]^2 \cdot \left.\frac{\omega}{\omega\nu_t}\right|_{H_B} = \frac{32\gamma}{\left[1 + \frac{\gamma-1}{\sigma}\right]^2}\left[\frac{R}{r\nu_t}\right]^4 \tag{164}$$

and for incompressible flow

$$\Omega_{H_B} = 32\left[\frac{R}{r\nu_t}\right]^4 \tag{165}$$

The entire set of constant LRC model attenuation curves, Figure 36, can be reduced exactly to a single curve, Figure 37, valid for all Reynolds numbers and line cross sections by using the dimensionless frequency ratio ω/ω_{ν_t} and expressing the dimensionless attenuation as

$$\bar{\alpha}_{L_t} = \frac{r_{\nu_t}^2 c a}{k\nu} \alpha_{L_t} \tag{166}$$

where α_{L_t} is the real part of Γ_{L_t} in equation (150).

It is seen from equations (150), (157), and (162), and shown in Figure 37, that $\bar{\alpha}_{L_t}$ and all asymptotic parameters are principally functions of ω_{ν_t} or ω/ω_{ν_t}. Equation (166), with α_{L_t} determined from equation (148) and $K = \sqrt{\gamma}$, is plotted in Figure 37, together with the appropriate asymptotes and corner frequencies. A second curve, which has been normalized such that the plateau value of dimensionless attenuation is unity ($K = 4\sqrt{\gamma}$), is also shown in Figure 37. It can be shown via considerable algebra that this curve is also identical to the ratio $\sqrt{\gamma}\, c/c_a$ (or $\sqrt{\gamma}\, \lambda/\lambda_a$) obtained when using the constant LRC model.

Mid-Frequency Domain-Turbulent Mean Flow

If r_{ν_t} is used in place of r_o in equations (142) through (144), Nichols' circular line theory predicts the low frequency attenuation very accurately at or below the low frequency break ($\omega/\omega_{\nu_t} = 1/2$), and can be adjusted to predict the high frequency parameters also. However, in the mid-frequency range, $\omega \approx \omega_{\nu_t}$, Nichols' theory does not predict the extent of the attenuation plateau; in this region the constant LRC model is used and the plateau extended approximately to

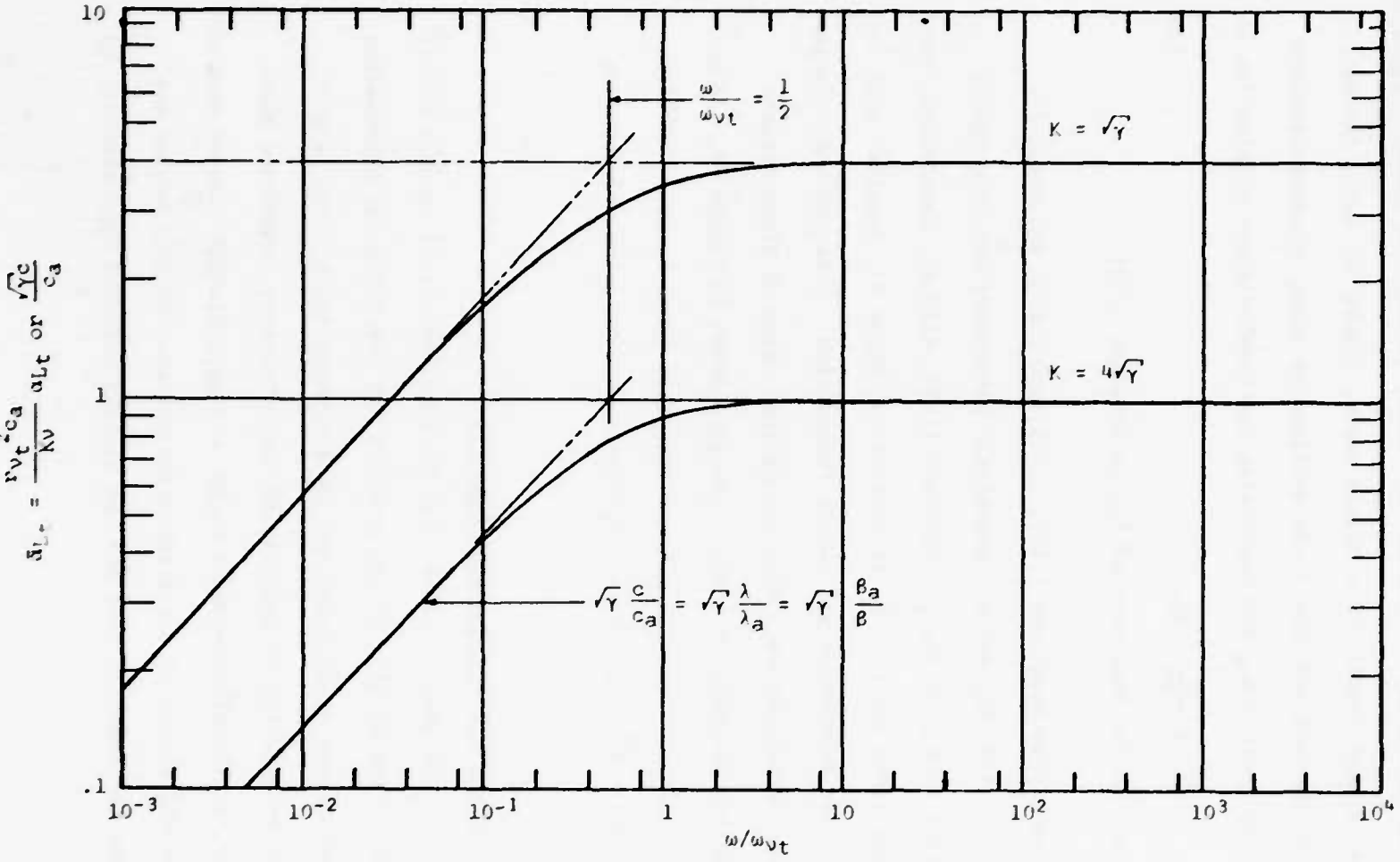

Figure 37. Attenuation and Phase Velocity in Circular or Noncircular Lines, Laminar or Turbulent Mean Flow, Constant LRC Model

the high frequency laminar reference. Accordingly, the results plotted in Figures 36 and 37 and the equations describing the constant LRC model are extended to include the mid-frequency range. This model is easily understood and applied, and is in sufficient agreement with experimental data [15,27,32]. Furthermore, in the region of the intersection of the constant LRC model plateau and the high frequency laminar reference (called the high corner or high frequency break), experimental anomalies have been encountered which are not amenable to linear analysis. In a recent paper by Margolis and Brown [27], unexpected and dramatic variations in both attenuation and phase velocity were encountered in the transition region between the quasi-steady (constant LRC), and high frequency (laminar oscillatory) regions of flow in water-filled circular lines carrying turbulent mean flow. This same behavior was also observed by Vining [32] in a recent experimental investigation involving air-filled rectangular lines carrying turbulent mean flow. Vining and the author conducted a thorough search for experimental anomalies or errors to no avail. The data was repeatable from day to day, after extensive experimental equipment replacement and recalibration. A similar exhaustive search was made by Margolis and Brown, and they were eventually persuaded that the experimental data was correct. Details of the cited behavior and discussion of the possible causes are best given in [27,32]. However, the behavior is worthy of illustration, see Figures 38 and 39. It is strongly suspected that resonance phenomena involving coupling between turbulent vortices and the superposed oscillatory signal is present.

In [27], and as seen in Figures 38 and 39, the experimental data corroborates the use of a quasi-steady model for dimensionless frequency

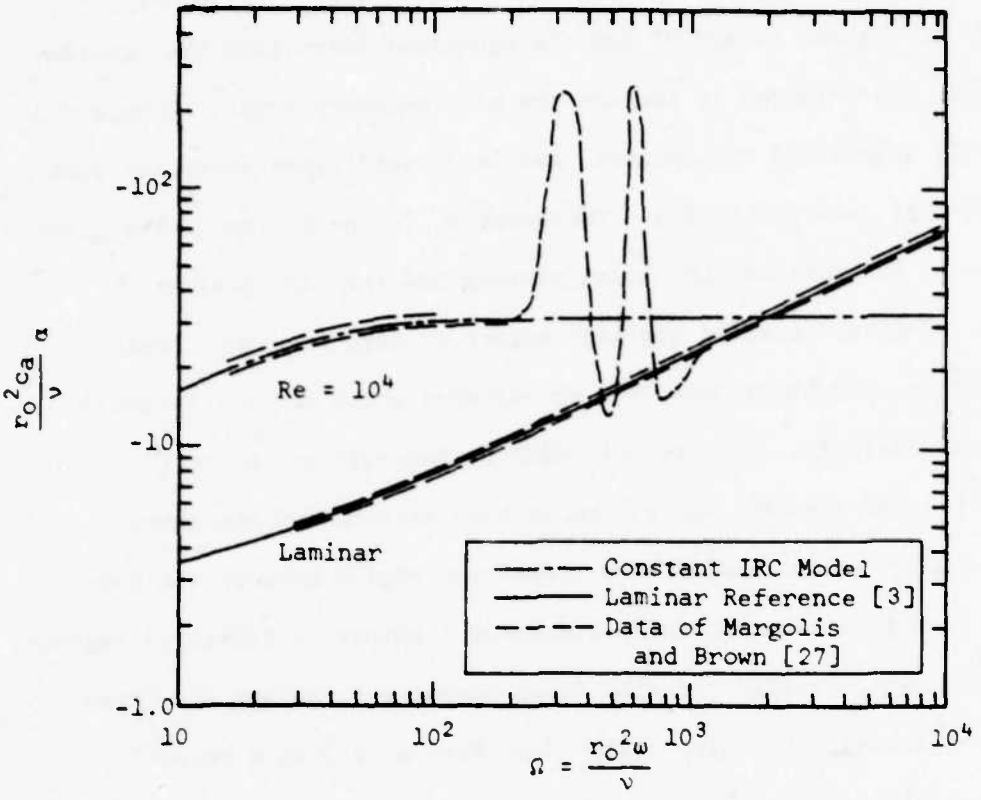

Figure 38. Normalized Attenuation Data in Water Medium

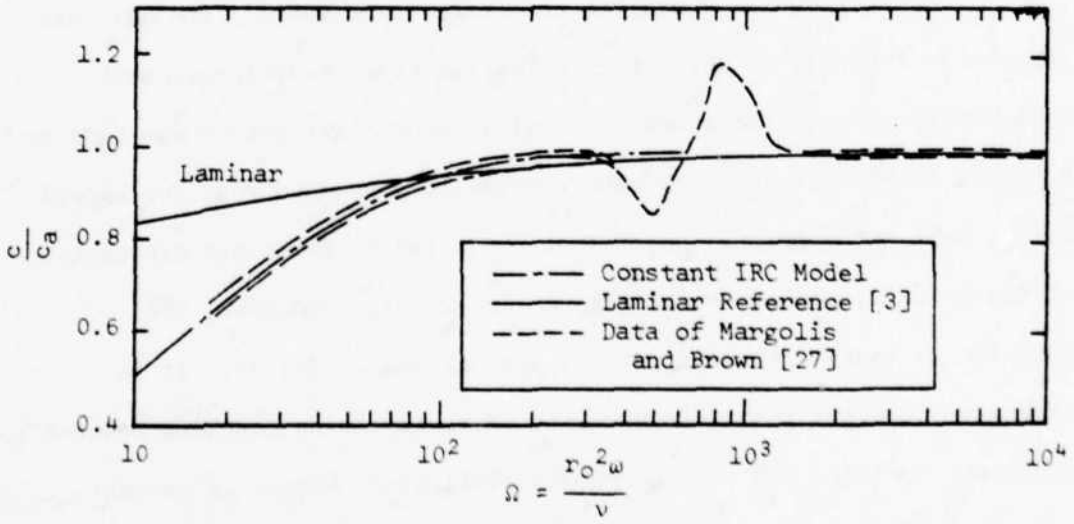

Figure 39. Phase Velocity Ratio Data in Water Medium

ratios below and up to the transition region, and the use of a laminar oscillatory model at ratios above this region. The experimental evidence in [27,32] further emphasizes the futility of attempting to develop a rigorous, complicated, smooth transition model as was done in [15,25]; attenuation and phase velocity behavior in the transition region is far from smooth. Fortunately, the transition frequency bandwidth is predictable [27], and can be avoided in any attempted transmission of information through the developed turbulent mean flow. In view of the experimental evidence, it is thought sufficient to use the constant LRC model for dimensionless frequency ratios in the mid-range and up to those at which the laminar oscillatory model becomes valid.

High Frequency Domain - Turbulent Mean Flow. In the high frequency domain ($\omega >> \omega_{\nu_t}$), the flow becomes frequency dependent. At high frequency, the laminar oscillatory boundary layer becomes considerably thinner than the equivalent mean flow boundary layer ($\delta_\omega << \delta_{\nu_t}$) as previously discussed in this section. Thus the high frequency behavior becomes essentially independent of the mean flow, and approaches the laminar oscillatory behavior associated with the line being investigated. The normalized laminar oscillatory behavior of both circular and noncircular lines was shown to be nearly identical when plotted against the laminar characteristic frequency ratio $\omega_{\nu_\ell} = R_{\nu_\ell}/L_a$. It remains to determine the transition from middle to high frequency and to normalize the high frequency domain results such that they are applicable to circular and noncircular lines carrying laminar or turbulent mean flow over a practical range of Reynolds number. Results are sought which are similar to the single curves of Figure 37. These curves include

both low and mid-frequency performance of circular and noncircular lines carrying a compressible or incompressible fluid at the specified Reynolds number.

If Nichols' equations (142 through 145) are used together with r_{ν_t}, the predicted high frequency attenuation is too high, as shown in Figure 40. Thus r_{ν_t} cannot be used as the characteristic radius in the high frequency region unless other adjustments are made. Experimental evidence supports the use of the laminar oscillatory model in the high frequency regions, and the following development will provide the mathematical relationships and adjustments needed in the high frequency domain.

Equation (144) may be expanded using equations (142) and (143) with $\nu = \nu_T$ to give

$$\Gamma = \alpha + j\beta = \frac{j\omega}{c_a}\left[\frac{1 + (\gamma-1)\,J(\phi)}{1 - J(\phi)}\right]^{1/2} = \frac{j\omega}{c_a}\,g(\phi) \qquad (167)$$

where

$$J(\phi) = \frac{2J_1(\phi)}{\phi J_0(\phi)} \qquad (168)$$

and

$$\phi = \sqrt{\frac{\omega}{\nu}}\, r_o j^{3/2} \qquad (169)$$

The normalized impedance ratio is obtained from equations (142), (143), (145), and (36):

$$\frac{Z_0}{Z_{s_0}} = \left\{\left[1 - J(\phi)\right]\left[1 + (\gamma-1)\,J(\phi)\right]\right\}^{-1/2} = h(\phi) \qquad (170)$$

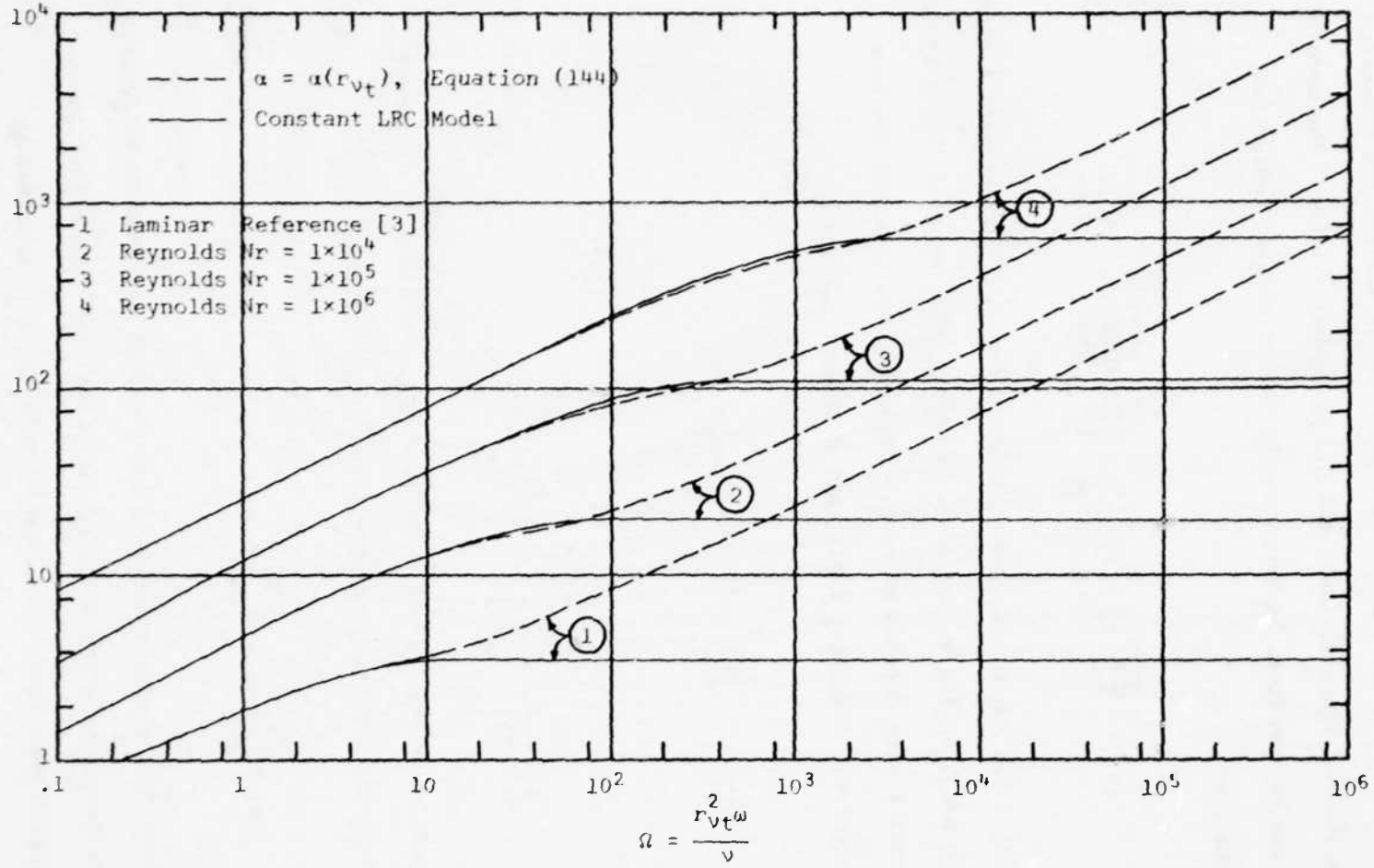

Figure 40. Variation of Unadjusted Frequency Dependent Attenuation with Reynolds Number in Circular and Noncircular Lines

It is clear that the argument ϕ completely determines the bracketed expression of equation (167) and all of equation (170). The modulus of ϕ can be rewritten in terms of the characteristic radius and frequency as

$$|\phi| = \sqrt{\frac{\omega}{\nu}}\, r_\nu = \sqrt{2}\ \frac{r_\nu}{\delta_\omega} = \sqrt{\frac{\omega}{\nu}}\sqrt{\frac{8\nu}{\omega_\nu}} = 2\sqrt{\frac{2\omega}{\omega_\nu}} \qquad (171)$$

where $r_\nu = r_o$, r_{ν_ℓ} or r_{ν_t}, and similarly for ω_ν. The argument ϕ depends only on ω/ω_ν, or its equivalents. However, from equation (167) it is seen that Γ also depends on ω/c_a. Supposing two lines of the same characteristic frequency ratio, but different ω_ν, i.e.,

$$\left.\frac{\omega}{\omega_\nu}\right|_1 = \left.\frac{\omega}{\omega_\nu}\right|_2 \quad , \quad \text{and} \quad \omega_{\nu_1} \neq \omega_{\nu_2}$$

implies

$$\frac{\omega_1}{\omega_2} = \frac{\omega_{\nu_1}}{\omega_{\nu_2}} = \left[\frac{r_{\nu_2}}{r_{\nu_1}}\right]^2 \quad , \text{ for all } \omega. \qquad (172)$$

Consequently, α (and β) may be adjusted between lines of different characteristic frequency to obtain the proper values:

$$\alpha_1 = \frac{\omega_{\nu_1}}{\omega_{\nu_2}}\,\alpha_2 = \left[\frac{r_{\nu_2}}{r_{\nu_1}}\right]^2 \alpha_2 \qquad (173)$$

It follows that a single baseline curve can be constructed to describe the high frequency attenuation of all lines, carrying either laminar or turbulent mean flow. One form of this curve is obtained by

normalizing α, equation (167), in a manner similar to Brown [15]:

$$\frac{r_\nu^2 c_a}{\nu}\,\alpha = \frac{r_\delta^2 c_a}{\nu}\,\frac{\omega}{c_a}\,\text{Real}\,[jg(\Phi)] = \frac{\delta\omega}{\omega_\nu}\,\text{Real}\left[jg\left(\sqrt{\frac{\delta\omega}{\omega_\nu}}\right)\right] \tag{174}$$

when $\alpha = \alpha(r_\nu)$. Equation (174) shows that the normalized attenuation is a function of ω/ω_ν only. Equation (174) is plotted in Figure 41. The high frequency behavior as shown in Figure 41 (above $\omega/\omega_{\nu_t} \cong 2$), may be adjusted to the appropriate laminar reference (asymptote) by using the known high frequency behavior and the approach leading to equations (172) and (173), or by noting that the correct characteristic frequency ratio at high frequencies is ω/ω_{ν_ℓ}, whether the underlying steady flow is laminar or turbulent, and interpreting Figure 41 accordingly.

It is convenient to normalize α such that the onset of frequency dependent behavior begins at unity value on the mid-frequency plateau and joins the laminar oscillatory limit curve of the fluid line being considered. The normalized high frequency attenuation is to be determined in terms of ω/ω_{ν_t}. The appropriate asymptotes are given in equations (157) and (98) for the middle and high frequency regions, respectively. These are used to define a new, extremely simple, single expression for the middle and high frequency dimensionless attenuation. The two asymptotes are:

$$\alpha_M/\alpha_M = 1 \tag{175}$$

$$\frac{\alpha_H}{\alpha_M} = \frac{\frac{1}{4}\,c_a\left[1 + \frac{\gamma-1}{\sigma}\right]\sqrt{\omega\omega_{\nu_\ell}}}{\frac{\sqrt{\gamma}}{2c_a}\,\omega_{\nu_t}} \tag{176}$$

and for σ = 1,

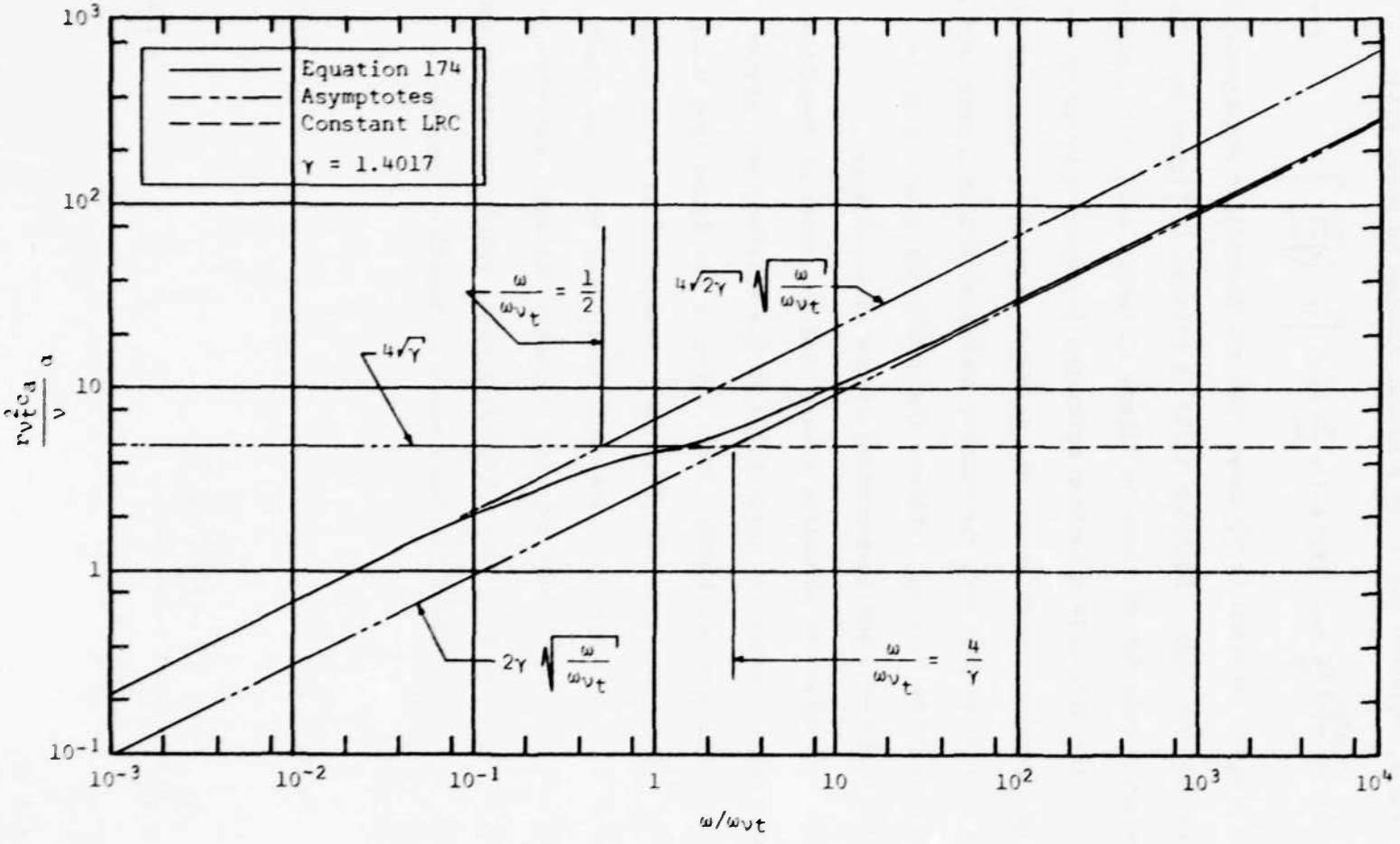

Figure 41. Frequency Dependent Attenuation in Circular and Noncircular Lines, Laminar or Turbulent Mean Flow

$$\frac{\alpha_H}{\alpha_M} = \frac{\sqrt{\gamma}}{2}\sqrt{\left(\frac{\omega_{\nu_\ell}}{\omega_{\nu_t}}\right)\left(\frac{\omega}{\omega_{\nu_t}}\right)} = \frac{\sqrt{\gamma}}{2}\left(\frac{r_{\nu_t}}{r_{\nu_\ell}}\right)\sqrt{\frac{\omega}{\omega_{\nu_t}}} \qquad (177)$$

Equations (175) and (177) are combined into a single function, called $\bar{\alpha}_{H_t}$:

$$\bar{\alpha}_{H_t} \cong \frac{\alpha}{\alpha_M} = \sqrt{1 + \frac{\gamma}{4}\left(\frac{r_{\nu_t}}{r_{\nu_\ell}}\right)^2 \frac{\omega}{\omega_{\nu_t}}} \qquad (178)$$

This function represents the middle and high frequency dimensionless attenuation of laminar oscillatory signals in circular and noncircular lines, carrying fully developed laminar or turbulent throughflow. The inclusion of γ in this equation also accounts for compressibility effects. Equation (178) is plotted in Figure 42. The high corner (break) frequency occurs at the intersection of the two asymptotes, as previously shown in the development of equations (161) through (165). A new dimensionless grouping, the abscissa of Figure 42, is formed which combines mean flow, geometry, and frequency dependent parameters. This new grouping facilitates comparisons with previous work, notably that of Funk and Wood [25], as discussed in the following subsection.

Comparison of High Frequency Results with Previous Work

In comparing the above results with those of Brown, et al. [15,27], and Funk and Wood [25,26], it is necessary to establish a common basis among the references. This basis assumes: (1) lines of circular cross section ($r_{\nu_\ell} = r_o$ or R); (2) nearly incompressible fluids ($\gamma = 1$); (3) unity Prandtl Number ($\sigma = 1$); (4) constant phase velocity ($c = c_a$);

(5) developed turbulent mean flow; (6) relatively small amplitude oscillatory signals; (7) small attenuation per line wavelength; and (8) high or near high signal frequencies ($\omega/\omega_{\nu_t} \geq 1$), for all turbulent Reynolds numbers. Since Funk and Wood [25] have compared their work to that of Brown, et al. [15], the comparison herein deals primarily with Reference [25]. The dimensionless parameters of Brown, equations (152) and (153), will be used for overall comparisons, since these parameters have found wide use in the literature.

The model developed by Funk and Wood [25] assigns all viscous effects to a single fictitious laminar boundary layer whose thickness (Δ) is based on steady flow laminar and turbulent friction factor data:

$$\frac{\Delta}{R} = \frac{16}{(fRe)_t} \tag{179}$$

where R is the radius of the circular line. All other effects are assigned to an inertial plug-flow core (i.e., $L \geq La$). The model makes use of the eight assumptions listed above, and results in a single dissipation function (Φ) such that the attenuation can be expressed as

$$\alpha = \frac{\nu\Phi}{Rc_a\Delta} \tag{180}$$

The attenuation itself is assumed to be small, and only first order effects are considered in the expansion of the dynamic pressure ratio:

$$\left|\frac{\Delta P_r}{\Delta P_s}\right| = e^{-\alpha z} \geq 1 - \alpha z \tag{181}$$

The model of Funk and Wood still requires the computation of a complex transfer function relating the local velocity gradient to the core velocity, and also requires numerical integration of the dissipation function across the boundary layer. Both of these requirements are avoided by the model given in equation (178) and plotted in Figure 42. From equations (65), (75), (76), and (141) it is easily shown that for the same circular line carrying turbulent mean flow,

$$\frac{\omega_{\nu_\ell}}{\omega_{\nu_t}} = \left(\frac{r_{\nu_t}}{R}\right)^2 = \frac{R_{\nu_\ell}}{R_{\nu_t}} = \frac{(fRe)_\ell}{(fRe)_t} = \frac{64}{(fRey)_t} \tag{182}$$

The model of Funk and Wood and the author's model are related through the turbulent mean flow parameters. Comparing equations (179) and (182),

$$\frac{\Delta}{R} = \frac{1}{4}\left(\frac{r_{\nu_t}}{R}\right)^2 \tag{183}$$

The relationship between Φ and the parameters developed herein is obtained by comparing expressions for the dimensionless attenuation. From equation (180),

$$\frac{R^2 c_a}{\nu}\alpha = \frac{R^2 c_a}{\nu} \cdot \frac{\nu\Phi}{R c_a \Delta} = \frac{R}{\Delta}\Phi \tag{184}$$

and from equations (178) and (183),

$$\frac{R^2 c_a}{\nu}\alpha = \frac{R^2 c_a}{\nu}\alpha_M \bar{\alpha}_{H_t} = 4\left(\frac{R}{r_{\nu_t}}\right)^2 \bar{\alpha}_{H_t} = \frac{R}{\Delta}\bar{\alpha}_{H_t} \tag{185}$$

It follows that equivalence is of the form $\Phi = \bar{\alpha}_{H_t}$. From equations (178), (183), and (185), with $\gamma = \sigma = 1$, and $r_{\nu_\ell} = R$ for comparison with [25],

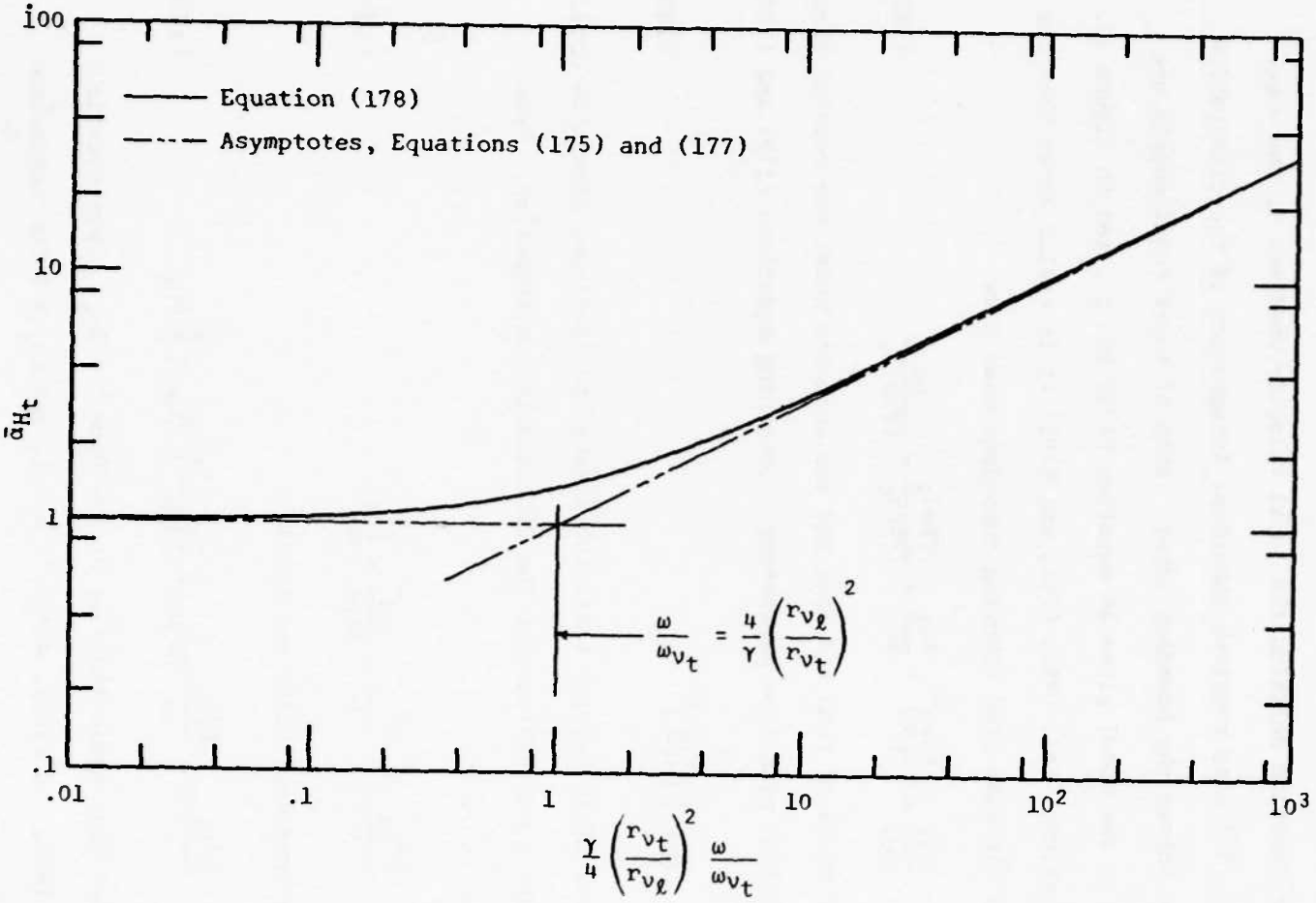

Figure 42. Attenuation in Circular and Noncircular Lines, Laminar or Turbulent Mean Flow, High Frequency Model

$$\frac{R^2 c_a}{\nu}\alpha = \frac{R}{\Delta}\left[1 + \frac{1}{4}\left(\frac{r_{\nu_t}}{R}\right)^2 \frac{\omega}{\omega_{\nu_t}}\right]^{1/2} = \frac{R}{\Delta}\left[1 + \frac{\Delta}{R}\frac{\omega}{\omega_{\nu_t}}\right]^{1/2}$$

$$\frac{R^2 c_a}{\nu}\alpha = \frac{R}{\Delta}\left[1 + \frac{\Delta}{R}\left(\frac{R\Delta}{\delta_\omega{}^2}\right)\right]^{1/2} = \frac{R}{\Delta}\left[1 + \left(\frac{\Delta}{\delta_\omega}\right)^2\right]^{1/2} \qquad (186)$$

Equation (186) indicates the significant influence of the steady and dynamic boundary layers on the line response. At high frequency ratios,

$$\lim_{\omega\to\infty} \frac{R^2 c_a}{\nu}\alpha = \lim_{\omega\to\infty} \frac{R}{\Delta}\left[1 + \left(\frac{\Delta}{\delta_\omega}\right)^2\right]^{1/2} = \frac{R}{\Delta}\cdot\frac{\Delta}{\delta_\omega} = \frac{R}{\delta_\omega} \qquad (187)$$

and at low frequency ratios,

$$\lim_{\omega\to 0} \frac{R^2 c_a}{\nu}\alpha \cong \frac{R}{\Delta}[1 + 0]^{1/2} \cong \frac{R}{\Delta} \qquad (188)$$

and the high corner (break) frequency occurs at $\Delta = \delta_\omega$. From Nichols [3] and Karam [20], the high frequency laminar oscillatory attenuation was approximated by equation (98). Equation (98) reduces to equation (187) as shown in the following development ($\gamma = \sigma = 1$).

$$\alpha_H = \frac{1}{4c_a}\left[1 + \frac{\gamma - 1}{\sigma}\right]\sqrt{\omega\omega_{\nu_\ell}} = \frac{1}{4c_a}\sqrt{\omega\omega_{\nu_\ell}} \qquad (189)$$

Using the definitions of ω_{ν_ℓ} and δ_ω, together with equation (189) and Brown's notation, gives

$$\frac{R^2 c_a}{\nu}\alpha_H = \frac{R^2}{4\nu}\sqrt{\omega\omega_{\nu_\ell}} = 2\sqrt{\frac{\omega}{\omega_{\nu_\ell}}} = \frac{R}{\delta_\omega} \qquad (190)$$

It remains to show the equivalence of the mid-frequency asymptotes, i.e., that $(R^2 c_a/\nu)\,\alpha_M = R/\Delta$, with $\gamma = \sigma = 1$:

$$\frac{R^2 c_a}{\nu}\,\alpha_M = \frac{R^2 c_a}{\nu} \cdot \frac{\sqrt{\gamma}}{2}\,\frac{\omega \nu_t}{c_a} = \frac{R^2}{2\nu} \cdot \frac{8\nu}{r_{\nu_t}^2} = 4\left(\frac{R}{r_{\nu_t}}\right)^2 = \frac{R}{\Delta} \qquad (191)$$

The last two terms of the above equation are identical to those of equation (183).

The attenuation model embodied in equations (178) and (186), applicable to the middle and high frequency regions, constitutes a very significant simplification when compared to the models given in [15] and [25]. An appreciation of this model can only be realized by comparison with the cited references.

The results of Brown, et al. [15,27], Funk and Wood [25], and the author are plotted for comparison in Figure 43 at two Reynolds numbers, Re = 1×10^4 and 1×10^5, for $r_{\nu_\ell} = R$. In view of the experimental data, the author's model is as valid as any of the referenced models for circular lines, and is comparatively much simpler. Furthermore, the model is applicable to any fluid line of arbitrary cross section, carrying laminar or turbulent mean flow. The other models are not.

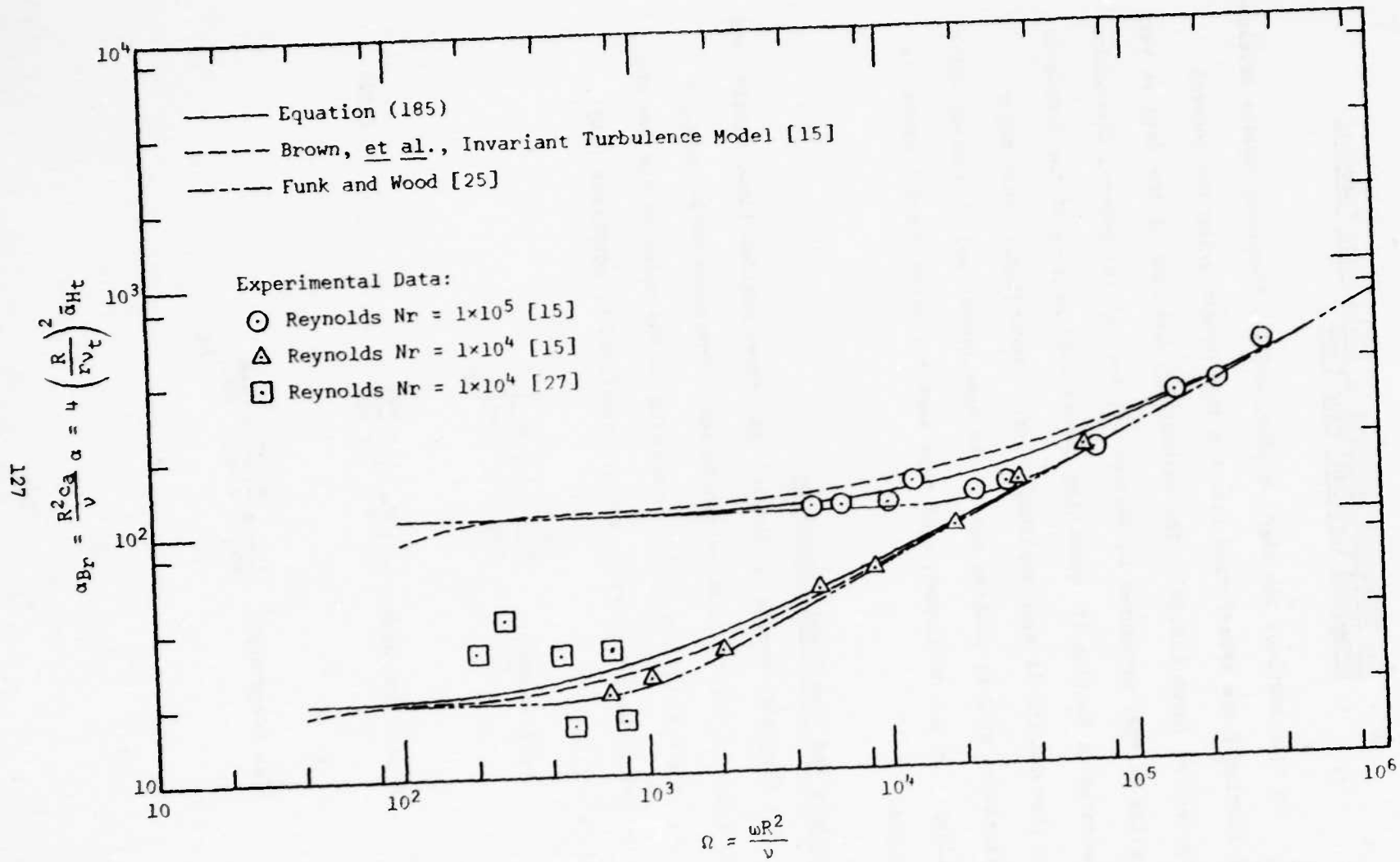

Figure 43. Comparison of Experimental and Predicted Results for Attenuation Factor in Circular Lines, Turbulent Mean Flow

VI. The Transient Response of Fluid Lines Carrying Developed Turbulent Mean Flow

In this section, the high, middle, and low frequency models developed in Section V are transformed into the time domain using the general approach of Karam [19,20]. The methodology and form of the data is very similar to that presented in Section IV; much of the general discussion presented in Section IV concerning the various regions of the frequency and time domains is also applicable here. Accordingly, only major differences will be pointed out in the development and discussion which follows. In all developments of this section, unity Prandtl number is assumed.

Frequency and Time Domain Equations

The frequency domain is divided into three regions (low, middle, and high) based on the turbulent characteristic frequency ratio, $\omega/\omega_{\nu_t} = R_{\nu_t}/La$. The regions are divided according to the value of the low and high corner (break) frequency ratios, as defined by equations (150), (157), and (162):

$$\text{Low frequency:} \quad \frac{\omega}{\omega_{\nu_t}} \leq \frac{1}{2} = \left.\frac{\omega}{\omega_{\nu_t}}\right|_{L_B}$$

$$\text{Middle frequency:} \quad \frac{1}{2} \leq \frac{\omega}{\omega_{\nu_t}} \leq \frac{4}{\gamma}\frac{\omega_{\nu_t}}{\omega_{\nu_\ell}} \tag{192}$$

$$\text{High frequency:} \quad \frac{\omega}{\omega_{\nu_t}} \geq \frac{4}{\gamma}\frac{\omega_{\nu_t}}{\omega_{\nu_\ell}} = \left.\frac{\omega}{\omega_{\nu_t}}\right|_{H_B}$$

It is seen that the regions are highly dependent on both the laminar and turbulent steady flow parameters. A new characteristic time, $t_c = 1/\omega_{\nu_t}$, is used to redefine the dimensionless time parameters, such that:

$$\tau = \omega_{\nu_t} t = t/t_c$$

$$\tau_0 = \omega_{\nu_t} T = T/t_c \qquad (193)$$

$$1 = \omega_{\nu_t} t_c = t_c/t_c$$

The above frequency regions and dimensionless time parameters are used in developing expressions for the various pressure and flow transient responses presented in this section.

Line Attenuation Factor

To facilitate the use of Karam's methodology, the attenuation in turbulent mean flow is expressed in terms of the three logarithmic line segments (asymptotes) corresponding to the three frequency regions of equations (192):

$$\alpha_{L_t} \cong \frac{\omega_{\nu_t}}{c_a}\sqrt{\frac{\gamma}{2}\frac{\omega}{\omega_{\nu_t}}} = K_L\sqrt{\omega}$$

$$\alpha_M = \frac{1}{2}\frac{\omega_{\nu_t}}{c_a}\sqrt{\gamma} \qquad (194)$$

$$\alpha_{H_t} \cong \frac{\gamma}{4c_a}\sqrt{\omega\omega_{\nu_\ell}} = \frac{\gamma\omega_{\nu_t}}{4c_a}\left(\frac{\nu_{\nu_t}}{\nu_{\nu_\ell}}\right)\sqrt{\frac{\omega}{\omega_{\nu_t}}} = K_H\sqrt{\omega}$$

It is seen that the high and low frequency attenuation are of the form $\alpha = K\sqrt{\omega}$. Consequently, the solutions of Metzger and Vabre [23] and

Karam [20] may be adapted to obtain the various transient responses. The attenuation ratio, α/α_H, is redefined as

$$\frac{\alpha}{\alpha_H} = \frac{K}{K_H} = \begin{cases} 1 & \text{for } \tau \le \frac{\gamma}{4}\left(\frac{r_{\nu t}}{r_{\nu \ell}}\right)^2 \\ k\tau^m & \text{for } \frac{\gamma}{4}\left(\frac{r_{\nu t}}{r_{\nu \ell}}\right)^2 \le \tau \le 2 \\ \sqrt{\frac{s}{\gamma}}\left(\frac{r_{\nu \ell}}{r_{\nu t}}\right) & \text{for } \tau \ge 2 \end{cases} \qquad (195)$$

where

$$m = \frac{1}{2} \quad \text{and} \quad k = \frac{2}{\sqrt{\gamma}}\left(\frac{r_{\nu \ell}}{r_{\nu t}}\right)$$

Pressure (Flow) Response to a Step Input of Pressure (Flow), Turbulent Mean Flow

The general solution for the transient downstream pressure (flow) response to a step input of pressure (flow) was given by equation (102). Using the attenuation ratios of equations (195) above, together with equations (102) and (193), the generalized transient response may be expressed as

$$P_{r_t} = \operatorname{erfc}\left[\frac{\frac{\gamma}{4}\left(\frac{r_{\nu t}}{r_{\nu \ell}}\right)\left(\frac{K}{K_H}\right)\tau_0}{\sqrt{2(\tau-\tau_0)}}\right] U(\tau-\tau_0) \qquad (196)$$

where subscript t denotes applicability to turbulent mean flow conditions. The dimensionless step responses for long and short times corresponding to equations (107) and (108) are, respectively:

$$Pr_{L_t} = \operatorname{erfc}\left[\frac{\frac{\gamma}{4}\left(\frac{r_{\nu t}}{r_{\nu \ell}}\right)\left(\frac{K_L}{K_H}\right)\tau_0}{\sqrt{2(\tau-\tau_0)}}\right]U(\tau-\tau_0)$$

$$= \operatorname{erfc}\left[\frac{1}{2}\left(\frac{\gamma\tau_0^2}{\tau-\tau_0}\right)^{1/2}\right]U(\tau-\tau_0) \qquad (197)$$

and

$$Pr_{H_t} = \operatorname{erfc}\left[\frac{\frac{\gamma}{4}\left(\frac{r_{\nu t}}{r_{\nu \ell}}\right)\tau_0}{\sqrt{2(\tau-\tau_0)}}\right]U(\tau-\tau_0) \qquad (198)$$

For completeness, the intermediate or middle time solution is

$$Pr_{M_t} = \operatorname{erfc}\left[\frac{\frac{\gamma}{4}\left(\frac{r_{\nu t}}{r_{\nu \ell}}\right)k\tau^m\tau_0}{\sqrt{2(\tau-\tau_0)}}\right]U(\tau-\tau_0)$$

$$= \operatorname{erfc}\left[\frac{1}{2}\left(\frac{\gamma}{2}\frac{\tau_0^2\tau}{\tau-\tau_0}\right)^{1/2}\right]U(\tau-\tau_0) \qquad (199)$$

It is seen that the middle and long time transient response is completely determined for a given fluid, τ, and τ_0. It is also noted that equation (197) is identical to equation (107); in the latter equation the times are nondimensionalized with respect to ω_c. Equations (197) and (199) describe the transient response of arbitrary lines filled with a compressible fluid carrying laminar or turbulent mean flow. For laminar mean flow, $\omega_{\nu_\ell} = R_{\nu_\ell}/La$ is used to define the dimensionless time (i.e., $\tau = \omega_{\nu_\ell} t$); for turbulent mean flow, $\omega_{\nu_t} = R_{\nu_t}/La$ is used. The short

time response, equation (198), retains some dependence on the ratio of the turbulent to laminar characteristic radii. The physical interpretation is that the high corner break frequency, which essentially marks the division of influence between steady turbulent mean flow behavior and frequency dependent laminar oscillatory behavior must include influences from both phenomena. The ratio r_{ν_t}/r_{ν_ℓ} essentially adjusts the transient response to account for the various arbitrary line geometries and turbulent Reynolds numbers, and is therefore not solely dependent on the turbulent characteristic frequency (ω_{ν_t}).

Equation (196) is plotted in Figure 44 as a function of $\tau = \omega_{\nu_t} t$, for two values of the ratio r_{ν_t}/r_{ν_ℓ}, which correspond to the following tabulated conditions for circular lines ($r_{\nu_\ell} = R$).

TABLE VII

Equivalent Circular Line Steady Flow Parameters for Figures 44, 45, and 46

$\frac{r_{\nu_t}}{r_{\nu_\ell}}$	γ	Re	fRe	$\frac{\gamma}{4}\left(\frac{r_{\nu_t}}{r_{\nu_\ell}}\right)$	$R(=r_{\nu_\ell})$
.44975	1.4017	1×10^4	316.4	.15760	.0935
.07998	1.4017	1×10^6	1779.2	.02803	.0935

The influence of r_{ν_t}/r_{ν_ℓ} on the short time response is small and nearly negligible, as can be seen in Figure 44. In the middle or long time regions, there is no influence, which is evident from equations (197) and (199). For the large differences in mean flow parameters given in Table VII, the nearly unnoticeable effect on the pressure and flow parameters plotted in Figure 44 indicates that the transient responses

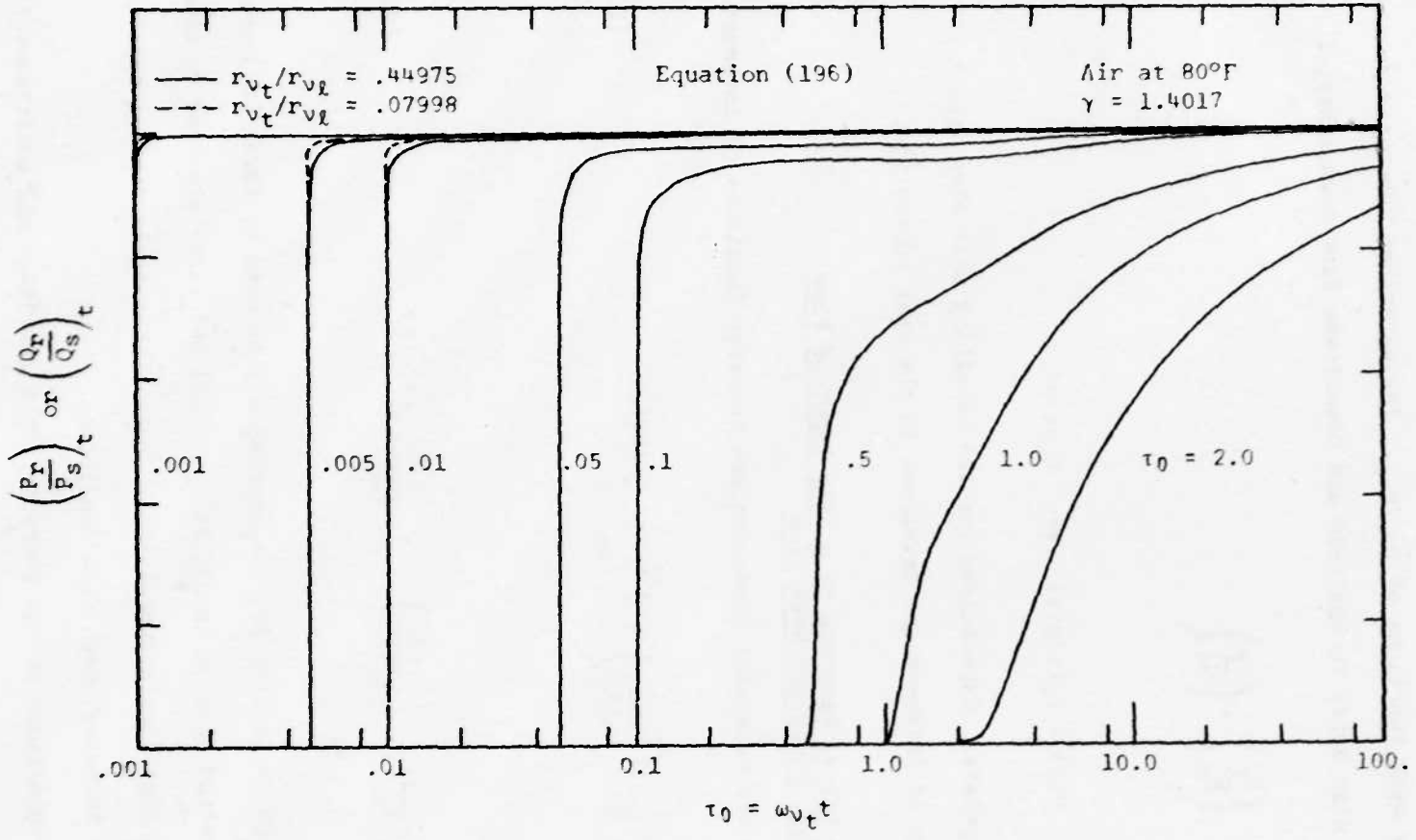

Figure 44. Pressure (Flow) Response to a Step Input of Pressure (Flow) for Air-Filled Lines of Arbitrary Cross Section, Carrying Turbulent Mean Flow

are very weak functions of r_{ν_t}/r_{ν_ℓ}. The equations developed in this section also apply to upstream and downstream flow transients; i.e.,

$$\left(\frac{P_r}{P_s}\right)_t = \left(\frac{Q_r}{Q_s}\right)_t$$

and

$$U(t) = P_s(t)u(t) \quad \text{or} \quad Q_s(t)u(t)$$

as appropriate. Expressions for the remaining unit step inputs and responses of interest are developed in the next subsection.

Pressure (Flow) Response to a Step Input of Flow (Pressure), Turbulent Mean Flow

The two remaining dimensionless transfer functions of interest are:

$$\frac{1}{Z_{so}}\left(\frac{P_r(s)}{Q_s(s)}\right)_t = \frac{1}{s}\frac{Z_o(s)}{Z_{so}}\, e^{-\ell\Gamma_t(s)} \tag{200}$$

and

$$\frac{1}{Y_{so}(s)}\left(\frac{Q_r(s)}{P_s(s)}\right)_t = \frac{1}{s}\,\frac{Y_o(s)}{Y_{so}}\, e^{-\ell\Gamma_t(s)} \tag{201}$$

As was done in Section IV, the approximations used by Karam [20] are adapted, with $\tau = \omega_{\nu_t} t$, and equations (113) and (114) are used to obtain the final time domain expressions. Subscript t again denotes applicability to turbulent mean flow conditions.

Approximations of the characteristic impedance and admittance for the long time (small s) and short time (large s) regions, adapted to turbulent mean flow conditions, are respectively:

$$Z_{oL_t} = \frac{1}{Y_{oL_t}} = \sqrt{\frac{Rv_t}{C_i s}} = \sqrt{\frac{L_a}{C_a}\frac{\omega v_t}{\gamma s}} = Z_{so}\sqrt{\frac{\omega v_t}{\gamma s}} \tag{202}$$

$$Z_{oH_t} = \frac{1}{Y_{oH_t}} = Z_{so} \tag{203}$$

Performing the required integrations yields:

$$\int_o^t Z_{oL_t}(\lambda)d(\lambda) = L^{-1}\left[\frac{Z_{so}}{s}\sqrt{\frac{\omega v_t}{\gamma s}}\right] = 2Z_{so}\sqrt{\frac{\omega v_t t}{\gamma \pi}} = 2Z_{so}\sqrt{\frac{\tau}{\gamma \pi}} \tag{204}$$

$$\int_o^t Z_{oH_t}(\lambda)d\lambda = L^{-1}\left[\frac{Z_{so}}{s}\right] = Z_{so} \tag{205}$$

$$\int_o^t Y_{oL_t}(\lambda)d\lambda = L^{-1}\left[\frac{Y_{so}}{s}\sqrt{\frac{\gamma s}{\omega v_t}}\right] = Y_{so}\sqrt{\frac{\gamma}{\pi \tau}} \tag{206}$$

$$\int_o^t Y_{oH_t}(\lambda)d\lambda = L^{-1}\left[\frac{Y_{so}}{s}\right] = Y_{so} \tag{207}$$

As before, it is convenient to combine the impedance and admittance into a single function applicable to the entire time interval:

$$\frac{1}{Z_{so}} \int_o^t Z_o(\lambda)d\lambda = \left(1 + \frac{4\tau}{\gamma\pi}\right)^{1/2} \tag{208}$$

$$\frac{1}{Y_{so}} \int_o^t Y_o(\lambda)d\lambda = \left(1 + \frac{\pi\tau}{\gamma}\right)^{-1/2} \tag{209}$$

Using the form of equations (113) and (114) together with equations (196), (208), and (209), the desired dimensionless step responses are obtained as follows:

$$\frac{1}{Z_{so}} \left(\frac{P_r}{Q_s}(\tau)\right)_t = \left[\frac{P_r}{Q_s}(\tau)\right]_t \left[1 + \frac{4\tau}{\gamma\pi}\right]^{1/2} \tag{210}$$

$$Z_{so} \left(\frac{Q_r}{P_s}(\tau)\right)_t = \left[\frac{P_r}{P_s}(\tau)\right]_t \left[1 + \frac{\pi\tau}{\gamma}\right]^{-1/2} \tag{211}$$

Equations (210) and (211) are plotted in Figures 45 and 46, respectively, for the parameters given in Table VII.

Physical Implications of the Fluid Line Step Response with Turbulent Mean Flow

It is of interest to discuss the physical implications of the dimensionless step responses shown in Figures 44, 45, and 46. For lines with the same value of τ_0, the computed responses will be identical for values of $\tau \geq (\gamma/4)\ (\omega_{v\ell}/\omega_{vt})$, and will be nearly identical for smaller values of τ. However, two lines of identical τ_0 and working

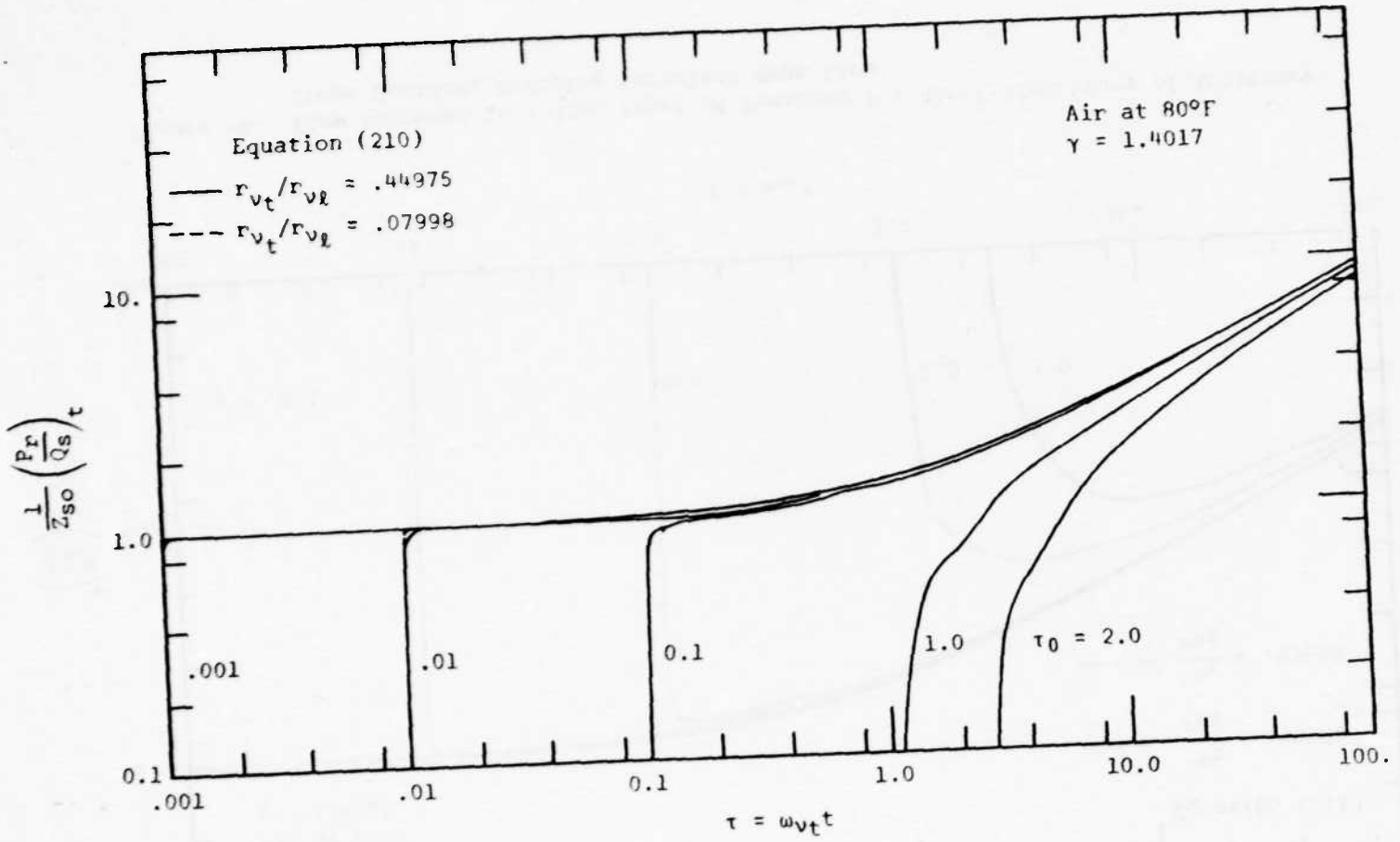

Figure 45. Pressure Response to a Step Input of Flow for Air-Filled Lines of Arbitrary Cross Section, Carrying Turbulent Mean Flow

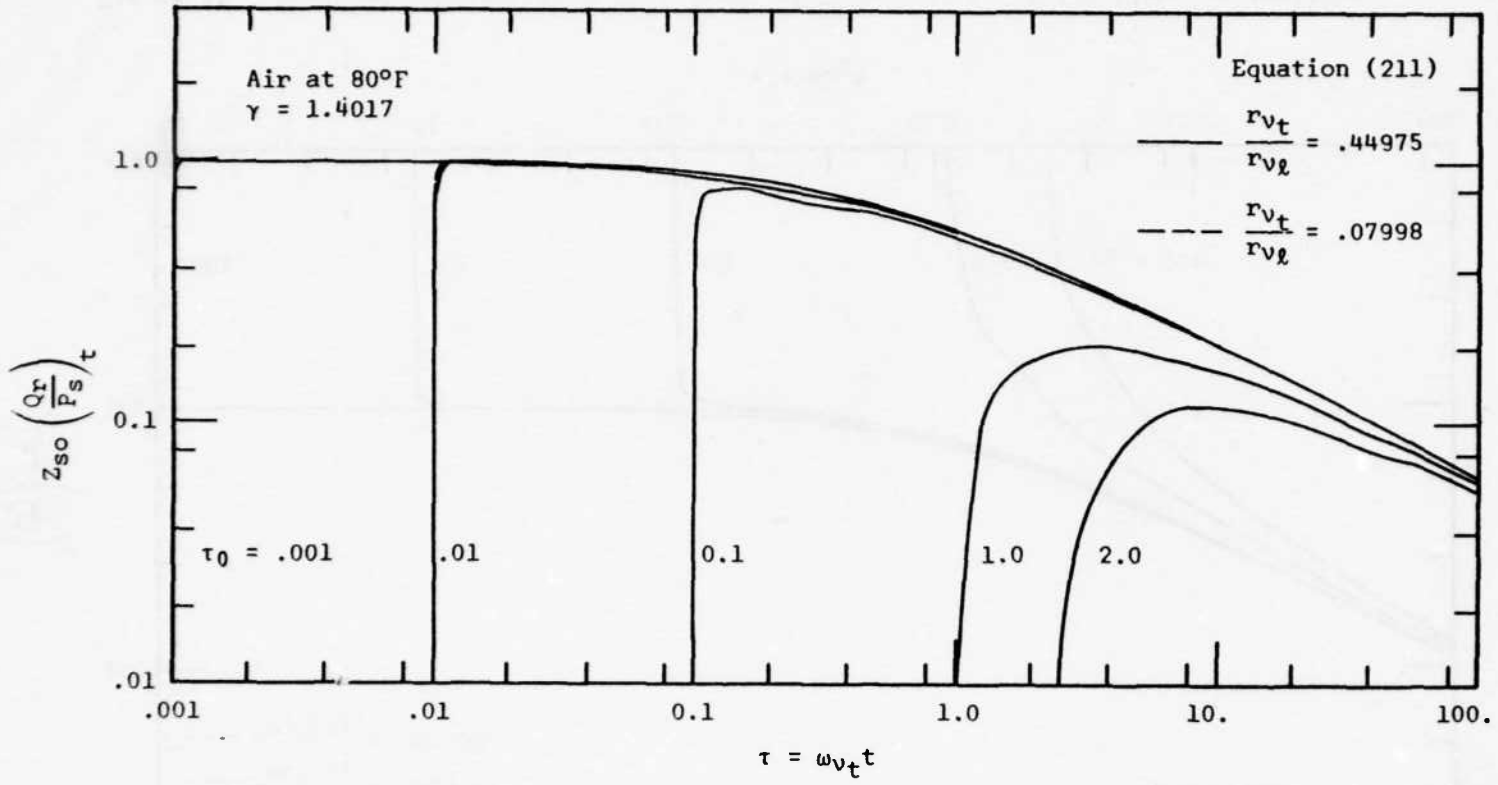

Figure 46. Flow Response to a Step Input of Pressure for Air-Filled Lines of Arbitrary Cross Section, Carrying Turbulent Mean Flow

fluid, but different turbulent characteristic frequencies necessarily imply different physical lengths down the lines. The line having the larger turbulent characteristic frequency will exhibit a faster rise to a given ratio of P_r/P_s or Q_r/Q_s, in a shorter length, and will approach a diffusive RC line more rapidly. Comparing the two circular pneumatic lines for the conditions of Table VII with $\tau_0 = 2$, it is seen that an increase in Reynolds number from $R_e = 10^4$ to $R_e = 10^6$ decreases the adiabatic delay time ($T = \ell/c_a$) by the ratio of 31.6/1! The implication of this example is that increases in the turbulent flow Reynolds number greatly accelerate the transition to diffusive RC line behavior; consequently, high turbulent Reynolds numbers should be avoided in any attempt to transmit information.

In terms of the equivalent laminar and turbulent steady flow boundary layers, equation (183), it is seen that the condition

$$\tau \geq \frac{\gamma}{4}\left(\frac{\omega\nu_\ell}{\omega\nu_t}\right)$$

is equivalent to

$$\tau \geq \gamma\,\frac{\Delta}{R}$$

for circular lines or

$$\tau \geq \frac{\gamma\Delta}{r\nu_\ell}$$

for arbitrary lines. Thus the break time between short time and intermediate time domain responses is a strong function of the equivalent steady flow boundary layer parameters.

VII. Conclusions and Recommendations

This section contains a summary of the conclusions reached as a consequence of this work. Recommendations for extensions of this work are addressed.

Conclusions

1. In general, the very close analogy between the small-signal response of fluid and electrical transmission lines has been reinforced for a wide range of fluid line geometries, mean flow conditions, fluid media, and heat transfer effects. The significant role of the equivalent electrical transmission line properties in describing the fluid line response has been demonstrated. Distributed line parameters such as resistance, inductance, conductance and capacitance, derived from the series impedance and shunt admittance of an equivalent electrical transmission line, are shown to be the key parameters in determining the line response.
2. A closed form, distributed parameter, analytical solution for the small-signal frequency response of fluid transmission lines of annular cross section has been obtained. The solution considers shear flow effects, fluid compressibility, and heat transfer effects, and is applicable to blocked lines or lines carrying developed laminar mean flow. The solution was shown to be in very good agreement with experimental data for blocked annular pneumatic transmission lines over a wide range of annular radius ratios and signal frequencies. In comparing the annular line results with those previously obtained for rectangular lines, it was shown that for large radius and aspect ratios the solutions converge. The

annular line solution contains the circular line solution as a special case.

3. Lines of arbitrary cross section can be accurately modeled as equivalent circular lines having the same ratio of steady flow resistance to inertia properties. The concept of an equivalent characteristic frequency and radius can be applied to transmission lines of arbitrary cross section to predict both the frequency response and transient behavior of these lines, including either laminar or turbulent mean flow effects. In solving practical problems involving fluid systems, this equivalence should be of significant value in simplifying the system modeling task.

4. The characteristic radius is analogous to the hydraulic radius used to represent circular and noncircular lines in steady flow analysis. However, the characteristic radius more accurately accounts for the actual viscous and inertial effects and was shown to be clearly superior to the hydraulic radius in modeling the frequency response of noncircular lines. In view of the much closer agreement with existing data and analytical solutions for both rectangular and annular lines, the characteristic radius should be used instead of the hydraulic radius to determine the equivalent circular line for all noncircular lines.

5. Very significant simplifications have been achieved regarding the modeling of the frequency and temporal response of circular lines carrying turbulent mean flow. Comparison of the simplified models with existing models and experimental data on circular lines shows that the simplified models are as accurate as any existing models

in predicting the frequency response. Furthermore, the simplified models are not restricted to circular lines or incompressible fluids.

6. Of the four equivalent circuit components, the steady flow viscous resistance is the most influential parameter in determining the frequency and temporal response of fluid transmission lines. For developed laminar flow, the steady flow resistance is determined by the line geometry and fluid, and is not influenced by changes in the Reynolds number. For developed turbulent mean flow, the resistance is strongly dependent on the Reynolds number. In all cases, the thickness of the frequency dependent laminar oscillatory boundary layer relative to the equivalent steady flow boundary layer is a key parameter in determining whether the frequency or transient response exhibits predominantly viscous, isothermal behavior or inertial, adiabatic behavior.

Recommendations

1. The small signal transient response of both circular and non-circular lines carrying laminar throughflow should be determined experimentally and compared with the analytical results presented in this work. The experiment should include both compressible and incompressible fluid flow, and should be repeated for turbulent throughflow.
2. More analytical and experimental work is also needed to extend the applicability of the concepts. The frequency and temporal responses of fluid transmission lines to large amplitude excitation signals are of particular interest. The assumption of essentially constant

mean fluid properties and small perturbation of a steady mean flow, valid for small-signal excitation, would have to be re-examined. A possible approach would begin with a sensitivity analysis of the amplitude and frequency dependence in the initial formulation of the governing equations, followed by the addition of corrective terms to the simplified equations of this work to account for the first order dependence on excitation signal amplitude.

3. An analytical model which adequately describes the behavior of the signal attenuation and phase velocity at or near the high frequency corner, or break frequency, should be developed. The anomalous behavior is associated with the transition of small-signal dependence from quasi-steady turbulent mean flow dependence to laminar oscillatory frequency dependence. A companion experiment which would include flow visualization and high-speed photography of the disturbances might provide significant physical insights in developing the model.

Bibliography

1. Iberall, A.S., "Attenuation of Oscillatory Pressures in Instrument Lines," Journal of Research, National Bureau of Standards, Vol. 45, 1959, pp. 85-108.

2. Brown, F.T., "The Transient Response of Fluid Lines," Journal of Basic Engineering, Trans. ASME, Series D, Vol. 84, No. 3, Sept. 1962, pp. 547-553.

3. Nichols, N. B., "The Linear Properties of Pneumatic Transmission Lines," Transactions of the Instrument Society of America, Vol. 1, 1962, pp. 5-14.

4. Schaedel, H., "A Theoretical Investigation of Fluidic Transmission Lines with Rectangular Cross-Section," Third Cranfield Fludics Conference, 8-10 May 1968, Turin, Paper K-3.

5. McLachlan, N.W., Bessel Functions for Engineers, 2nd edition, Oxford University Press, London, England, 1955.

6. Handbook of Mathematical Functions, edited by M. Abramowitz and I.A. Stegun, U.S. Government Printing Office, November 1970.

7. Goodson, R.E. and Leonard, R.G., "A Survey of Modeling Techniques for Fluid Line Transients," Journal of Basic Engineering, Trans. ASME, Series D, Vol. 94, No. 2, June 1972, pp. 474-482.

8. Ebert, W.A. and Sparrow, E.M., "Slipflow in Rectangular and Annular Ducts," Journal of Basic Engineering, Trans. ASME, Series D, Vol. 87, No. 4, December 1965, pp. 1018-1024.

9. Karam, J.T., Jr. and Franke, M.E., "The Frequency Response of Pneumatic Lines," Journal of Basic Engineering, Trans. ASME, Series D, Vol. 89, June 1967, pp. 371-378.

10. Farney, G.R., "Dynamic Characteristics of Blocked Pneumatic Annular Transmission Lines," M.S. Thesis No. GA/ME/73-2, The Air Force Institute of Technology, June 1973.

11. Weber, E., Linear Transient Analysis, Volume II, John Wiley and Sons, Inc., New York, 1956.

12. Franke, M.E., Wilda, R.W., Miller, R.N., and Fada, C.V., "The Frequency Response of Volume-Terminated Pneumatic Lines with Circular and Rectangular Cross Sections," Proceedings of the 1969 Joint Automatic Control Conference, University of Colorado, Boulder, Colorado, 1969.

13. Healey, A.J. and Carlson, R.J., "Frequency Response of Rectangular Pneumatic Transmission Lines," ASME Paper No. 69-WA/FLCS-5, 1969.

14. Franke, M.E., Lymburner, F.C., and Karam, J.T., Jr., "Experimental Frequency Response of Fluidic Transmission Lines," Proceedings of the Fourth Cranfield Fluidics Conference, Paper E1, March 1970, Coventry, England, The British Hydromechanics Research Association, Cranfield, Bedford, England.

15. Brown, F.T., Margolis, D.L., and Shaw, R.P., "Small-Amplitude Frequency Behavior of Fluid Lines with Turbulent Flow," Journal of Basic Engineering, Trans. ASME, Series D, Vol. 91, No. 4, 1969, pp. 678-693.

16. Goldschmied, R.R., "On the Frequency Response of Viscous Compressible Fluids as a Function of Stokes Number," NASA TM X-53785, September 1968, NASA Marshall Space Flight Center.

17. Moore, E.F. and Franke, M.E., "The Small Signal Response of Annular Pneumatic Transmission Lines," Journal of Fluids Engineering, Trans. ASME, Series I, Vol. 96, December 1974, pp. 377-383.

18. Lundgren, T.S., Sparrow, E.M., and Starr, J.B., "Pressure Drop Due to the Entrance Region in Ducts of Arbitrary Cross Section," Journal of Basic Engineering, Trans. ASME, Vol. 86, Series D, No. 3, 1964, pp. 620-626.

19. Karam, J.T., Jr., "A Simple But Complete Solution for the Step Response of a Semi-Infinite, Circular Fluid Transmission Line," ASME Paper No. 71-WA/FE-10, 1971.

20. Karam, J.T., Jr., "A Simple Time Domain Model for Fluid Transmission Line Systems," Ph.D. Thesis, Purdue University, January 1972.

21. Sneddon, I.A., Fourier Transforms, McGraw-Hill Book Co., Inc., New York, 1951.

22. Brown, F.T. and Nelson, S.E., "Step Responses of Liquid Lines with Frequency-Dependent Effects of Viscosity," Journal of Basic Engineering, Trans. ASME, Series D, Vol. 87, June 1965, pp. 504-510.

23. Metzger, G. and Vabre, J-P., Transmission Lines with Pulse Excitation, Academic Press, New York, 1969.

24. Kantola, R., "Transient Response of Fluid Lines Including Frequency Modulated Inputs," ASME Paper No. 70-WA/Flcs-1, December 1970.

25. Funk, J.E. and Wood, D.J., "Frequency Response of Fluid Lines with Turbulent Flow," Journal of Fluids Engineering, Trans. ASME, Series I, Vol. 96, December 1974, pp. 365-369.

26. Wood, D.J. and Funk, J.E., "A Boundary-Layer Theory for Transient Viscous Losses in Turbulent Flow," Journal of Basic Engineering, Trans. ASME, Series D, Vol. 92, December 1970, pp. 865-873.

27. Margolis, D.L. and Brown, F.T., "Measurement of the Propagation of Long-Wavelength Disturbances Through Turbulent Flow in Tubes," Journal of Fluids Engineering, Trans. ASME, Series I, Vol. 98, No. 1, March 1976, pp. 70-78.

28. Holmboe, E.L. and Rouleau, W.J., "The Effect of Viscous Shear on Transients in Liquid Lines," Journal of Basic Engineering, Trans. ASME, Series D, Vol. 89, March 1967, pp. 174-180.

29. Trikha, A.K., "An Efficient Method for Simulating Frequency-Dependent Friction in Transient Liquid Flow," Journal of Fluids Engineering, Trans. ASME, Series I, Vol. 97, No. 1, March 1975, pp. 97-105.

30. Schlichting, H., Boundary Layer Theory, Fourth Edition, McGraw-Hill Book Company, Inc., New York, June 1962.

31. Hinze, J.O., Turbulence, First Edition, McGraw-Hill Book Company, New York, 1959.

32. Vining, J.D., "Through Flow Effects on the Dynamic Characteristics of Pneumatic Transmission Lines," M.S. Thesis, Air Force Institute of Technology, No. GAE/AE/75J-21, June 1975.

Appendix A

DC Resistance and DC Inductance of Fluid Transmission Lines Carrying Developed Laminar Flow

In general, the DC resistance (R_v) and DC inductance (L_v) are determined from the steady flow parameters of the rigid transmission line. These parameters will be functions of the line geometry, fluid properties and steady flow profiles. The DC resistance is defined by

$$R_v = \frac{-\partial P/\partial z}{Q} = \frac{-\partial P/\partial z}{A\bar{u}} \tag{A-1}$$

and the DC inductance is defined as

$$L_v = \left[\frac{1}{A}\int \left(\frac{u}{\bar{u}}\right)^2 dA\right] L_a = K_L \cdot L_a \tag{A-2}$$

where u is the steady flow velocity (either laminar or turbulent); $\bar{u}$ is the average velocity, $\bar{u} = 1/A \int u dA$; and $L_a = \rho/A$ is the adiabatic inductance.

For circular lines, R_v and L_v are constants. For steady developed laminar flow, R_v and L_v are obtained from the classical Hagen-Poiseuille flow:

$$R_v = \frac{-\partial P/\partial z}{Q} = \frac{8\pi\mu}{A^2} \tag{A-3}$$

The Hagen-Poiseuille velocity ratio is [30]

$$\frac{u}{\bar{u}} = 2\left[1 - \left(\frac{r}{r_o}\right)^2\right] \tag{A-4}$$

where r is the radial coordinate and r_o is the inner radius of the circular line. Using this ratio in equation (A-2),

$$L_v = \frac{L_a}{\pi r_o^2} \int_o^{r_o} 4\left[1 - \left(\frac{r}{r_o}\right)^2\right]^2 2\pi r dr = \frac{4}{3} L_a \qquad \text{(A-5)}$$

For annular and rectangular lines R_v and L_v will depend on the radius or aspect ratio, respectively. For the annular line [8],

$$\frac{\bar{u}}{r_o^2/4\mu\ (-dP/dz)} = \frac{1}{2}\left[1 + r_i^{*2} + \frac{1-r_i^{*2}}{\ln r_i^*}\right] \qquad \text{(A-6)}$$

From which R_{v_n} is easily obtained as

$$R_{v_n} = \frac{-\partial P/\partial z}{Q} = \frac{8\pi\mu}{A_n^2}\left[\frac{1+r_i^{*2}}{1-r_i^{*2}} + \frac{1}{\ln r_i^*}\right]^{-1} \qquad \text{(A-7)}$$

where $r_i^* = r_i/r_o$, is the radius ratio of the annular cross section. The velocity ratio is [8]:

$$\frac{u}{\bar{u}} = \frac{[1-r^{*2}] \ln r_i^* - [1-r_i^{*2}] \ln r^*}{\frac{1}{2}[(1+r_i^{*2}) \ln r_i^* + (1-r_i^{*2})]} \qquad \text{(A-8)}$$

where $r^* = r/r_o$ and the dependence on geometry is obvious. The notation $r^* = r_i/r_o$ is generally used in the body of this work. However, for this appendix only, it is necessary to distinguish between the dimensionless ratio $r^* = r/r_o$ and $r_i^* = r_i/r_o$. Using equations (A-2) and (A-8),

$$L_{v_n} = K_L \cdot L_a = \frac{8L_a}{d^2}\left\{(\ln r_i^*)^2\left[\frac{1}{2} - \frac{2}{3}\left(1 + r_i^*\right) + \frac{1}{4}\left(1 + r_i^{*2}\right) + \frac{r_i^{*2}}{2}\right] - \ln r_i^*\left(\frac{3}{8} r_i^{*4}\right) + \frac{1}{4}\left(1 - r_i^{*2}\right)^2\right\} \quad \text{(A-9)}$$

where

$$d^2 = \left[\left(1 + r_i^{*2}\right)\ln r_i^* + \left(1 - r_i^{*2}\right)\right]^2 \quad \text{(A-10)}$$

For the rectangular line [8] of aspect ratio a = h/b,

$$\frac{u}{\frac{h^2}{4\mu}\left(\frac{-\partial P}{\partial z}\right)} = 2\sum_{i=1}^{\infty}\frac{\sin\alpha_i}{\alpha_i^3}\cos(\alpha_i\eta)\left[1 - \frac{\cosh\left(\frac{\alpha_i}{a}\xi\right)}{\cosh\left(\frac{\alpha_i}{a}\right)}\right] \quad \text{(A-11)}$$

where $\eta = y/h$, $\xi = x/b$, and $\alpha_i = \pi/2(2i-1)\pi/2(2i-1) \quad i = 1,2,3,\ldots$

The average velocity is

$$\frac{\bar{u}}{\frac{h^2}{4\mu}\left(\frac{-\partial P}{\partial z}\right)} = 2\sum_{i=1}^{\infty}\frac{a}{\alpha_i^5}\sin^2\alpha_i\left[\frac{\alpha_i}{a} - \tanh\frac{\alpha_i}{a}\right] \quad \text{(A-12)}$$

The DC resistance for the rectangular line is easily found as

$$R_{v_r} = \frac{-\partial P/\partial z}{Q} = \frac{2\mu}{aA^2}\left[\sum_{i=1}^{\infty}\frac{a}{\alpha_i^5}\sin^2\alpha_i\left(\frac{\alpha_i}{a} - \tanh\frac{\alpha_i}{a}\right)\right]^{-1} \quad \text{(A-13)}$$

The velocity ratio is given by

$$\frac{u}{\bar{u}} = \frac{\sum_{i=1}^{\infty}\frac{\sin\alpha_i}{\alpha_i^3}\cos\alpha_i\eta\left[1 - \frac{\cosh\left(\frac{\alpha_i}{a}\xi\right)}{\cosh(\alpha_i/a)}\right]}{\sum_{i=1}^{\infty}\frac{a}{\alpha_i^5}\sin^2\alpha_i\left[\frac{\alpha_i}{a} - \tanh\frac{\alpha_i}{a}\right]} \quad \text{(A-14)}$$

The DC inductance is

$$L_{v_r} = \frac{L_a}{A} \int \left(\frac{u}{\bar{u}}\right)^2 dA = \frac{L_a}{d^2} \int_{-1}^{+1} \int_{-1}^{+1} \left[\sum_{i=1}^{\infty} \frac{\sin\alpha_i}{\alpha^3} \cos\alpha_i\eta \left(1 - \frac{\cosh\left(\frac{\alpha_i}{a}\right)\xi}{\cosh\left(\frac{\alpha_i}{a}\right)} \right) \right]^2 d\xi d\eta \qquad \text{(A-15)}$$

where $d = \sum_{i=1}^{\infty} \frac{a}{\alpha_i^5} \left[\frac{\alpha_i}{a} - \tanh \frac{\alpha_i}{a} \right]$

The integrand is of the form

$$\left[\sum_{i=1}^{\infty} y_i(\eta) x_i(\xi) \right]^2 = \sum_{j=1}^{\infty} \sum_{i=1}^{\infty} y_i(\eta) x_i(\xi) y_j(\eta) x_j(\xi) \qquad \text{(A-16)}$$

where

$$x_i(\xi) = \left[1 - \frac{\cosh \frac{\alpha_i}{a} \xi}{\cosh \frac{\alpha_i}{a}} \right]$$

and

$$y_i(\eta) = \frac{\sin\alpha_i}{\alpha_i^3} \cos\alpha_i\eta$$

The integrand is sufficiently well-behaved to permit interchanging the orders of summation and integration. Thus, the integral of equation (A-15) may be written as

$$I = \sum_{j=1}^{\infty} \sum_{i=1}^{\infty} \int_{-1}^{+1} y_i(\eta) y_j(\eta)\, d\eta \int_{-1}^{+1} x_i(\xi) x_j(\xi) d\xi \qquad \text{(A-17)}$$

The integration is greatly simplified by noting that

$$\left.\begin{aligned} \int_{-1}^{1} y_i(\eta) y_j(\eta) d\eta &= 0, \quad i \neq j \\ &= \frac{1}{\alpha_i^4}, \quad i = j \end{aligned}\right\} \tag{A-18}$$

The integral is evaluated, and L_{v_r} becomes:

$$L_{v_r} = \frac{L_a}{4d^2} \sum_{i=1}^{\infty} \frac{1}{\alpha_i^6} \left(3 - \frac{3a}{\alpha_i} \tanh \frac{\alpha_i}{a} - \tanh^2 \frac{\alpha_i}{a} \right) \tag{A-19}$$

It is of interest to include the case of steady developed laminar flow between parallel plates, because this case represents limiting values of both radius ratio for annular lines and aspect ratio for rectangular lines. As $r_i^* \to 1$ $(a \to 0)$, the pairs R_{v_n}, L_{v_n} and R_{v_r}, L_{v_r} will approach the values obtained for parallel plate flow. Taking a unit width of flow between parallel plates where 2b is the distance separating the plates [30] and y is measured from the center plane between the plates,

$$u = - \frac{1}{2\mu} \frac{\partial P}{\partial x} (b^2 - y^2) \tag{A-20}$$

$$\bar{u} = \frac{-\partial P/\partial x}{3\mu} b \tag{A-21}$$

And the DC resistance per unit width is

$$R_{v_p} = \frac{-\partial P/\partial x}{Q} = \frac{3\mu}{2b^3} \tag{A-22}$$

The DC inductance is easily calculated as

$$L_v = \frac{L_a}{A} \int \left(\frac{u}{\bar{u}}\right)^2 dA = \frac{L_a}{2b} \int_{-b}^{b} \left(\frac{3}{2}\right)^2 \left[1 - \left(\frac{y}{b}\right)^2\right]^2 dy = 1.2\, L_a \qquad \text{(A-23)}$$

Thus, the low frequency (DC) inductance does not vary greatly over the range of aspect or radius ratios for rectangular or annular lines. With inside radius $r_i = 0$ for annular lines, $K_{L_n} = K_{L_c} = 4/3$. As $r_i \to r_o$, $K_{L_n} \to 1.2$. For rectangular lines, K_{L_r} has its maximum at $a = 1$ where $K_{L_r} = 1.3785$, and approaches $K_{L_r} = 1.2$ as $a \to 0$.

A similar approach may be used to obtain the low frequency (DC) viscous laminar resistances and inductances for other noncircular lines, provided the steady flow velocity profile is known.

Appendix B

High Frequency Approximations for Annular Lines

First order approximations of the system variables describing the performance of annular fluid transmission lines at high frequency ratios ($\omega/\omega_\nu >> 1$) are obtained from equivalent circuit considerations and analysis of the asymptotic behavior of the Bessel function solutions. In general at high frequency ratios, the flow is approaching inertial, adiabatic behavior. As was pointed out by Nichols [3], the velocity profile is characterized by a large central plug wherein inertial effects are predominant, and a viscous skin region wherein viscous shear effects are predominant. The viscous region is characterized by a skin depth δ_ν which is proportional to $\sqrt{\nu/\omega}$. As frequency (ω) increases, δ_ν decreases. Similarly heat transfer effects may be separated into a relatively large adiabatic core region bounded by a nonadiabatic region, the latter being characterized by a thermal boundary layer thickness δ_T which is proportional to $\sqrt{\nu_T/\omega}$. For the annular line, there are two boundary layers and their influence on the velocity and temperature profiles vary with radius ratio. The behavior is described in the velocity and temperature profiles, equations (11) and (12), respectively. In general, the Bessel function $J_0\left(\phi_j^{\frac{3}{2}}\right)$ has its greatest influence on the solution at the outer wall ($r = r_o$) while $K_0\left(\phi_j^{\frac{1}{2}}\right)$ is most influential at the inner wall. At high frequencies the following inequalities apply:

$$J_0(r_o) >> J_0(r_i) \qquad K_0(r_i) >> K_0(r_o)$$
$$J_1(r_o) >> J_1(r_i) \qquad K_1(r_i) >> K_1(r_o) \tag{B-1}$$

$$J_0(r_o)K_0(r_i) >>> J_0(r_i)K_0(r_o) \tag{B-2}$$

where for J_0, J_1 the argument (r) is presumed to be $\left(\sqrt{\omega/\nu}\ rj^{3/2}\right)$ and for K_0, K_1 the argument is presumed to be $\left(\sqrt{\omega/\nu}\ rj^{1/2}\right)$. For the energy equations ν is replaced by ν_T.

With the foregoing approximations the parameters appearing in equations (11) and (12) may be greatly simplified. The coefficients B, D, and M of equations (13), (14), and (18) become:

$$B \approx B' = -\frac{K_0(r_i)}{J_0(r_o)K_0(r_i)} = -\frac{1}{J_0(r_o)} \tag{B-3}$$

$$D \approx D' = -\frac{J_0(r_o)}{J_0(r_o)K_0(r_i)} = -\frac{1}{K_0(r_i)} \tag{B-4}$$

$$M \approx M' = -\left[\frac{r_o J_1(r_o)}{J_0(r_o)} + j\,\frac{r_i K_1(r_i)}{K_0(r_i)}\right] \tag{B-5}$$

From [5,6] the first order approximations of the Bessel functions are given in Table B-I. Using the expressions given in Table B-I and keeping only first order terms, the high frequency series impedance becomes

$$Z_{HI} = j\omega L_a \left\{1 + \frac{\pi r_o}{A_n}\sqrt{\frac{2\nu}{\omega}}\left[(r^*-1) + j(r^*+1)\right]\right\}^{-1} \tag{B-6}$$

and the shunt admittance is

$$Y_{HI} = j\omega C_a \left\{1 - \left(\frac{\gamma-1}{\sigma}\right)\frac{\pi r_o}{A_n}\sqrt{\frac{2\nu}{\omega}}\left[(r^*-1) + j(r^*+1)\right]\right\} \tag{B-7}$$

TABLE B-I

First Order High Argument Approximations of J_0, J_1, K_0, K_1

Bessel Function	Modulus	Phase
$J_0\left(xj^{\frac{3}{2}}\right) = M_0 e^{j\theta_0}$	$M_0 = \frac{e^{x/\sqrt{2}}}{\sqrt{2\pi x}}\left(1 + \frac{1}{8\sqrt{2}x}\right)$	$\theta_0 = \frac{x}{\sqrt{2}} - \frac{\pi}{8} - \frac{1}{8\sqrt{2}x}$
$J_1\left(xj^{\frac{3}{2}}\right) = M_1 e^{j\theta_1}$	$M_1 = \frac{e^{x/\sqrt{2}}}{\sqrt{2\pi x}}\left(1 - \frac{3}{8\sqrt{2}x}\right)$	$\theta_1 = \frac{x}{\sqrt{2}} + \frac{3\pi}{8} + \frac{3}{8\sqrt{2}\,x}$
$K_0\left(xj^{\frac{1}{2}}\right) = N_0 e^{j\phi_0}$	$N_0 = \frac{e^{-x/\sqrt{2}}}{\sqrt{\pi/2x}}\left(1 - \frac{1}{8\sqrt{2}x}\right)$	$\phi_0 = -\frac{x}{\sqrt{2}} - \frac{\pi}{8} + \frac{1}{8\sqrt{2}x}$
$K_1\left(xj^{\frac{1}{2}}\right) = N_1 e^{j\phi_1}$	$N_1 = \frac{e^{-x/\sqrt{2}}}{\sqrt{\pi/2x}}\left(1 + \frac{3}{8\sqrt{2}x}\right)$	$\phi_1 = -\frac{x}{\sqrt{2}} - \frac{5\pi}{8} - \frac{3}{8\sqrt{2}x}$

The high frequency components of the equivalent circuit are easily obtained from equations (B-6) and (B-7) by separating real and imaginary parts:

$$R_{HI} = \text{Real}(Z_{HI}) = \frac{\sqrt{2\nu\omega}\,L_a}{r_o(1-r^*)} = \frac{1}{2}\sqrt{\omega\omega_\nu}\,L_a \cdot \sqrt{\frac{1+r_i^*}{1-r_i^*}} \qquad \text{(B-8)}$$

$$L_{HI} = \text{Imag}(Z_{HI})/\omega = L_a \qquad \text{(B-9)}$$

$$G_{HI} = \text{Real}(Y_{HI}) = \frac{\sqrt{2\nu_T\omega}\,(\gamma-1)C_a}{r_o(1-r^*)} = \frac{1}{2}\sqrt{\omega\omega_\nu}\left(\frac{\gamma-1}{\sigma}\right)C_a \cdot \sqrt{\frac{1+r_i^*}{1-r_i^*}} \qquad \text{(B-10)}$$

$$C_{HI} = \text{Imag}(Y_{HI})/\omega \simeq C_a \qquad \text{(B-11)}$$

In the high frequency regime and using the approximations $R/\omega L << 1$, $G/\omega C << 1$, the attenuation α and phase lag β are given by Weber [11] as

$$\alpha_{HI} = \frac{LG+RC}{2\sqrt{LC}} \qquad \beta_{HI} = \omega\sqrt{LC} \tag{B-12}$$

Using equations (B-8) through(B-11) in the above equations

$$\alpha_{HI} = \frac{\frac{1}{2} L_a C_a \sqrt{\omega\omega_\nu} \sqrt{\frac{1+r_i^*}{1-r_i^*}\left(1 + \frac{\gamma-1}{\sigma}\right)}}{2\sqrt{L_a C_a}} \tag{B-13}$$

$$\beta_{HI} = \omega\sqrt{L_a C_a}$$

The foregoing approximations are accurate to within 1% for $\omega/\omega_\nu \geq 100$ and $r_i^* \leq 0.9$ and are accurate within 10% for $\omega/\omega_\nu \geq 10$ and $r_i^* \leq 0.5$. The smaller is r_i^* the greater is the accuracy for a given range of ω/ω_ν.

Appendix C

Derivation of Small Signal Equations in Cylindrical Coordinates

In this appendix, the continuity, momentum and energy equations governing the small signal propagation of pressure waves through a fluid-filled line are developed from the more general equations of fluid mechanics and thermodynamics. The equations are expressed in a cylindrical coordinate system (r, θ, z). The radial, angular and axial velocities in this coordinate system are u_r, u_θ, and u_z, respectively, and $\vec{u}$ is the vector velocity. In the following developments

$$\frac{D}{Dt} = \frac{\partial}{\partial t} + u_r \frac{\partial}{\partial r} + \frac{u_\theta}{r} \frac{\partial}{\partial \theta} + u_z \frac{\partial}{\partial z}$$

$$\nabla \cdot \vec{u} = \frac{1}{r} \frac{\partial}{\partial r} (r u_r) + \frac{1}{r} \frac{\partial u_\theta}{\partial \theta} + \frac{\partial u_z}{\partial z}$$

$$\nabla^2 = \frac{\partial^2}{\partial r^2} + \frac{1}{r} \frac{\partial}{\partial r} + \frac{1}{r^2} \frac{\partial^2}{\partial \theta^2} + \frac{\partial^2}{\partial z^2}$$

Momentum Equations

The Navier-Stokes equations of motion for a compressible fluid are as follows:

$$\rho \left[\frac{Du_r}{Dt} - \frac{u_\theta^2}{r} \right] = -\frac{\partial p}{\partial r} + F_r + \mu \left[\nabla^2 u_r - \frac{u_r}{r^2} - \frac{2}{r^2} \frac{\partial u_\theta}{\partial \theta} \right]$$

$$+ \frac{1}{3} \mu \frac{\partial}{\partial r} (\nabla \cdot \vec{u}) \qquad \text{(C-1)}$$

$$\rho\left[\frac{Du_\theta}{Dt} + \frac{u_r u_\theta}{r}\right] = -\frac{1}{r}\frac{\partial P}{\partial \theta} + F_\theta + \mu\left[\nabla^2 u_\theta + \frac{2}{r^2}\frac{\partial u_r}{\partial \theta} - \frac{u_\theta}{r^2}\right]$$

$$+ \frac{1}{3}\mu\left[\frac{1}{r}\frac{\partial}{\partial \theta}(\nabla\cdot\vec{u})\right] \qquad \text{(C-2)}$$

$$\rho\left[\frac{Du_z}{Dt}\right] = -\frac{\partial P}{\partial z} + F_z + \mu\nabla^2 u_z + \frac{1}{3}\mu\frac{\partial}{\partial z}(\nabla\cdot\vec{u}) \qquad \text{(C-3)}$$

The principal direction of small signal wave motion is the axial direction; thus, it is assumed that the flow is axially symmetrical. This further implies $u_\theta = \partial/\partial\theta = 0$. This assumption eliminates the momentum considerations of Equation (C-2). In addition, the body forces (F_r, F_θ, F_z) are also assumed negligible. The momentum equations are thus reduced to the following:

$$\rho\left[\frac{\partial u_r}{\partial t} + u_r\frac{\partial u_r}{\partial r} + u_z\frac{\partial u_r}{\partial z}\right] = -\frac{\partial p}{\partial r} + \mu\left[\frac{\partial^2 u_r}{\partial r^2} + \frac{1}{r}\frac{\partial u_r}{\partial r} + \frac{\partial^2 u_r}{\partial z^2} - \frac{u_r}{r^2}\right]$$

$$+ \frac{1}{3}\mu\frac{\partial}{\partial r}\left[\frac{1}{r}(ru_r) + \frac{\partial u_z}{\partial z}\right] \qquad \text{(C-4)}$$

$$\rho\left[\frac{\partial u_z}{\partial t} + u_r\frac{\partial u_z}{\partial r} + u_z\frac{\partial u_z}{\partial z}\right] = -\frac{\partial p}{\partial z} + \mu\left[\frac{\partial^2 u_z}{\partial r^2} + \frac{1}{r}\frac{\partial u_z}{\partial r} + \frac{\partial^2 u_z}{\partial z^2}\right]$$

$$+ \frac{1}{3}\mu\frac{\partial}{\partial z}\left[\frac{1}{r}\frac{\partial(ru_r)}{\partial r} + \frac{\partial u_z}{\partial z}\right] \qquad \text{(C-5)}$$

The wavelengths of interest are assumed large compared to the cross-sectional dimensions of the line, which implies that the radial component of velocity, u_r, and its derivatives may be neglected. The above equations are further reduced to the following:

$$0 = -\frac{\partial P}{\partial r} + \frac{1}{3}\mu\frac{\partial}{\partial r}\quad\frac{\partial u_z}{\partial z} \tag{C-6}$$

$$\rho\left[\frac{\partial u_z}{\partial t} + u_z\frac{\partial u_z}{\partial z}\right] = -\frac{\partial P}{\partial z} + \frac{4}{3}\mu\frac{\partial^2 u_z}{\partial z^2} + \mu\left[\frac{\partial^2 u_z}{\partial r^2} + \frac{1}{r}\frac{\partial u_z}{\partial r}\right] \tag{C-7}$$

This assumption may be expressed as the following condition: $\lambda >> r_d$ where r_d is the principal dimension of the cross section in the radial direction. Since $c = f\lambda$, and $f = \omega/2\pi$ this condition is equivalently expressed as

$$\cdot\ r_d << \frac{2\pi c}{\omega} \tag{C-8}$$

where c = speed of sound in the line. It is next assumed that the pressure is uniform across any line cross section. This assumption removes the dependence of P on r and eliminates the radial momentum equation

$$\frac{\partial P}{\partial r} = \frac{1}{3}\mu\frac{\partial}{\partial r}\left(\frac{\partial u_z}{\partial z}\right) = 0 \tag{C-9}$$

It is necessary to define the conditions under which the axial variation of u_z is negligible, and to remove this dependence. The pressure, velocity, and density may be written in terms of a mean value and a small perturbation about this value as follows:

$$\begin{aligned} \rho &= \bar{\rho} + \rho' \\ P &= \bar{p} + p' \\ u &= \bar{u} + u' \end{aligned} \tag{C-10}$$

and the subscript z has been dropped from velocity, since only the axial velocity remains in the momentum equation. Substituting these variables into equation (C-7), and separating the steady and dynamic terms gives:

$$\bar{\rho}\,\frac{\partial \bar{u}}{\partial t} + \bar{\rho}\bar{u}\,\frac{\partial \bar{u}}{\partial z} = -\frac{\partial \bar{P}}{\partial z} + \frac{4}{3}\,\mu\,\frac{\partial^2 \bar{u}}{\partial z^2} + \mu\left[\frac{\partial^2 \bar{u}}{\partial r^2} + \frac{1}{r}\,\frac{\partial \bar{u}}{\partial r}\right] \tag{C-11}$$

$$(\bar{\rho}+\rho')\,\frac{\partial u'}{\partial t} + (\bar{\rho}\bar{u}+\bar{\rho}u'+\bar{u}\rho'+u'\rho')\,\frac{\partial u'}{\partial z} = -\frac{\partial P'}{\partial z} + \frac{4}{3}\,\mu\,\frac{\partial^2 u'}{\partial z^2}$$

$$+ \mu\left[\frac{\partial^2 u'}{\partial r^2} + \frac{1}{r}\,\frac{\partial u'}{\partial r}\right] \tag{C-12}$$

It is assumed that the steady part of the velocity is constant in both the axial direction and time. Thus $\partial\bar{u}/\partial t = \partial\bar{u}/\partial z = 0$, and the above equations are rewritten as follows:

$$0 = -\frac{\partial \bar{P}}{\partial z} + \mu\left[\frac{\partial^2 \bar{u}}{\partial r^2} + \frac{1}{r}\,\frac{\partial \bar{u}}{\partial r}\right] \tag{C-13}$$

$$(\bar{\rho}+\rho')\,\frac{\partial u'}{\partial t} + (\bar{\rho}+\rho')u'\,\frac{\partial u'}{\partial z} = -\frac{\partial P'}{\partial z} + \frac{4}{3}\,\mu\,\frac{\partial^2 u'}{\partial z^2} + \mu\left[\frac{\partial^2 u'}{\partial r^2} + \frac{1}{r}\,\frac{\partial u'}{\partial r}\right] \tag{C-14}$$

Equation (C-14) can be further reduced by neglecting higher order terms involving products of perturbation quantities:

$$\bar{\rho}\,\frac{\partial u'}{\partial t} = -\frac{\partial P'}{\partial z} + \frac{4}{3}\,\mu\,\frac{\partial^2 u'}{\partial z^2} + \mu\left[\frac{\partial^2 u'}{\partial r^2} + \frac{1}{r}\,\frac{\partial u'}{\partial r}\right] \tag{C-15}$$

It is now possible to solve the steady flow problem, equation (C-13), by standard techniques. The combined homogeneous and particular solution for velocity is as follows:

$$\bar{u} = C_1 \ln r + C_2 + \frac{r^2}{4\mu} \frac{\partial \bar{P}}{\partial z} \qquad \text{(C-16)}$$

where C_1 and C_2 are arbitrary constants, subject to the boundary conditions of either circular or annular lines. For circular lines, the boundary conditions are:

$$\begin{aligned} &\bar{u} \text{ remains finite at } r = 0 \\ &\bar{u} = 0 \quad \text{at} \quad r = r_o \end{aligned} \qquad \text{(C-17)}$$

Applying these conditions to equation (C-16) leads to the well-known Hagen-Poiseuille velocity distribution:

$$\bar{u} = - \frac{\partial P}{\partial z} \frac{1}{4\mu} (r_o^2 - r^2) \qquad \text{(C-18)}$$

For the annular line, the boundary conditions are:

$$\begin{aligned} &\bar{u} = 0 \quad \text{at} \quad r = r_i \ (\text{or } r^* = r_i^*) \\ &\bar{u} = 0 \quad \text{at} \quad r = r_o \ (\text{or } r^* = 1) \end{aligned} \qquad \text{(C-19)}$$

where $r^* = r/r_o$ and $r_i^* = r_i/r_o$, and r_i, r_o are the inside and outside radii which bound the annular cross section of the line. Applying these conditions to equation (C-16) gives the steady developed laminar flow velocity profile in an annular region.

$$\bar{u} = - \frac{r_o^2}{4\mu} \frac{\partial P}{\partial z} \left[(1 - r^{*2}) - (1 - r_i^{*2}) \frac{\ln r^*}{\ln r_i^*} \right] \qquad \text{(C-20)}$$

Returning to the dynamic problem, equation (C-15), it is necessary to develop the conditions for which

$$\frac{4}{3}\mu\frac{\partial^2 u'}{\partial z^2} << -\frac{\partial P'}{\partial z} \tag{C-21}$$

This is done by assuming the dynamic pressure to be of the following form:

$$p' = \Delta p e^{-\Gamma z} e^{j\omega t} \tag{C-22}$$

and Γ is the propagation operator defined in Section II, which defines the lengthwise dependence of the dynamic pressure. Differentiating equation (C-22) gives

$$\frac{\partial P'}{\partial z} = -\Delta p\Gamma e^{-\Gamma z} e^{j\omega t} \tag{C-23}$$

To a first approximation, the axial sensitivity of the perturbation velocity is

$$\frac{\partial u'}{\partial z} = \frac{1}{\bar{\rho} c_a^2}\frac{\partial P'}{\partial t} \tag{C-24}$$

Substituting equation (C-22) into (C-24), then differentiating equation (C-24) with respect to z gives

$$\frac{\partial^2 u'}{\partial z^2} = -\Delta P\Gamma\frac{j\omega}{\bar{\rho} c_a^2} e^{-\Gamma z} e^{j\omega t} \tag{C-25}$$

Comparing equations (C-21), (C-23) and (C-25) it is seen that

$$\frac{4}{3}\mu\frac{\partial^2 u'}{\partial z^2} << -\frac{\partial P'}{\partial z}$$

when

$$\omega << \frac{3}{4}\frac{\bar{\rho}c_a^2}{\mu} = \frac{3}{4}\frac{c_a^2}{\nu} \qquad \text{(C-26)}$$

For air at standard conditions this amounts to requiring that $\omega << 3.2\times10^7$ rad/sec. The radian frequencies considered in this work are well within this restriction. Using equation (C-26) in equation (C-15), and rearranging terms

$$-\frac{\nu}{r}\frac{\partial}{\partial r}\left[r\frac{\partial u'}{\partial r}\right] + \frac{\partial u'}{\partial t} = -\frac{1}{\bar{\rho}}\frac{\partial P'}{\partial z} \qquad \text{(C-27)}$$

Equation (C-27) is identical with equation (2), Section II. The continuity equation is considered in the following development.

Continuity Equation. The continuity equation for a general compressible fluid expressed in cylindrical coordinates is:

$$\frac{\partial \rho}{\partial t} + \frac{1}{r}\frac{\partial}{\partial r}(\rho r u_r) + \frac{1}{r}\frac{\partial}{\partial \theta}(\rho u_\theta) + \frac{\partial}{\partial z}(\rho u_z) = 0 \qquad \text{(C-28)}$$

By previous assumption, $u_r = u_\theta = \partial/\partial\theta = 0$; thus

$$\frac{\partial \rho}{\partial t} + \frac{\partial}{\partial z}(\rho u_z) = 0 \qquad \text{(C-29)}$$

Expanding equation (C-29) gives

$$\frac{\partial \rho}{\partial t} + \rho\frac{\partial u_z}{\partial z} + u_z\frac{\partial \rho}{\partial z} = 0 \qquad \text{(C-30)}$$

Energy Equation. For a compressible fluid with constant thermal conductivity, k, the energy equation is

$$\rho \frac{Dh}{Dt} - \frac{DP}{Dt} = \frac{\partial q}{\partial t} + \Phi + k\nabla^2 T - \nabla \cdot \vec{q}_r \qquad \text{(C-31)}$$

where h is the specific enthalpy, q is the internal heat generation other than by viscous dissipation, Φ is the mechanical or viscous dissipation function, and $\vec{q}_r$ is the radiation heat flux vector. For small signal propagation the dissipation Φ is assumed negligible. Radiation effects ($\vec{q}_r$) and internal heat generation by chemical or other like means (q) are not considered. With these assumptions, equation (C-31) reduces to

$$\rho \frac{Dh}{Dt} - \frac{DP}{Dt} = k\nabla^2 T \qquad \text{(C-32)}$$

Expanding equation (C-32) in cylindrical coordinates,

$$\rho\left[\frac{\partial h}{\partial t} + u_r \frac{\partial h}{\partial r} + \frac{u_\theta}{r}\frac{\partial h}{\partial \theta} + u_z \frac{\partial h}{\partial z}\right] - \left[\frac{\partial P}{\partial t} + u_r \frac{\partial P}{\partial r} + \frac{u_\theta}{r}\frac{\partial P}{\partial \theta} + u_z \frac{\partial P}{\partial z}\right]$$

$$= k\left[\frac{\partial^2 T}{\partial r^2} + \frac{1}{r}\frac{\partial T}{\partial r} + \frac{1}{r^2}\frac{\partial^2 T}{\partial \theta^2} + \frac{\partial^2 T}{\partial z^2}\right] \qquad \text{(C-33)}$$

From the assumptions made previously on simplifying the momentum equations, such as $u_r = u_\theta = \partial/\partial\theta = 0$, the above equation becomes

$$\rho\left[\frac{\partial h}{\partial t} + u_z \frac{\partial h}{\partial z}\right] - \left[\frac{\partial P}{\partial t} + u_z \frac{\partial P}{\partial z}\right] = k\left[\frac{\partial^2 T}{\partial r^2} + \frac{1}{r}\frac{\partial T}{\partial r} + \frac{\partial^2 T}{\partial z^2}\right] \qquad \text{(C-34)}$$

Since only the axial velocity remains, the subscript z is dropped at this point. As before, the variables are defined as mean values and small perturbation quantities:

$$\begin{aligned} \rho &= \bar{\rho} + \rho' \\ P &= \bar{p} + p' \\ T &= \overline{T} + T' \end{aligned} \tag{C-35}$$

These variables are substituted into equation (C-34) to obtain the small signal energy equation. The result is

$$\bar{\rho}\,\frac{\partial h'}{\partial t} - \frac{\partial P'}{\partial t} = k\left[\frac{\partial^2 T'}{\partial r^2} + \frac{1}{r}\frac{\partial T'}{\partial r} + \frac{\partial^2 T'}{\partial z^2}\right] \tag{C-36}$$

Using the relation $dh = C_p dT$ and dividing by the quantity $\bar{\rho}C_p$ gives

$$\frac{\partial T'}{\partial t} - \frac{1}{\bar{\rho}C_p}\frac{\partial P'}{\partial t} = \frac{k}{\bar{\rho}C_p}\left[\frac{\partial^2 T'}{\partial r^2} + \frac{1}{r}\frac{\partial T'}{\partial r} + \frac{\partial^2 T'}{\partial z^2}\right] \tag{C-37}$$

The Prandtl number $\sigma^2 = \mu C_p/k$, together with the relation $\mu/\bar{\rho} = \nu$, gives

$$\frac{k}{\bar{\rho}C_p} = \frac{\mu}{\bar{\rho}\sigma^2} = \frac{\nu}{\sigma^2} = \nu_T \tag{C-38}$$

and ν_T is the thermal diffusivity. Substituting equation (C-38) into (C-37), and rearranging

$$\frac{\nu_T}{r}\frac{\partial}{\partial r}\left[r\frac{\partial T'}{\partial r}\right] + \frac{\beta_p \overline{T}}{\rho C_p}\frac{\partial P'}{\partial t} = \frac{\partial T'}{\partial t} + \nu_T \frac{\partial^2 T'}{\partial z^2} \tag{C-39}$$

It is necessary to determine the conditions for which

$$\frac{\partial T'}{\partial t} >> \nu_T \frac{\partial^2 T'}{\partial z^2} \tag{C-40}$$

Assuming the dynamic perturbation of temperature is of the following form

$$T' = \Delta T\, e^{-\Gamma z}\, e^{j\omega t} \tag{C-41}$$

then

$$\frac{\partial^2 T'}{\partial z^2} = \Gamma^2\, \Delta T\, e^{-\Gamma z}\, e^{j\omega t} \tag{C-42}$$

and

$$\frac{\partial T'}{\partial t} = j\omega \Delta T\, e^{-\Gamma z}\, e^{j\omega t} \tag{C-43}$$

Since the modulus of Γ is approximately equal to ω/c_a it is seen by comparing equations (C-42) and (C-43) that the condition of equation (C-40) is satisfied when

$$\omega << \frac{c_a^2}{\nu_T} \quad \frac{c_a^2 \sigma^2}{\nu} \tag{C-44}$$

For air, $\sigma^2 = .7$ so that the condition expressed in equation (C-44) is nearly identical to that of equation (C-26). The final form of the energy equation is

$$\frac{\nu_T}{r} \frac{\partial}{\partial r} \left[r \frac{\partial T'}{\partial r} \right] - \frac{\partial T'}{\partial t} = - \frac{\beta p \bar{T}}{\bar{\rho} C_p} \frac{\partial P'}{\partial t} \tag{C-45}$$

which is in agreement with equation (3), Section II.

Temporal Derivative of Density

It is thought necessary to show the derivation of equation (22), since this equation is crucial to the development of the line shunt properties. The density is assumed to depend on pressure and temperature, $\rho = \rho(P,T)$.

$$d\rho = \left(\frac{\partial \rho}{\partial P}\right)_T dp + \left(\frac{\partial \rho}{\partial T}\right)_P dT \tag{C-46}$$

The isothermal compressibility ε is defined as

$$\varepsilon = -\frac{1}{V}\left(\frac{\partial V}{\partial p}\right)_T = \frac{1}{\rho}\left(\frac{\partial \rho}{\partial p}\right)_T \tag{C-47}$$

where V is the specific volume. The coefficient of thermal expansion β_p is defined as

$$\beta_p = \frac{1}{V}\left.\frac{\partial V}{\partial T}\right|_p = -\frac{1}{\rho}\left(\frac{\partial p}{\partial T}\right)_P \tag{C-48}$$

For an ideal gas, $\beta_p T = 1$ and $\varepsilon P = 1$.

Equation (C-43) may be rewritten in terms of the temporal derivative as

$$\frac{\partial p}{\partial t} = \rho\left[\varepsilon \frac{\partial p}{\partial t} - \beta \frac{\partial T}{\partial t}\right] \tag{C-49}$$

From the definition of the specific enthalpy, h:

$$dh = de + d\left(\frac{p}{\rho}\right) \tag{C-50}$$

where e is the specific internal energy. For a perfect gas

$$dh = C_p dT \quad \text{and} \quad de = C_v dT \tag{C-51}$$

Using equations (C-51) in equation (C-50) gives

$$C_p dT = C_v dT + \frac{1}{\rho} dp - \frac{p}{\rho^2} \rho \tag{C-52}$$

Rearranging terms and using equation (C-49) together with the ideal gas relations, $\beta_p T = \varepsilon P = 1$,

$$(C_p - C_v) dT = \frac{dp}{\rho} (1 - \varepsilon p) + \frac{P}{\rho} \beta_p dT = \frac{\beta^2 T}{\rho \varepsilon} dT \tag{C-53}$$

or

$$C_p - C_v = \frac{\beta_p^2 T}{\rho \varepsilon} = C_p \left(\frac{\gamma - 1}{\gamma} \right) \tag{C-54}$$

The pressure term in equation (C-49) may now be expanded as follows

$$\rho \varepsilon \frac{\partial p}{\partial t} = \frac{\beta_p^2 T}{C_p} \left(\frac{\gamma}{\gamma - 1} \right) \frac{\partial p}{\partial t} = \frac{\rho \varepsilon}{\gamma} + \frac{\beta_p^2 T}{C_p} \frac{\partial p}{\partial t} \tag{C-55}$$

Substituting equation (C-55) into equation (C-49) leads directly to equation (22) repeated here for convenience:

$$\frac{\partial \rho}{\partial t} = \frac{\rho \varepsilon}{\gamma} \frac{\partial p}{\partial t} + \beta_p \rho \left[\frac{\beta_p T}{\rho C_p} \frac{\partial p}{\partial t} - \frac{\partial T}{\partial t} \right] \tag{22}$$

The development of the remaining equations in Section II is relatively straightforward.

*U.S.Government Printing Office: 1978 — 757-080/565


EN
DAT
FILM